

DOKUZ EYLÜL UNIVERSITY
GRADUATE SCHOOL OF NATURAL AND APPLIED
SCIENCES

FAILURE ANALYSIS OF COMPOSITE JOINTS
UNDER PRELOAD MOMENT AND MOISTURE

by
Servet KAPTI

September, 2011

İZMİR

FAILURE ANALYSIS OF COMPOSITE JOINTS UNDER PRELOAD MOMENT AND MOISTURE

A Thesis Submitted to the

Graduate School of Natural and Applied Sciences of Dokuz Eylül University

In Partial Fulfillment of the Requirements for the Degree of Master of Science

in Mechanical Engineering, Mechanics Program

by

Servet KAPTI

September, 2011

İZMİR

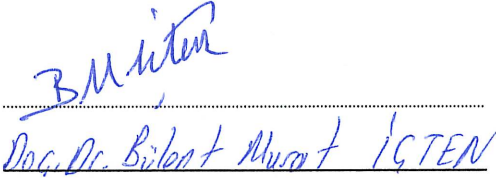
M.Sc THESIS EXAMINATION RESULT FORM

We have read the thesis entitled “**FAILURE ANALYSIS OF COMPOSITE JOINTS UNDER PRELOAD MOMENT AND MOISTURE**” completed by **SERVET KAPTI** under supervision of **PROF. DR. ONUR SAYMAN** and we certify that in our opinion it is fully adequate, in scope and in quality, as a thesis for the degree of Master of Science.

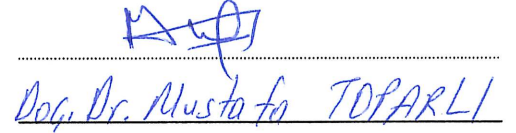


Prof. Dr. Onur SAYMAN

Supervisor



(Jury Member)



(Jury Member)



Prof. Dr. Mustafa SABUNCU

Director

Graduate School of Natural and Applied Sciences

ACKNOWLEDGEMENTS

First of all, I would like to thank and express my deep sense of appreciation to my supervisor Prof. Dr. Onur SAYMAN for his continuous help, patient guidance and valuable encouragement throughout this study.

I would like to extend my special thanks to research assistant Mustafa ÖZEL for his instructive help, moral supporting and sincere friendship.

I also would like to thank to research assistant Semih BENLİ.

Finally, special thanks to my parents, and my brother for their tolerance and understanding while preparing this thesis. I would like to dedicate this work to my family.

Servet KAPTI

**FAILURE ANALYSIS OF COMPOSITE JOINTS UNDER PRELOAD
MOMENT AND MOISTURE
ABSTRACT**

In this study, a failure analysis was performed under various conditions numerically and experimentally to investigate the behavior of laminated composite plates which have pin-loaded holes. The main aim of the study is searching the effects of preload moment, moisture and interference-fit on bearing strength, failure load and failure mode in pin-jointed and bolted carbon-epoxy composite plates which were subjected to a traction force. Some of the specimens were kept in the seawater for sixty days before the experimental tests to observe the effect of moisture.

Each laminated plates consisted of four laminas and had same stacking sequences. Two different geometrical parameters, end distance to pin diameter ratio and width to pin diameter ratio were considered. End distance to pin diameter ratio and width to pin diameter ratios were determined ranging from one to four and from two to four, respectively. The pre-load moments were applied to the specimens as three and six newton-meter for observing the failures under preload moment. Also, for investigating effect of interference-fit, a pin was produced which has a bigger diameter than hole diameter.

The experiments were performed in tension mode on the Instron-1114 Tensile Machine of a crosshead speed of 1mm per minute. Then the average bearing strength values were found. The load versus pin displacement curves were plotted in the experiments. For the numerical study, three-dimensional non-linear contact analyses were conducted using commercial program ANSYS v10.

Keywords: Failure analysis, mechanical fastening, carbon fibers, laminated composites.

KOMPOZİT BAĞLANTILARIN MOMENT VE NEM ETKİSİ ALTINDA HASAR ANALİZİ

ÖZ

Bu çalışmada, pim deliğine sahip tabakalı kompozit plakların, çeşitli durumlar altındaki davranışlarını incelemek için bir hasar analizi gerçekleştirilmiştir. Çalışmanın asıl amacı, çeki kuvvetine tabi tutulan pimli ve cıvatalı karbon-epoxy kompozit plaklarda, ön gerilme momenti, nem ve sıkı geçmenin, yatak mukavemeti, hasar kuvveti ve hasar modu üzerindeki etkisini araştırmaktır. Nem etkisini gözlemlemek için bazı numuneler testlerden önce altmış gün boyunca suda bekletilmiştir.

Her tabakalı kompozit plak dört tabakadan oluşmaktadır ve aynı tabaka dizilişine sahiptir. Pim delik merkezi ile plak ucu arasındaki uzaklığın, delik çapına oranı birden dörde, plak genişliğinin delik çapına oranı ikiden dörde kadar değişecek şekilde iki geometrik parametre belirlenmiştir. Ön gerilme momenti altındaki hasarları gözlemlemek için numunelere üç ve altı newton-metre olmak üzere ön gerilme momenti uygulanmıştır. Ayrıca, sıkı geçme etkisini araştırmak için delik çapından daha büyük bir pim üretilmiştir.

Deneyler, çeki modundaki çene hızı dakikada 1mm olan Instron-1114 Çekme Cihazı üzerinde gerçekleştirilmiştir. Daha sonra ortalama yatak mukavemet değerleri bulunmuştur. Yük-deplasman eğrileri deneylerde çizdirilmiştir. Nümerik çalışma için, üç boyutlu nonlinear kontakt analizler ANSYS v10 ticari programı kullanılarak gerçekleştirilmiştir.

Anahtar Sözcükler: Hasar analizi, mekanik sabitleme, karbon lifler, tabakalı kompozitler.

CONTENTS

	Page
M.Sc THESIS EXAMINATION RESULT FORM.....	ii
ACKNOWLEDGEMENTS	iii
ABSTRACT.....	iv
ÖZ	v
CHAPTER ONE - INTRODUCTION	1
1. 1 Overview	1
1. 2 Objectives of Present Study	3
CHAPTER TWO - COMPOSITE MATERIALS	4
2. 1 Introduction	4
2. 2 Constituents of Composite Laminates.....	5
2. 2. 1 Functions of Fibers	7
2. 2. 1. 1 Carbon Fibers and Manufacturing	7
2. 2. 1. 2 Glass Fibers and Manufacturing.....	10
2. 2. 1. 3 Aramid Fibers and Manufacturing	12
2. 2. 1. 4 Extended Chain Polyethylene Fibers and Manufacturing.....	15
2. 2. 1. 5 Boron Fibers and Manufacturing.....	16
2. 2. 2 Functions of Matrix	17
2. 2. 2. 1 Thermoset Resins	18
2. 2. 2. 1. 1 Epoxies	19
2. 2. 2. 1. 2 Phenolics	21
2. 2. 2. 1. 3 Polyesters	21
2. 2. 2. 1. 4 Vinylesters	22
2. 2. 2. 1. 5 Cyanate esters.....	22
2. 2. 2. 1. 6 Bismaleimide (BMI) and Polyimide.....	22

2. 2. 2. 1. 7 Polyurethane	23
2. 2. 2. 2 Thermoplastic Resins	23
2. 2. 2. 2. 1 Nylons.....	25
2. 2. 2. 2. 2 Polypropylene (PP)	25
2. 2. 2. 2. 3 Polyetheretherketone (PEEK)	26
2. 2. 2. 2. 4 Polyphenylene Sulfide (PPS).....	26
2. 2. 2. 3 Metal Matrix.....	26
2. 2. 2. 4 Ceramic Matrix	28
CHAPTER THREE - MECHANICALLY FASTENED JOINTS	29
3. 1 Introduction	29
3. 2 General Design Considerations.....	30
CHAPTER FOUR - STRESS ANALYSIS OF COMPOSITE MATERIALS ...	33
4.1 Introduction	33
4.2 Stress – Strain Relations For Anisotropic Materials	34
4.3 Stress – Strain Relations For Plane Stress in an Orthotropic Material.....	40
4.4 Material Orientation	42
4.5 Tsai-Wu Tensor Failure Criterion	44
CHAPTER FIVE - EXPERIMENTAL STUDY	48
5.1 Introduction	48
5.2 Fabrication Of Laminated Composites	48
5.3 Mechanical Test Procedure	48
5.4 Problem Statement	52
5.5 Results Of Experimental Studies.....	54
5. 5. 1 Failure Modes	54
5. 5. 2 The Effect Of End Distance – Pin Diameter Ratio (E/D).....	58
5. 5. 3 The Effect Of The Preload Moment $M=3$ And $M=6$ Nm.....	59

5. 5. 4 The Effect Of Side Distance – Pin Diameter Ratio (W/D).....	61
5. 5. 5 The Effect Of The Interference-Fit On The Failure Mode.....	64
CHAPTER SIX - NUMERICAL STUDY	66
6.1 Modeling of The Composite Plates and Applying The Boundary Conditions..	66
CHAPTER SEVEN - CONCLUSIONS	81
REFERENCES.....	82

CHAPTER ONE

INTRODUCTION

1.1 Overview

Composite materials have a wide application area in aircraft industry due to their high mechanical properties and low weights. On these applications, mechanical fasteners, such as pinned and bolted joints are generally used for joining parts to each others in assemblies because of their simplicity and easiness to disassemble. On the other hand, pinned and bolted joints require holes in the composite structure. These holes cause large stress concentrations decrease the load holding capacity and increase the complexity of the numerical analysis. It can be said that the joint properties have a significant effect on failure as well as composite properties have. There are a lot of studies about mechanically fastened composites in literature which have been made by increasing number of investigators in years.

Choi et al. (2008) have used the failure area index (FAI) method to predict the failure load of a composite joint subjected to a clamping force. The failure load could be predicted within %23 via the FAI method. İçten and Karakuzu (2002) have investigated bearing strength and failure modes of pin loaded carbon-epoxy composite plates. They have used Hashin and Hoffman failure criteria to predict the failure loads and the failure modes. Sayman et.al. (2007) have carried out a failure analysis to determine bearing strength of mechanically fastened joints with single bolt in glass-epoxy laminated composite plates. The experimental results showed that the magnitudes of bearing strengths in bolted joints were strictly influenced from increasing value of applied preload moments, changing W/D and E/D ratios, and also ply orientations of laminated composite plates. Whitworth et al. (2003) performed an analysis to evaluate the bearing strength of pin-loaded composite joints. The analysis involved using the Chang–Scott–Springer characteristic curve model and a two-dimensional finite element analysis to evaluate the stress distribution around the fastener hole. Pierron, Cerisier and Grediac (2000) have carried out a numerical and experimental study to determine the stiffness and the bearing strength of bolted

woven composite joints. Zhang, Ganesan and Hoa (2000) have performed an investigation to study the effects of friction on the three-dimensional stress state around pin-loaded holes in laminated composites. They showed that the effects of friction on magnitude and distribution are significant. Aktaş and Karakuzu (1999) have used two dimensional finite element method to determine the failure load and mode using Tsai-Hill and fiber tensile- compressive failure criteria. Okutan (2002) carried out a numerical and experimental study to find out the failure of mechanically fastened fiber-reinforced laminated composite joints. Tests were performed on single pinned joints in [0/90/0]_s and [90/0/90]_s laminated composites. İçten and Sayman (2003) examined failure load and failure mode in an aluminum–glass–epoxy sandwich composite plate, with a circular hole, which was subjected to a traction force by a pin, experimentally. Aktaş and Dirikolu (2003) studied a pin loaded carbon epoxy composite laminate with different stacking sequences in order to determine its safe and maximum bearing strengths, experimentally. The laminate with [90/45/-45/0]_s and [0/45/-45/90]_s stacking sequences had a 62% fiber volume fraction. Shokrieh and Lessard (1996) have established a three-dimensional nonlinear finite element code to analyze the effect of material nonlinearity on the state of stress and failure prediction near the stress concentrations of a pin-loaded composite plate. They emphasize that especially for highly induced cases like [45₄/- 45₄]_s is important in failure analysis of composite laminates using stress based failure criteria. Kiral (2010) have made a study to investigate the effects of clearance and interference-fit on the failure loads and modes of mechanically fastened joints. It was observed that interference for all pin-loaded joint configurations is beneficial. Pradhan and Babu (2007) have created three-dimensional finite element model to investigate beneficial effects of interference-fit in pin-loaded FRP composites. They emphasized that fatigue life of the joint can be improved by interference-fit. Kootsookos and Mouritz (2004) have investigated the effect of seawater immersion on the durability of glass- and carbon-fibre reinforced polymer composites. They showed that when immersed in seawater at a temperature of 30°C for over two years, the composites experienced significant moisture absorption and suffered chemical degradation of resin matrix and fibre/matrix inter phase region. Aktaş and Uzun (2008) have investigated the effect of the seawater on the bearing strength behavior of the woven glass fiber

composite experimentally. They showed that failure distance of pin displacement increase with the increasing of immersing period owing to softening of the specimen.

1.2 Objectives of Present Study

This study deals with the effects of the geometrical parameters, pre-load moment, seawater and interference-fit on the failure loads, failure modes and bearing strengths of the pinned and bolted carbon-epoxy composites. The tests were carried out both applied preload moments as 3 and 6 Nm and without any preload moments under dry and wet conditions. Additionally, three-dimensional non-linear contact analyses were conducted using Tsai-Wu failure criteria via commercial ANSYS v10 program.

CHAPTER TWO

COMPOSITE MATERIALS

2.1 Introduction

In the most general of terms, a composite is a material that consists of two or more constituent materials or phases. Traditional engineering materials (steel, aluminum, etc.) contain impurities that can represent different phases of the same material and fit the broad definition of a composite, but are not considered composites because the elastic modulus or strength of the impurity phase is nearly identical to that of the pure material. The definition of a composite material is flexible and can be augmented to fit specific requirements. In this text a composite material is considered to be one that contains two or more distinct constituents with significantly different macroscopic behavior and a distinct interface between each constituent (on the microscopic level). This includes the continuous fiber laminated composites of primary concern herein, as well as a variety of composites not specifically addressed (Staab, 1999).

Fiber-reinforced composite materials consist of fibers of high strength and modulus embedded in or bonded to a matrix with distinct interfaces (boundaries) between them. In this form, both fibers and matrix retain their physical and chemical identities, yet they produce a combination of properties that cannot be achieved with either of the constituents acting alone. In general, fibers are the principal load-carrying members, while the surrounding matrix keeps them in the desired location and orientation, acts as a load transfer medium between them, and protects them from environmental damages due to elevated temperatures and humidity, for example. Thus, even though the fibers provide reinforcement for the matrix, the latter also serves a number of useful functions in a fiber reinforced composite material. The principal fibers in commercial use are various types of glass and carbon as well as Kevlar 49. Other fibers, such as boron, silicon carbide, and aluminum oxide, are used in limited quantities. All these fibers can be incorporated into a matrix either in continuous lengths or in discontinuous (short) lengths. The matrix material may be a

polymer, a metal, or a ceramic. Various chemical compositions and microstructural arrangements are possible in each matrix category. The most common form in which fiber-reinforced composites are used in structural applications is called a laminate, which is made by stacking a number of thin layers of fibers and matrix and consolidating them into the desired thickness. Fiber orientation in each layer as well as the stacking sequence of various layers in a composite laminate can be controlled to generate a wide range of physical and mechanical properties for the composite laminate (Mallick, 1993).

2.2 Constituents of Composite Laminates

Manufacturing of a composite structure starts with the incorporation of a large number of fibers into a thin layer of matrix to form a lamina (ply). The thickness of a lamina is usually in the range of 0.1–1 mm (0.004–0.04 in.). If continuous (long) fibers are used in making the lamina, they may be arranged either in a unidirectional orientation (i.e., all fibers in one direction, Figure 2.1a), in a bidirectional orientation (i.e., fibers in two directions, usually normal to each other, Figure 2.1b), or in a multidirectional orientation (i.e., fibers in more than two directions, Figure 2.1c). The bi- or multidirectional orientation of fibers is obtained by weaving or other processes used in the textile industry. (...) For a lamina containing unidirectional fibers, the composite material has the highest strength and modulus in the longitudinal direction of the fibers. However, in the transverse direction, its strength and modulus are very low. For a lamina containing bidirectional fibers, the strength and modulus can be varied using different amounts of fibers in the longitudinal and transverse directions. For a balanced lamina, these properties are the same in both directions. A lamina can also be constructed using discontinuous (short) fibers in a matrix. The discontinuous fibers can be arranged either in unidirectional orientation (Figure 2.1c) or in random orientation (Figure 2.1d). Discontinuous fiber-reinforced composites have lower strength and modulus than continuous fiber composites. However, with random orientation of fibers (Figure 2.1e), it is possible to obtain equal mechanical and physical properties in all directions in the plane of the lamina (Mallick, 2007).

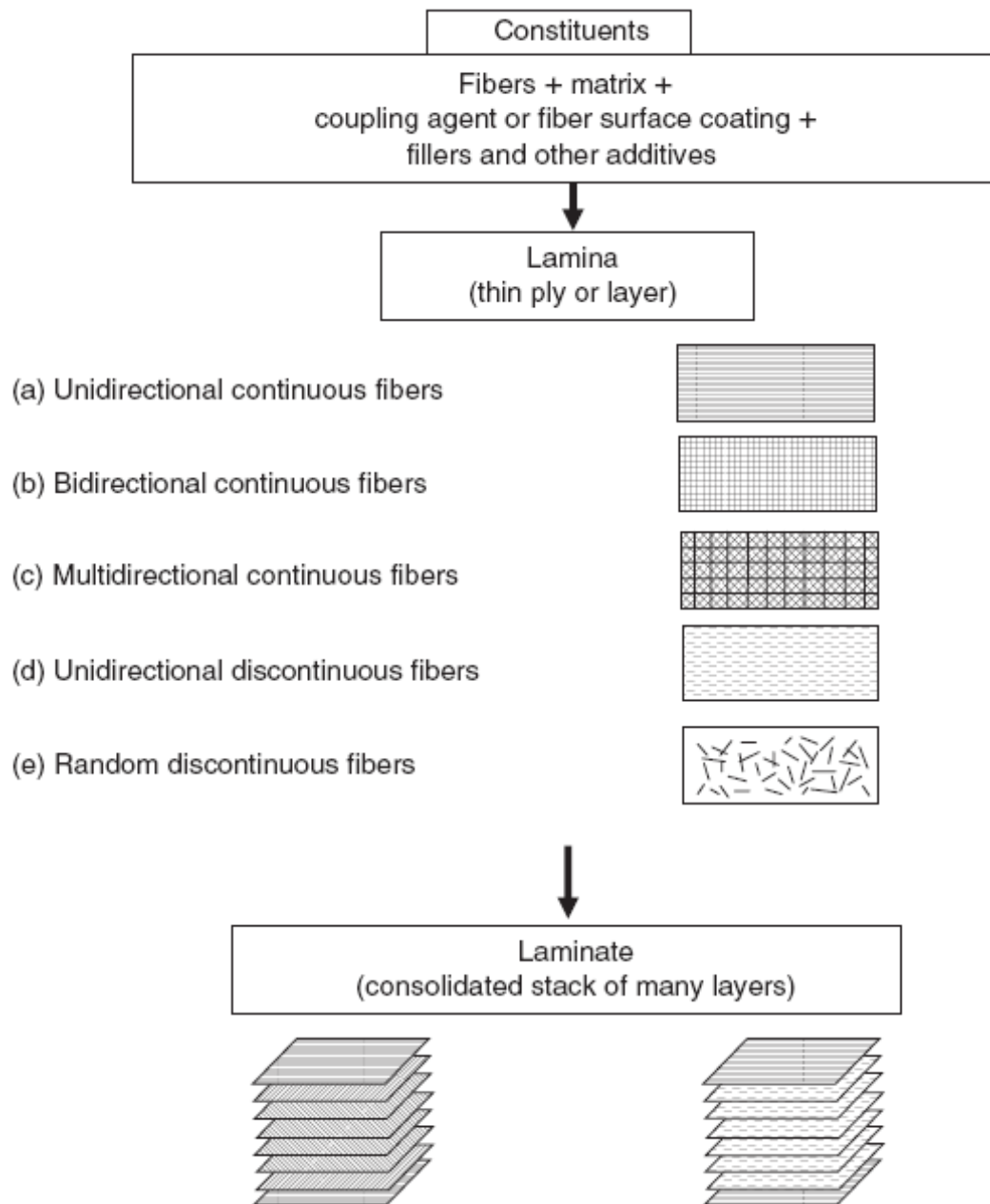


Figure 2.1 Basic building blocks in fiber-reinforced composites (Mallick, 2007)

2.2.1 Functions of Fibers

A composite material is formed by reinforcing plastics with fibers. To develop a good understanding of composite behavior, one should have a good knowledge of the roles of fibers and matrix materials in a composite. The important functions of fibers and matrix materials are discussed below.

The main functions of the fibers in a composite are:

- To carry the load. In a structural composite, 70 to 90% of the load is carried by fibers.
- To provide stiffness, strength, thermal stability, and other structural properties in the composites.
- To provide electrical conductivity or insulation, depending on the type of fiber used (Mazumdar, 2001).

2.2.1.1 Carbon Fibers and Manufacturing

Carbon fibers are commercially available with a variety of tensile modulus values ranging from 207 GPa (303106 psi) on the low side to 1035 GPa (1503106 psi) on the high side. In general, the low-modulus fibers have lower density, lower cost, higher tensile and compressive strengths, and higher tensile strains-to-failure than the high-modulus fibers. Among the advantages of carbon fibers are their exceptionally high tensile strength–weight ratios as well as tensile modulus–weight ratios, very low coefficient of linear thermal expansion (which provides dimensional stability in such applications as space antennas), high fatigue strengths, and high thermal conductivity (which is even higher than that of copper). The disadvantages are their low strain-to-failure, low impact resistance, and high electrical conductivity, which may cause “shorting” in unprotected electrical machinery. Their high cost has so far excluded them from widespread commercial applications. They are used mostly in the aerospace industry, where weight saving is considered more critical than cost. Structurally, carbon fibers contain a blend of amorphous carbon and graphitic

carbon. Their high tensile modulus results from the graphitic form, in which carbon atoms are arranged in a crystallographic structure of parallel planes or layers. The carbon atoms in each plane are arranged at the corners of interconnecting regular hexagons. The distance between the planes (3.4 Å) is larger than that between the adjacent atoms in each plane (1.42 Å). Strong covalent bonds exist between the carbon atoms in each plane, but the bond between the planes is due to van der Waals-type forces, which is much weaker. This results in highly anisotropic physical and mechanical properties for the carbon fiber (Mallick, 2007).

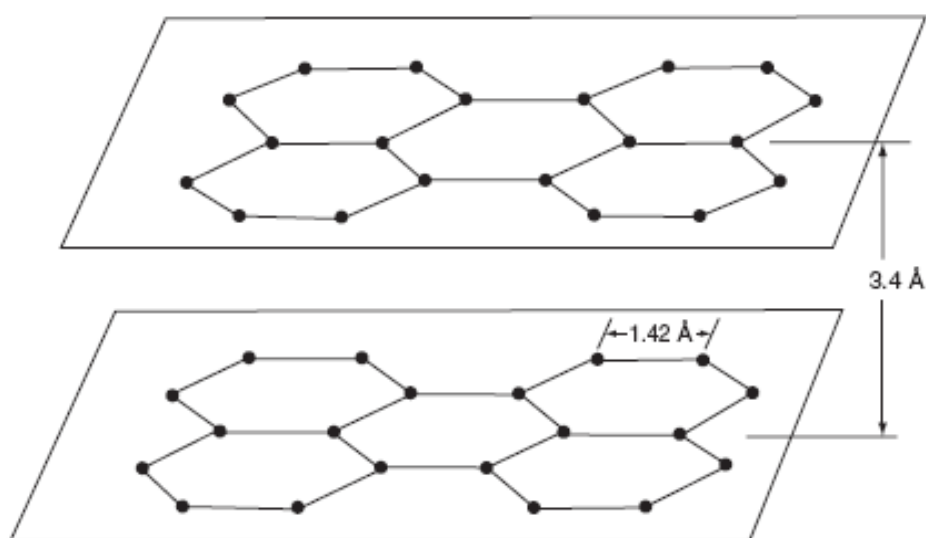


Figure 2.2 Arrangement of carbon atoms in a graphite crystal (Mallick, 2007)

Carbon and graphite fibers are produced using PAN-based or pitch-based precursors. The precursor undergoes a series of operations. In the first step, the precursors are oxidized by exposing them to extremely high temperatures. Later, they go through carbonization and graphitization processes. During these processes, precursors go through chemical changes that yield high stiffness-to-weight and strength-to-weight properties. The successive surface treatment and sizing process improves its resin compatibility and handleability. PAN refers to polyacrylonitrile, a polymer fiber of textile origin. Pitch fiber is obtained by spinning purified petroleum or coal tar pitch. PAN-based fibers are most widely used for the fabrication of carbon fibers. Pitch-based fibers tend to be stiffer and more brittle. The cost of carbon fiber depends on the cost of the raw material and process. The PAN-based precursor costs

around \$1.50 to \$2.00/lb. During oxidation and carbonization processes, the weight reduces to almost 50% of the original weight. Considering the weight loss, the cost of fibers based on raw material alone becomes \$3.00 to \$4.00/lb. The fabrication method for the production of carbon fibers is slow and capital intensive. Therefore, higher tow count is produced to lower the cost of the fibers. There is a limitation on increasing the tow size. For example, a tow size more than 12K creates processing and handling difficulties during filament winding and braiding operations. Pitch-based carbon fibers are produced in the same way as PAN-based fibers but pitch is more difficult to spin and the resultant fiber is more difficult to handle. Pitch itself costs pennies a kilogram, but processing and purifying it to the fiber form are very expensive. Generally, pitch-based fibers are more expensive than PAN-based fibers. The cost of carbon fibers depends on the strength and stiffness properties as well as on the tow size (number of filaments in a fiber bundle). Fibers with high stiffness and strength properties cost more. The higher the tow size, the lower the cost will be. For example, 12K tow (12,000 filaments per fiber bundle) costs less than 6K tow (Mazumdar, 2001).

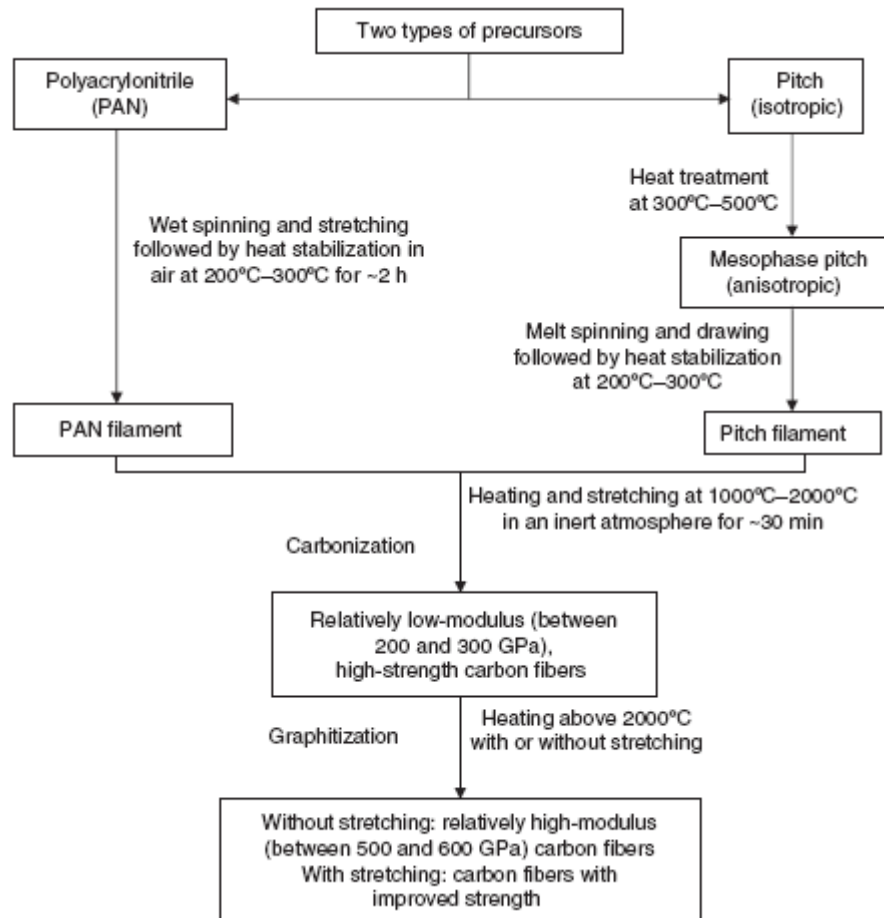


Figure 2.3 Flow diagram of carbon fiber manufacturing (Mallick, 2007)

2.2.1.2 Glass Fibers and Manufacturing

Glass fibers are the most common of all reinforcing fibers for polymeric matrix composites (PMC). The principal advantages of glass fibers are low cost, high tensile strength, high chemical resistance, and excellent insulating properties. The disadvantages are relatively low tensile modulus and high density (among the commercial fibers), sensitivity to abrasion during handling (which frequently decreases its tensile strength), relatively low fatigue resistance, and high hardness (which causes excessive wear on molding dies and cutting tools). The two types of glass fibers commonly used in the fiber-reinforced plastics (FRP) industry are E-glass and S-glass. Another type, known as C-glass, is used in chemical applications requiring greater corrosion resistance to acids than is provided by E-glass. E-glass has the lowest cost of all commercially available reinforcing fibers, which is the

reason for its widespread use in the FRP industry. S-glass, originally developed for aircraft components and missile casings, has the highest tensile strength among all fibers in use. However, the compositional difference and higher manufacturing cost make it more expensive than E-glass. A lower cost version of S-glass, called S-2-glass, is also available. Although S-2-glass is manufactured with less-stringent nonmilitary specifications, its tensile strength and modulus are similar to those of S-glass (Mallick, 2007).

The properties of fibers depend on how the fibers are manufactured. The raw materials used for making E-glass fibers are silica sand, limestone, fluorspar, boric acid, and clay. Silica accounts for more than 50% of the total ingredients. By varying the amounts of raw materials and the processing parameters, other glass types are produced. The raw materials are mixed thoroughly and melted in a furnace at 2,500 to 3,000°F. The melt flows into one or more bushings containing hundreds of small orifices. The glass filaments are formed as the molten glass passes through these orifices and successively goes through a quench area where water and/or air quickly cool the filaments below the glass transition temperature. The filaments are then pulled over a roller at a speed around 50 miles per hour. The roller coats them with sizing. The amount of sizing used ranges from 0.25 to 6% of the original fiber weight. All the filaments are then pulled into a single strand and wound onto a tube. Sizing is applied to the filaments to serve several purposes; it promotes easy fiber wetting and processing, provides better resin and fiber bonding, and protects fibers from breakage during handling and processing. The sizing formulation depends on the type of application; for example, sizing used for epoxy would be different than that used for polyester (Mazumdar, 2001).

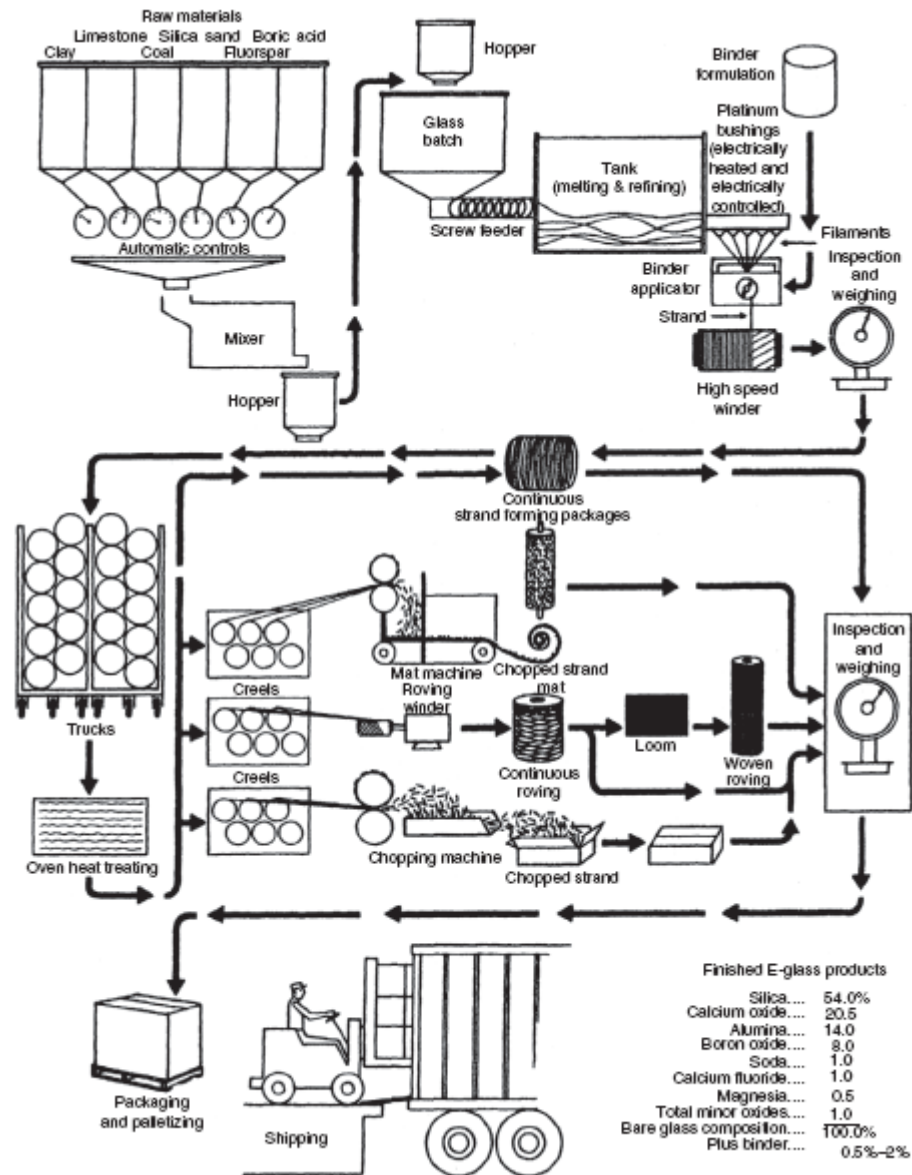


Figure 2.4 Flow diagram in glass fiber manufacturing (Mallick, 2007)

2.2.1.3 Aramid Fibers and Manufacturing

Aramid fibers are highly crystalline aromatic polyamide fibers that have the lowest density and the highest tensile strength-to-weight ratio among the current reinforcing fibers. Kevlar 49 is the trade name of one of the aramid fibers available in the market. As a reinforcement, aramid fibers are used in many marine and aerospace applications where lightweight, high tensile strength, and resistance to impact damage (e.g., caused by accidentally dropping a hand tool) are important. Like carbon fibers, they also have a negative coefficient of thermal expansion in the

longitudinal direction, which is used in designing low thermal expansion composite panels. The major disadvantages of aramid fiber-reinforced composites are their low compressive strengths and difficulty in cutting or machining. The molecular structure of aramid fibers is illustrated in Figure 2.5. The repeating unit in its molecules contains an amide ($-NH-$) group, which is also found in nylons and an aromatic ring represented by a hexagon. The aromatic ring gives it a higher chain stiffness (modulus) as well as better chemical and thermal stability over other commercial organic fibers, such as nylons (Mallick, 2007).

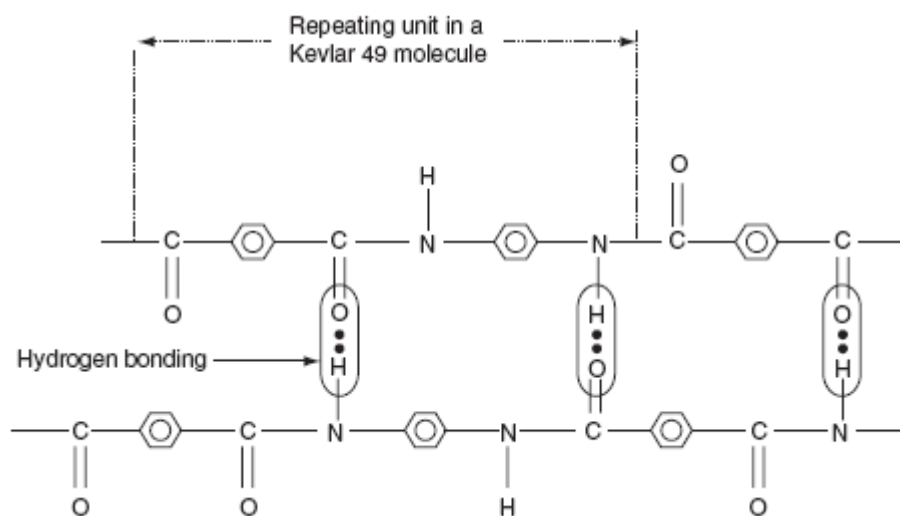


Figure 2.5 Molecular structure of Kevlar 49 fiber (Mallick, 2007)

Kevlar 49 filaments are manufactured by extruding an acidic solution of a proprietary precursor (a polycondensation product of terephthaloyl chloride and p-phenylene diamine) from a spinneret. During the filament drawing process, Kevlar 49 molecules become highly oriented in the direction of the filament axis. Weak hydrogen bonds between hydrogen and oxygen atoms in adjacent molecules hold them together in the transverse direction. The resulting filament is highly anisotropic, with much better physical and mechanical properties in the longitudinal direction than in the radial direction. Although the tensile stress–strain behavior of Kevlar 49 is linear, fiber fracture is usually preceded by longitudinal fragmentation, splintering, and even localized drawing. In bending, Kevlar 49 fibers exhibit a high degree of yielding on the compression side. Such a noncatastrophic failure mode is not

observed in glass or carbon fibers, and gives Kevlar 49 composites superior damage tolerance against impact or other dynamic loading. One interesting application of this characteristic of Kevlar 49 fibers is found in soft lightweight body armors and helmets used for protecting police officers and military personnel. A second-generation Kevlar fiber is Kevlar 149, which has the highest tensile modulus of all commercially available aramid fibers. The tensile modulus of Kevlar 149 is 40% higher than that of Kevlar 49; however, its strain-to-failure is lower. Kevlar 149 has the equilibrium moisture content of 1.2% at 65% relative humidity and 228C, which is nearly 70% lower than that of Kevlar 49 under similar conditions. Kevlar 149 also has a lower creep rate than Kevlar 49 (Mallick, 2007).

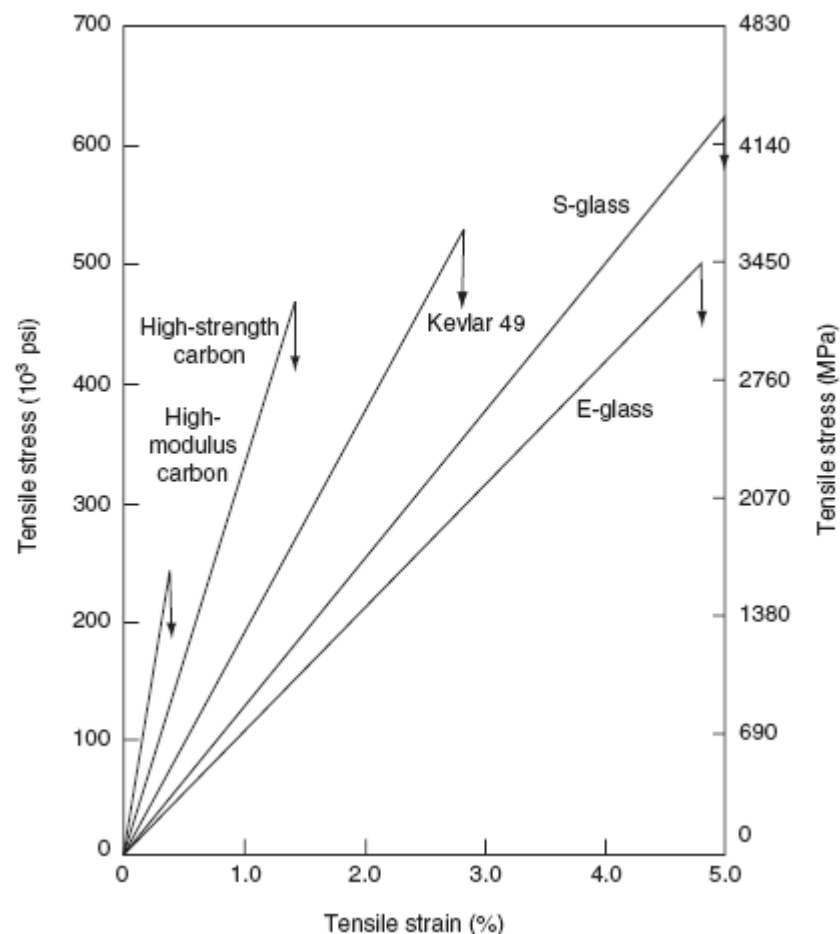


Figure 2.6 Tensile stress strain diagrams for various reinforcing fibers (Mallick, 2007)

2.2.1.4 Extended Chain Polyethylene Fibers and Manufacturing

High performance polyethylene fibers, with outstanding strength-to-weight and stiffness-to-weight performance, show promise in various specialized applications. While such fibers are not as widely known as aramid and carbon fibers, they possess many superior properties but they also have limitations that must be considered in design. (...) The process which is used to produce most commercial high strength, high modulus polyethylene fibers is called gel spinning, the name derived from the gel-like appearance of the as-spun and quenched fibers. Ultra-high molecular weight linear polyethylene is dissolved in a volatile solvent to form a dilute isotropic solution that is then spun through a spinneret and quenched in cold water to form a gel precursor fiber. Following solvent extraction, this fiber is then hot-drawn to a very high draw ratio (= 30), yielding a very highly oriented, highly crystalline, lightweight fiber (Peters, 1998).

Extended chain polyethylene fibers, commercially available under the trade name Spectra, are produced by gel spinning a high-molecular-weight polyethylene. Gel spinning yields a highly oriented fibrous structure with exceptionally high crystallinity (95%–99%) relative to melt spinning used for conventional polyethylene fibers. Spectra polyethylene fibers have the highest strength-to-weight ratio of all commercial fibers available to date. Two other outstanding features of Spectra fibers are their low moisture absorption (1% compared with 5%–6% for Kevlar 49) and high abrasion resistance, which make them very useful in marine composites, such as boat hulls and water skis. The melting point of Spectra fibers is 147 C; however, since they exhibit a high level of creep above 100 C, their application temperature is limited to 80 C–90 C. The safe manufacturing temperature for composites containing Spectra fibers is below 125 C, since they exhibit a significant and rapid reduction in strength as well as increase in thermal shrinkage above this temperature. Another problem with Spectra fibers is their poor adhesion with resin matrices, which can be partially improved by their surface modification with gas plasma treatment. Spectra fibers provide high impact resistance for composite laminates even at low temperatures and are finding growing applications in ballistic composites, such as

armors, helmets, and so on. However, their use in high-performance aerospace composites is limited, unless they are used in conjunction with stiffer carbon fibers to produce hybrid laminates with improved impact damage tolerance than all-carbon fiber laminates (Mallick, 2007).

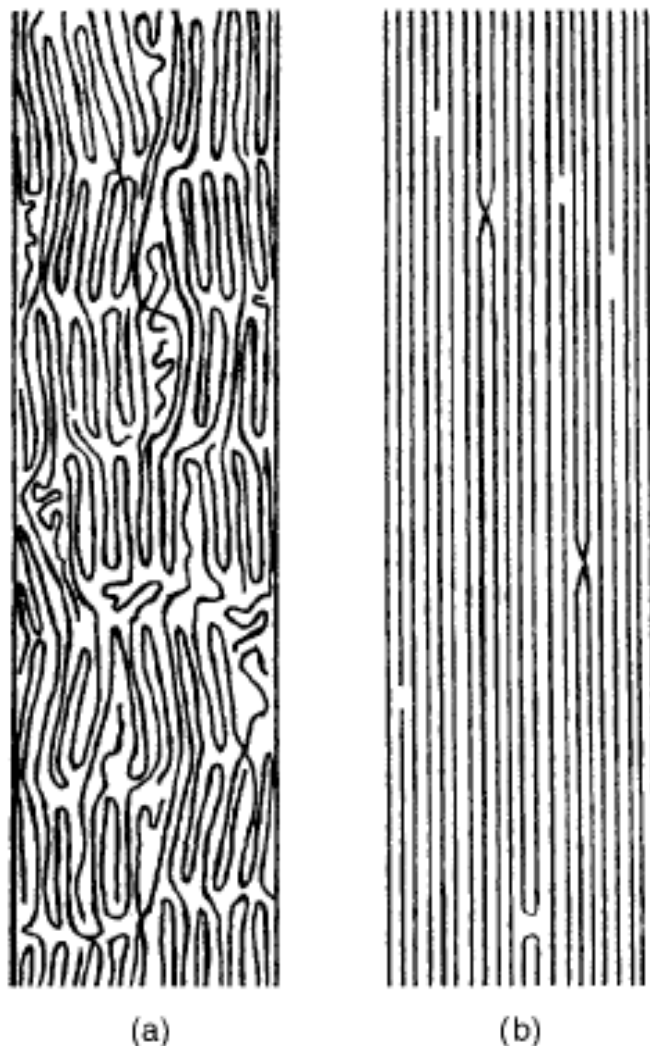


Figure 2.7 Schematic illustrating the difference between (a) conventional polyethylene fibers and (b) gel-spun extended chain fibers (Peters, 1998)

2.2.1.5 Boron Fibers and Manufacturing

The most prominent feature of boron fibers is their extremely high tensile modulus, which is in the range of 379–414 GPa (55–603106 psi). Coupled with their relatively large diameter, boron fibers offer excellent resistance to buckling, which in

turn contributes to high compressive strength for boron fiber-reinforced composites. The principal disadvantage of boron fibers is their high cost, which is even higher than that of many forms of carbon fibers. For this reason, its use is at present restricted to a few aerospace applications. Boron fibers are manufactured by chemical vapor deposition (CVD) of boron onto a heated substrate (either a tungsten wire or a carbon monofilament). Boron vapor is produced by the reaction of boron chloride with hydrogen: $2\text{BCL}_3 + 3\text{H}_2 = 2\text{B} + 6\text{HCL}$

The most common substrate used in the production of boron fibers is tungsten wire, typically 0.0127 mm (0.0005 in.) in diameter. It is continuously pulled through a reaction chamber in which boron is deposited on its surface at 11008C–13008C. The speed of pulling and the deposition temperature can be varied to control the resulting fiber diameter. Currently, commercial boron fibers are produced in diameters of 0.1, 0.142, and 0.203 mm (0.004, 0.0056, and 0.008 in.), which are much larger than those of other reinforcing fibers (Mallick, 2007).

2.2.2 Functions of Matrix

A matrix material fulfills several functions in a composite structure, most of which are vital to the satisfactory performance of the structure. Fibers in and of themselves are of little use without the presence of a matrix material or binder. The important functions of a matrix material include the following:

- The matrix material binds the fibers together and transfers the load to the fibers. It provides rigidity and shape to the structure.
- The matrix isolates the fibers so that individual fibers can act separately. This stops or slows the propagation of a crack.
- The matrix provides a good surface finish quality and aids in the production of net-shape or near-net-shape parts.
- The matrix provides protection to reinforcing fibers against chemical attack and mechanical damage (wear).

- Depending on the matrix material selected, performance characteristics such as ductility, impact strength, etc. are also influenced. A ductile matrix will increase the toughness of the structure. For higher toughness requirements, thermoplastic-based composites are selected.
- The failure mode is strongly affected by the type of matrix material used in the composite as well as its compatibility with the fiber (Mazumdar, 2001).

Table 2.1 Matrix materials (Mallick, 2007)

<i>Polymeric</i>
Thermoset polymers
Epoxyes: principally used in aerospace and aircraft applications
Polyesters, vinyl esters: commonly used in automotive, marine, chemical, and electrical applications
Phenolics: used in bulk molding compounds
Polyimides, polybenzimidazoles (PBI), polyphenylquinoxaline (PPQ): for high-temperature aerospace applications (temperature range: 250°C–400°C)
Cyanate ester
Thermoplastic polymers
Nylons (such as nylon 6, nylon 6,6), thermoplastic polyesters (such as PET, PBT), polycarbonate (PC), polyacetals: used with discontinuous fibers in injection-molded articles
Polyamide-imide (PAI), polyether ether ketone (PEEK), polysulfone (PSUL), polyphenylene sulfide (PPS), polyetherimide (PEI): suitable for moderately high temperature applications with continuous fibers
<i>Metallic</i>
Aluminum and its alloys, titanium alloys, magnesium alloys, copper-based alloys, nickel-based superalloys, stainless steel: suitable for high-temperature applications (temperature range: 300°C–500°C)
<i>Ceramic</i>
Aluminum oxide (Al ₂ O ₃), carbon, silicon carbide (SiC), silicon nitride (Si ₃ N ₄): suitable for high-temperature applications

2.2.2.1 Thermoset Resins

Thermoset materials once cured cannot be remelted or reformed. During curing, they form three-dimensional molecular chains, called cross-linking, as shown in Figure 2.8. Due to these cross-linkings, the molecules are not flexible and cannot be remelted and reshaped. The higher the number of cross-linkings, the more rigid and thermally stable the material will be. In rubbers and other elastomers, the densities of cross-links are much less and therefore they are flexible. Thermosets may soften to some extent at elevated temperatures. This characteristic is sometimes used to create

a bend or curve in tubular structures, such as filament-wound tubes. Thermosets are brittle in nature and are generally used with some form of filler and reinforcement. Thermoset resins provide easy processability and better fiber impregnation because the liquid resin is used at room temperature for various processes such as filament winding, pultrusion, and RTM. Thermosets offer greater thermal and dimensional stability, better rigidity, and higher electrical, chemical, and solvent resistance. The most common resin materials used in thermoset composites are epoxy, polyester, vinylester, phenolics, cyanate esters, bismaleimides, and polyimides. Some of the basic properties of selected thermoset resins are shown in Table 2.2 (Mazumdar, 2001).

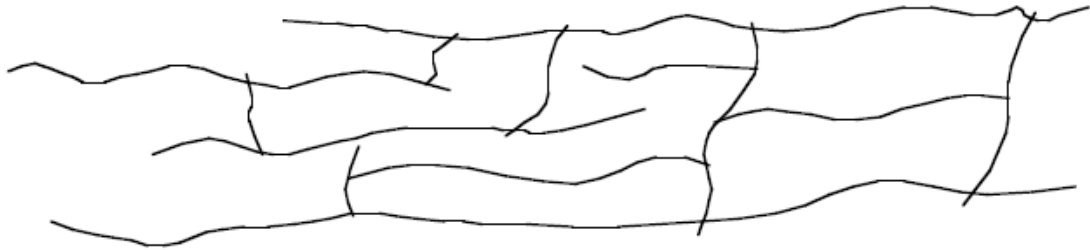


Figure 2.8 Cross-linking of thermoset molecules during curing (Mazumdar, 2001)

Table 2.2 Typical unfilled thermosetting resin properties (Mazumdar, 2001)

Resin Material	Density (g/cm ³)	Tensile Modulus GPa (10 ⁶ psi)	Tensile Strength MPa (10 ³ psi)
Epoxy	1.2–1.4	2.5–5.0 (0.36–0.72)	50–110 (7.2–16)
Phenolic	1.2–1.4	2.7–4.1 (0.4–0.6)	35–60 (5–9)
Polyester	1.1–1.4	1.6–4.1 (0.23–0.6)	35–95 (5.0–13.8)

2.2.2.1.1 Epoxies. Epoxy is a very versatile resin system, allowing for a broad range of properties and processing capabilities. It exhibits low shrinkage as well as excellent adhesion to a variety of substrate materials. Epoxies are the most widely used resin materials and are used in many applications, from aerospace to sporting goods. There are varying grades of epoxies with varying levels of performance to meet different application needs. They can be formulated with other materials or can be mixed with other epoxies to meet a specific performance need. By changing the formulation, properties of epoxies can be changed; the cure rate can be modified, the

processing temperature requirement can be changed, the cycle time can be changed, the drupe and tack can be varied, the toughness can be changed, the temperature resistance can be improved, etc. Epoxies are cured by chemical reaction with amines, anhydrides, phenols, carboxylic acids, and alcohols. An epoxy is a liquid resin containing several epoxide groups, such as diglycidyl ether of bisphenol A (DGEBA), which has two epoxide groups. In an epoxide group, there is a three-membered ring of two carbon atoms and one oxygen atom. In addition to this starting material, other liquids such as diluents to reduce its viscosity and flexibilizers to increase toughness are mixed. The curing (crosslinking) reaction takes place by adding a hardener or curing agent (e.g. diethylenetriamine [DETA]). During curing, DGEBA molecules form crosslinks with each other as shown in Figure 2.8. These cross-links grow in a three-dimensional network and finally form a solid epoxy resin. Cure rates can be controlled through proper selection of hardeners and/or catalysts. Each hardener provides different cure characteristics and different properties to the final product. The higher the cure rate, the lower the process cycle time and thus higher production volume rates. Epoxy-based composites provide good performance at room and elevated temperatures. Epoxies can operate well up to temperatures of 200 to 250°F, and there are epoxies that can perform well up to 400°F. For high-temperature and high-performance epoxies, the cost increases, but they offer good chemical and corrosion resistance. Epoxies come in liquid, solid, and semi-solid forms. Liquid epoxies are used in RTM, filament winding, pultrusion, hand lay-up, and other processes with various reinforcing fibers such as glass, carbon, aramid, boron, etc. Semi-solid epoxies are used in prepreg for vacuum bagging and autoclave processes. Solid epoxy capsules are used for bonding purposes. Epoxies are more costly than polyester and vinylesters and are therefore not used in cost-sensitive markets (e.g., automotive and marine) unless specific performance is needed. Epoxies are generally brittle, but to meet various application needs, toughened epoxies have been developed that combine the excellent thermal properties of a thermoset with the toughness of a thermoplastic. Toughened epoxies are made by adding thermoplastics to the epoxy resin by various patented processes (Mazumdar, 2001).

2.2.2.1.2 Phenolics. Phenolics meet FAA (and JAR) requirements for low smoke and toxicity. They are used for aircraft interiors, stowbins, and galley walls, as well as other commercial markets that require low-cost, flame-resistant, and low-smoke products. Phenolics are formed by the reaction of phenol (carbolic acid) and formaldehyde, and catalyzed by an acid or base. Urea, resorcinol, or melamine can be used instead of phenol to obtain different properties. Their cure characteristics are different than other thermosetting resins such as epoxies, due to the fact that water is generated during cure reaction. The water is removed during processing. In the compression molding process, water can be removed by bumping the press. Phenolics are generally dark in color and therefore used for applications in which color does not matter. The phenolic products are usually red, blue, brown, or black in color. To obtain light-colored products, urea formaldehyde and melamine formaldehyde are used. Other than flame-resistant parts, phenolic products have demonstrated their capabilities in various other applications where:

- High temperature resistance is required.
- Electrical properties are needed.
- Wear resistance is important.
- Good chemical resistance and dimensional stability are essential.

Phenolics are used for various composite manufacturing processes such as filament winding, RTM, injection molding, and compression molding. Phenolics provide easy processability, tight tolerances, reduced machining, and high strength. Because of their high temperature resistance, phenolics are used in exhaust components, missile parts, manifold spacers, commutators, and disc brakes (Mazumdar, 2001).

2.2.2.1.3 Polyesters. Polyesters are low-cost resin systems and offer excellent corrosion resistance. The operating service temperatures for polyesters are lower than for epoxies. Polyesters are widely used for pultrusion, filament winding, SMC, and RTM operations. Polyesters can be a thermosetting resin or a thermoplastic resin. Unsaturated polyesters are obtained by the reaction of unsaturated difunctional organic acids with a difunctional alcohol. The acids used include maleic, fumaric, phthalic, and terephthalic. The alcohols include ethylene glycol, propylene glycol, and halogenated glycol. For the curing or crosslinking process, a reactive monomer

such as styrene is added in the 30 to 50 wt% range. The carbon-carbon double bonds in unsaturated polyester molecules and styrene molecules function as the cross-linking site. With the growing health concerns over styrene emissions, the use of styrene is being reduced for polyester-based composite productions. In recent methods, catalysts are used for curing polyesters with reduced styrene (Mazumdar, 2001).

2.2.2.1.4 Vinylesters. Vinylesters are widely used for pultrusion, filament winding, SMC, and RTM processes. They offer good chemical and corrosion resistance and are used for FRP pipes and tanks in the chemical industry. They are cheaper than epoxies and are used in the automotive and other high-volume applications where cost is critical in making material selection. Vinylesters are formed by the chemical reaction of an unsaturated organic acid with an epoxide-terminated molecule. In vinylester molecules, there are fewer unsaturated sites for cross-linking than in polyesters or epoxies and, therefore, a cured vinylester provides increased ductility and toughness (Mazumdar, 2001).

2.2.2.1.5 Cyanate esters. Cyanate esters offer excellent strength and toughness, better electrical properties, and lower moisture absorption compared to other resins. If they are formulated correctly, their high-temperature properties are similar to bismaleimide and polyimide resins. They are used for a variety of applications, including spacecrafts, aircrafts, missiles, antennae, radomes, microelectronics, and microwave products. Cyanate esters are formed via the reaction of bisphenol esters and cyanic acid that cyclotrimerize to produce triazine rings during a second cure. Cyanate esters are more easily cured than epoxies. The toughness of cyanate esters can be increased by adding thermoplastics or spherical rubber particles (Mazumdar, 2001).

2.2.2.1.6 Bismaleimide (BMI) and Polyimide. BMI and polyimide are used for high-temperature applications in aircrafts, missiles, and circuit boards. The glass transition temperature (T_g) of BMIs is in the range of 550 to 600°F, whereas some polyimides offer T_g greater than 700°F. These values are much higher than for

epoxies and polyesters. The lack of use of BMIs and polyimides is attributed to their processing difficulty. They emit volatiles and moisture during imidization and curing. Therefore, proper venting is necessary during the curing of these resins; otherwise, it may cause process-related defects such as voids and delaminations. Other drawbacks of these resins include the fact that their toughness values are lower than epoxies and cyanate esters, and they have a higher moisture absorption ability (Mazumdar, 2001).

2.2.2.1.7 Polyurethane. Polyurethane is widely used for structural reaction injection molding (SRIM) processes and reinforced reaction injection molding (RRIM) processes, in which isocyanate and polyol are generally mixed in a ratio of 1:1 in a reaction chamber and then rapidly injected into a closed mold containing short or long fiber reinforcements. RRIM and SRIM processes are low-cost and high-volume production methods. The automotive industry is a big market for these processes. Polyurethane is currently used for automotive applications such as bumper beams, hoods, body panels, etc. Unfilled polyurethane is used for various applications, including truck wheels, seat and furniture cushions, mattress foam, etc. Polyurethane is also used for wear and impact resistance coatings. Polyurethane can be a thermosetting or thermoplastic resin, depending on the functionality of the selected polyols. Thermoplastic-based polyurethane contains linear molecules, whereas thermoset-based resin contains crosslinked molecules. Polyurethane is obtained by the reaction between polyisocyanate and a polyhydroxyl group. There are a variety of polyurethanes available by selecting various types of polyisocyanate and polyhydroxyl ingredients. Polyurethane offers excellent wear, tear, and chemical resistance, good toughness, and high resilience (Mazumdar, 2001).

2.2.2.2 Thermoplastic Resins

Thermoplastic materials are, in general, ductile and tougher than thermoset materials and are used for a wide variety of nonstructural applications without fillers and reinforcements. Thermoplastics can be melted by heating and solidified by cooling, which render them capable of repeated reshaping and reforming.

Thermoplastic molecules do not cross-link and therefore they are flexible and reformable. Thermoplastics can be either amorphous or semicrystalline, as shown in Figure 2.9. In amorphous thermoplastics, molecules are randomly arranged; whereas in the crystalline region of semi-crystalline plastics, molecules are arranged in an orderly fashion. It is not possible to have 100% crystallinity in plastics because of the complex nature of the molecules. Some of the properties of themoplastics are given in Table 2.3. Their lower stiffness and strength values require the use of fillers and reinforcements for structural applications. Thermoplastics generally exhibit poor creep resistance, especially at elevated temperatures, as compared to thermosets. They are more susceptible to solvents than thermosets. Thermoplastic resins can be welded together, making repair and joining of parts more simple than for thermosets. Repair of thermoset composites is a complicated process, requiring adhesives and careful surface preparation. Thermoplastic composites typically require higher forming temperatures and pressures than comparable thermoset systems. Thermoplastic composites do not enjoy as high a level of integration as is currently obtained with thermosetting systems. The higher viscosity of thermoplastic resins makes some manufacturing processes, such as hand lay-up and tape winding operations, more difficult. As a consequence of this, the fabrication of thermoplastic composite parts has drawn a lot of attention from researchers to overcome these problems (Mazumdar, 2001).

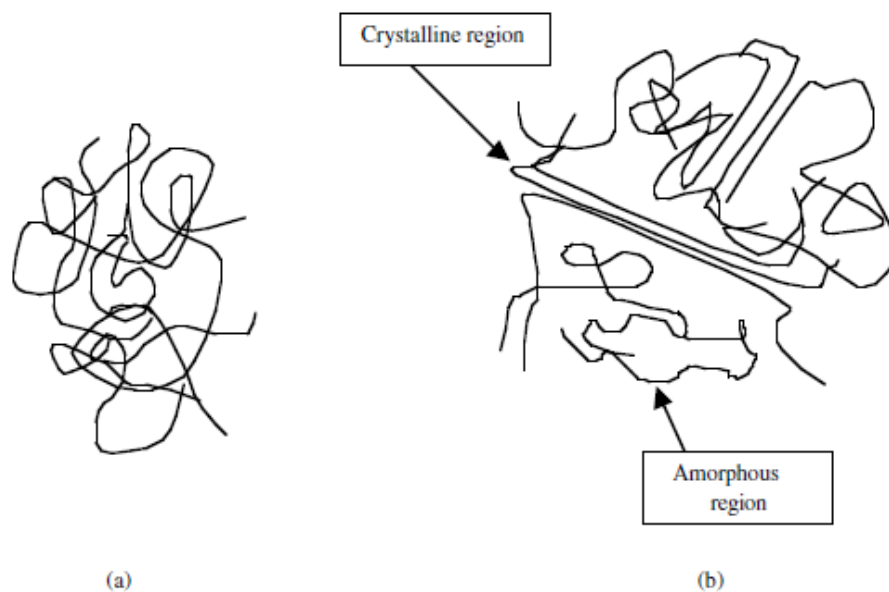


Figure 2.9 Molecular arrangements in (a) amorphous and (b) semi-crystalline polymers (Mazumdar, 2001)

Table 2.3 Typical Unfilled Thermoplastic Resin Properties (Mazumdar, 2001)

Resin Material	Density (g/cm ³)	Tensile Modulus GPa (10 ⁶ psi)	Tensile Strength MPa (10 ³ psi)
Nylon	1.1	1.3–3.5 (0.2–0.5)	55–90 (8–13)
PEEK	1.3–1.35	3.5–4.4 (0.5–0.6)	100 (14.5)
PPS	1.3–1.4	3.4 (0.49)	80 (11.6)
Polyester	1.3–1.4	2.1–2.8 (0.3–0.4)	55–60 (8–8.7)
Polycarbonate	1.2	2.1–3.5 (0.3–0.5)	55–70 (8–10)
Acetal	1.4	3.5 (0.5)	70 (10)
Polyethylene	0.9–1.0	0.7–1.4 (0.1–0.2)	20–35 (2.9–5)
Teflon	2.1–2.3	—	10–35 (1.5–5.0)

2.2.2.2.1 *Nylons*. Nylons are used for making intake manifolds, housings, gears, bearings, bushings, sprockets, etc. Glass-filled and carbon-filled nylons in pellet form are available for injection molding purposes. Nylons are most widely used for injection molding purposes, but are also available as prepregs with various reinforcements. Nylons have been used for various pultruded components. Nylons are also called polyamides. There are several types of nylon, including nylon 6, nylon 66, nylon 11, etc., each offering a variety of mechanical and physical properties; but as a whole, they are considered engineering plastics. Nylons provide a good surface appearance and good lubricity. The important design consideration with nylons is that they absorb moisture, which affects the properties and dimensional stability of the part. Glass reinforcement minimizes this problem and produces a strong, impact-resistant material. Impact resistance of long glass-filled nylon is higher than conventional engineering materials such as aluminum and magnesium (Mazumdar, 2001).

2.2.2.2.2 *Polypropylene (PP)*. Polypropylene (PP) is a low-cost, low-density, versatile plastic and is available in many grades and as a co-polymer (ethylene/propylene). It has the lowest density (0.9 g/cm³) of all thermoplastics and offers good strength, stiffness, chemical resistance, and fatigue resistance. PP is used for machine parts, car components (fans, fascia panels, etc.), and other household items, and has also been pultruded with various reinforcements (Mazumdar, 2001).

2.2.2.2.3 Polyetheretherketone (PEEK). PEEK is a new-generation thermoplastic that offers the possibility of use at high service temperatures. Carbon-reinforced PEEK composites (APC-2) have already demonstrated their usefulness in fuselage, satellite parts, and other aerospace structures; they can be used continuously at 250°C. The glass transition temperature (T_g) of PEEK is 143°C and crystalline melting temperature is ~336°C. PEEK/carbon thermoplastic composites (APC-2, aromatic polymer composites) have generated significant interest among researchers and in the aircraft industry because of their greater damage tolerance, better solvent resistance, and high-temperature usage. As well, PEEK has the advantage of almost 10 times lower water absorption than epoxies. The water absorption of PEEK is 0.5% at room temperature, whereas aerospace-grade epoxies have 4 to 5% water absorption. The drawback of PEEK-based composites is that the materials cost is very high, more than \$50.00/lb. PEEK/carbon is processed in the range of 380 to 400°C for autoclave, hot press, and diaphragm molding processes whereas for tape winding operation, more than 500°C is suggested for better interply consolidation. It is a semi-crystalline material with a maximum crystallinity of 48%. In general, the crystallinity of PEEK is 30 to 35%. The toughness offered by PEEK is 50 to 100 times higher than that of epoxies (Mazumdar, 2001).

2.2.2.2.4 Polyphenylene Sulfide (PPS). PPS is an engineering thermoplastic with a maximum crystallinity of 65%. It provides high operating temperatures and can be used continuously at 225°C. The T_g of PPS is 85°C and crystalline melt temperature is 285°C. Prepreg tape of PPS with several reinforcements is available. The trade names of PPS-based prepreg systems are Ryton and Techtron. It is processed in the temperature range of 300 to 345°C. PPS-based composites are used for applications where great strength and chemical resistance are required at elevated temperature (Mazumdar, 2001).

2.2.2.3 Metal Matrix

Metal matrix has the advantage over polymeric matrix in applications requiring a long-term resistance to severe environments, such as high temperature. The yield

strength and modulus of most metals are higher than those for polymers, and this is an important consideration for applications requiring high transverse strength and modulus as well as compressive strength for the composite. Another advantage of using metals is that they can be plastically deformed and strengthened by a variety of thermal and mechanical treatments. However, metals have a number of disadvantages, namely, they have high densities, high melting points (therefore, high process temperatures), and a tendency toward corrosion at the fiber–matrix interface. The two most commonly used metal matrices are based on aluminum and titanium. Both of these metals have comparatively low densities and are available in a variety of alloy forms. Although magnesium is even lighter, its great affinity toward oxygen promotes atmospheric corrosion and makes it less suitable for many applications. Beryllium is the lightest of all structural metals and has a tensile modulus higher than that of steel. However, it suffers from extreme brittleness, which is the reason for its exclusion as a potential matrix material. Nickel- and cobalt-based superalloys have also been used as matrix; however, the alloying elements in these materials tend to accentuate the oxidation of fibers at elevated temperatures. Aluminum and its alloys have attracted the most attention as matrix material in metal matrix composites. Commercially, pure aluminum has been used for its good corrosion resistance. Aluminum alloys, such as 201, 6061, and 1100, have been used for their higher tensile strength–weight ratios. Carbon fiber is used with aluminum alloys; however, at typical fabrication temperatures of 500°C or higher, carbon reacts with aluminum to form aluminum carbide (Al_4C_3), which severely degrades the mechanical properties of the composite. Protective coatings of either titanium boride (TiB_2) or sodium has been used on carbon fibers to reduce the problem of fiber degradation as well as to improve their wetting with the aluminum alloy matrix. Carbon fiber-reinforced aluminum composites are inherently prone to galvanic corrosion, in which carbon fibers act as a cathode owing to a corrosion potential of 1 V higher than that of aluminum. A more common reinforcement for aluminum alloys is SiC. Titanium alloys that are most useful in metal matrix composites are α , β alloys (e.g., Ti-6Al-9V) and metastable β -alloys (e.g., Ti-10V-2Fe-3Al). These titanium alloys have higher tensile strength–weight ratios as well as better strength retentions at 400°C–500°C over those of aluminum alloys. The thermal expansion coefficient of titanium

alloys is closer to that of reinforcing fibers, which reduces the thermal mismatch between them. One of the problems with titanium alloys is their high reactivity with boron and Al₂O₃ fibers at normal fabrication temperatures. Borsic (boron fibers coated with silicon carbide) and silicon carbide (SiC) fibers show less reactivity with titanium. Improved tensile strength retention is obtained by coating boron and SiC fibers with carbon-rich layers (Mallick, 2007).

2.2.2.4 Ceramic Matrix

Ceramics are known for their high temperature stability, high thermal shock resistance, high modulus, high hardness, high corrosion resistance, and low density. However, they are brittle materials and possess low resistance to crack propagation, which is manifested in their low fracture toughness. The primary reason for reinforcing a ceramic matrix is to increase its fracture toughness. Structural ceramics used as matrix materials can be categorized as either oxides or nonoxides. Alumina (Al₂O₃) and mullite (Al₂O₃-SiO₂) are the two most commonly used oxide ceramics. They are known for their thermal and chemical stability. The common nonoxide ceramics are silicon carbide (SiC), silicon nitride (Si₃N₄), boron carbide (B₄C), and aluminum nitride (AlN). Of these, SiC has found wider applications, particularly where high modulus is desired. It also has an excellent high temperature resistance. Si₃N₄ is considered for applications requiring high strength and AlN is of interest because of its high thermal conductivity. The reinforcements used in ceramic matrix composites are SiC, Si₃N₄, AlN, and other ceramic fibers. Of these, SiC has been the most commonly used reinforcement because of its thermal stability and compatibility with a broad range of both oxide and nonoxide ceramic matrices. The forms in which the reinforcement is used in ceramic matrix composites include whiskers (with length to diameter ratio as high as 500), platelets, particulates, and both monofilament and multifilament continuous fibers (Mallick, 2007).

CHAPTER THREE

MECHANICALLY FASTENED JOINTS

3.1 Introduction

The purpose of a joint is to transfer loads from one member to another in a structure. The design of joints has a special significance in fiber-reinforced composite structures for two reasons: (1) the joints are often the weakest areas in a composite structure and (2) the composite materials do not possess the forgiving characteristics of ductile metals, namely, their capacity to redistribute local high stresses by yielding. For composite laminates, the basic joints are either mechanical or bonded. Mechanical joints are created by fastening the substrates with bolts or rivets; bonded joints use an adhesive interlayer between the substrates (commonly called the adherends) (Mallick, 2007).

Intuitively, it may be concluded that mechanical fastening is an unsatisfactory means on joining composites because the fastener holes must cut fibers, destroying part of the load path. However, although considerable loss in strength occurs (typically to half of the original strength), acceptable joint can be made. Indeed, mechanically fastening is usually the only feasible or economic means of joining highly loaded (thick) composite components (Baker, Dutton and Kelly, 2004).

The advantages and disadvantages of mechanical joints:

1. Permit quick and repeated disassembly for repairs or replacements without destroying the substrates
2. Require little or no surface preparation
3. Are easy to inspect for joint quality
4. Require machining of holes that interrupt the fiber continuity and may reduce the strength of the substrate laminates
5. Create highly localized stress concentrations around the joints that may induce failure in the substrates

6. Add weight to the structure
7. May create a potential corrosion problem, for example, in an aluminum fastener if used for joining carbon fiber–epoxy laminates (Mallick, 2007).

3.2 General Design Considerations

Although the aim of achieving smooth load transfer from one joint element to another is similar in bonding and mechanical fastening, the load transfer mechanisms are very different. In mechanical fastening, load transfer accomplished by compression (bearing) on the faces of holes passing through the joint members by shear (and, less desirably, bending) of the fasteners. Some of the load is also transferred through friction on the face of the joint element if the clamping forces imposed by the fasteners is sufficient. However, although high clamping forces (bolt-tightening torque T) are very important to develop high-friction forces to maximize bearing strength, it may not be possible to maintain these levels of clamping force during prolonged service, for example, due to wear under service loading conditions. Because high through-thickness reinforcement is provided by the fasteners, peel failure of the composite is generally not a problem. However, problems can arise resulting from the relatively low bearing and transverse strength of the composite compared with those of metals. Bearing failure result in hole elongation, allowing bending and subsequent fatigue of the bolt or substructure. Alternatively, the fastener head may pull through the composite (Baker, Dutton and Kelly, 2004).

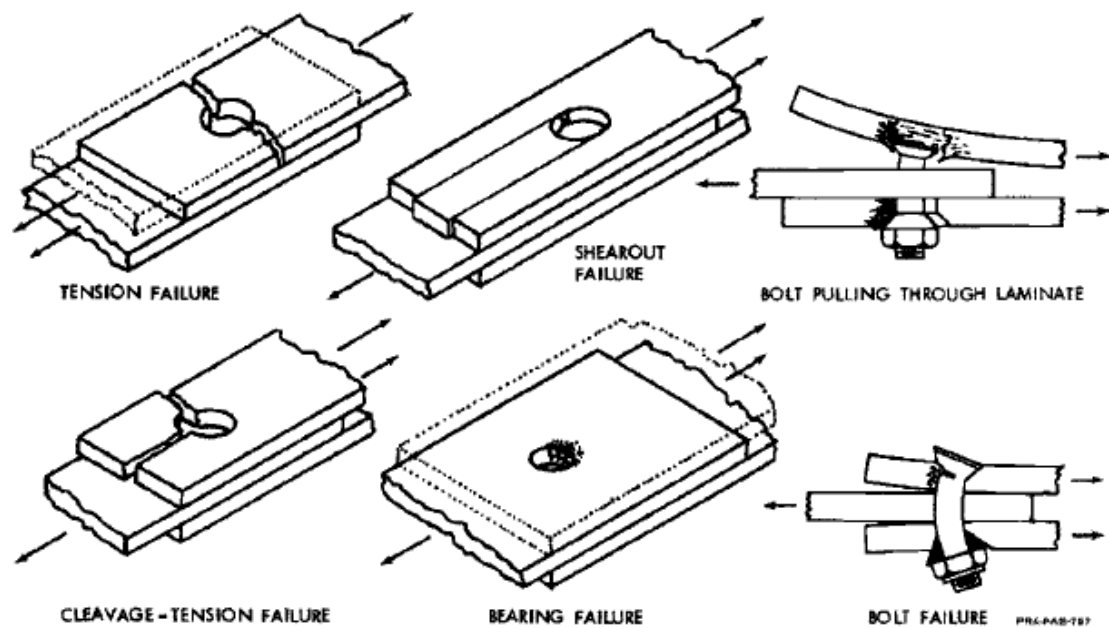


Figure 3.1 Schematic illustration of the main failure modes in mechanical joints

The allowable stresses in each of these modes is a function of :

- Geometry of the joint, including thickness
- Hole size, spacing, and bearing area, allowing for countersink
- Fastener loading, single or double shear; that is, loading symmetrical, as in a double-lap joint, or unsymmetrical, as in a single lap joint
- Fastener fit tolerance
- Clamping area and pressure, allowing for any countersink
- Fiber orientation and ply sequence
- Moisture content and service temperature
- Nature of stressing: tension, compression, shear; cyclic variation of stressing; any secondary bending, resulting in out-of-plane loading. Stresses due to thermal expansion mismatch in metal-to-composite joints may also have an effect, but these are rarely considered in mechanical joints (Baker, Dutton and Kelly, 2004).

It is clear that, in view of the very large number of variables involved, a complete characterization of joint behavior is impossible. Rather, the approach should be to determine as thoroughly as possible the behavior of basic joints and to hopefully

infer the influence of the more important parameters, from which the behavior of joints and materials can be predicted (Okutan, 2001).

In addition, to estimate the strength of single pin-loaded specimens, the static strengths are defined as (Okutan, 2001);

Net-tension Strength: The stress at net-tension section, at failure, is given by

$$(\sigma_t)_{ult} = \frac{P_{ult}}{(W-D).t} \quad (3.1)$$

where P_{ult} is the failing load of the member, W is the joint width at net-section, D is the hole diameter and t the joint thickness.

Bearing Strength: The bearing strength of a composite material is expressed in the form,

$$(\sigma_b)_{ult} = \frac{P_{ult}}{D.t} \quad (3.2)$$

Shearing Strength: The strength in this case is given as,

$$(\tau_s)_{ult} = \frac{P_{ult}}{2.E.t} \quad (3.3)$$

where E is the distance (parallel to the load) between the hole center and the free edge, usually known as the edge distance.

CHAPTER FOUR

STRESS ANALYSIS OF COMPOSITE MATERIALS

4.1 Introduction

The mechanics of materials deal with stresses, strains, and deformations in engineering structures subjected to mechanical and thermal loads. A common assumption in the mechanics of conventional materials, such as steels and aluminum, is that they are homogenous and isotropic continua. For a homogenous material, properties do not depend on the location, and for an isotropic material, properties do not depend on the orientation. Unless severely cold worked, grains in metallic materials are randomly oriented so that, on a statistical basis, the assumption of isotropy can be justified. Fiber-reinforced composites, on the other hand, are microscopically inhomogeneous and nonisotropic (orthotropic). As a result, the mechanics of fiber reinforced composites are far more complex than that of conventional materials. The mechanics of fiber-reinforced composite materials are studied two levels.

1. The micromechanics level, in which the interaction of the constituent materials is examined on a microscopic scale. Equations describing the elastic and thermal characteristics of a lamina are, in general, based on micromechanics formulations. An understanding of the interaction between various constituents is also useful in delineating the failure modes in a fiber-reinforced composite material.

2. The macromechanics level, in which the response of a fiber-reinforced composite material to mechanical and thermal loads is examined on a macroscopic scale. The material is assumed to be homogeneous. Equations of orthotropic elasticity are used to calculate stresses, strains, and deflections (Mallick, 1993).

4.2 Stress – Strain Relations For Anisotropic Materials

The generalized Hook's law relating stresses to strains can be written in contracted notation as (Jones, 1999),

$$\sigma_i = C_{ij} \varepsilon_j \quad i, j = 1, \dots, 6 \quad (4.1)$$

where σ_i are the stress components shown on a three-dimensional cube in x, y and z coordinates in Figure 4.1 (Jones, 1999), C_{ij} is the stiffness matrix, and ε_j are the strain components. The strains are defined as,

$$\begin{aligned} \varepsilon_1 &= \frac{\partial u}{\partial x} & \varepsilon_2 &= \frac{\partial v}{\partial y} & \varepsilon_3 &= \frac{\partial w}{\partial z} \\ \gamma_{23} &= \frac{\partial v}{\partial z} + \frac{\partial w}{\partial y} & \gamma_{31} &= \frac{\partial w}{\partial x} + \frac{\partial u}{\partial z} & \gamma_{12} &= \frac{\partial u}{\partial y} + \frac{\partial v}{\partial x} \end{aligned} \quad (4.2)$$

where u, v, and w are displacements in the x, y, and z directions (or the 1, 2, and 3 directions).

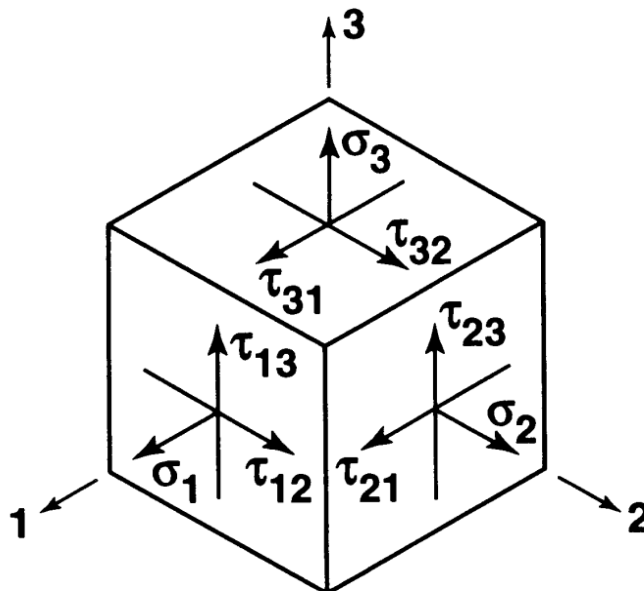


Figure 4.1 Stresses on an element (Jones, 1999)

The stiffness matrix has 36 constants in Equation 4.1. However, less than 36 of the constant can be shown to actually be independent for elastic materials when important characteristics of the strain energy are considered. Elastic materials for which an elastic potential or strain energy density function exists have incremental work per unit volume of

$$dW = \sigma_i d\varepsilon_i \quad (4.3)$$

when the stress σ_i act through strains $d\varepsilon_i$. However, because of the stress-strain relations, Equation (4.1), the incremental work becomes

$$dW = C_{ij} \varepsilon_j d\varepsilon_j \quad (4.4)$$

Upon integration for all strains, the work per unit of volume is

$$W = \frac{1}{2} C_{ij} \varepsilon_i \varepsilon_j \quad (4.5)$$

However, Hook's law, Equation (4.1), can be derived from Equation (4.5):

$$\frac{\partial W}{\partial \varepsilon_i} = C_{ij} \varepsilon_j \quad (4.6)$$

whereupon

$$\frac{\partial^2 W}{\partial \varepsilon_i \partial \varepsilon_j} = C_{ij} \quad (4.7)$$

Similarly,

$$\frac{\partial^2 W}{\partial \varepsilon_j \partial \varepsilon_i} = C_{ji} \quad (4.8)$$

But the order of differentiation of W is immaterial, so

$$C_{ij}=C_{ji} \quad (4.9)$$

Thus, the stiffness matrix is symmetric so only 21 of the constants are independent.

In similar manner, it can be show that

$$W=\frac{1}{2}S_{ij}\sigma_i\sigma_j \quad (4.10)$$

where S_{ij} is the compliance matrix defined by the inverse of the stress-strain relations, namely the strain-stress relations:

$$\varepsilon_i=S_{ij}\sigma_j \quad i, j=1, \dots, 6 \quad (4.11)$$

Reasoning similar to that in the preceding paragraph leads to

$$S_{ij}=S_{ji} \quad (4.12)$$

i.e., that the compliance matrix is symmetric hence, has only 21 independent constants. With the foregoing reduction from 36 to 21 independent constants, the stress-strain relations are

$$\begin{bmatrix} \sigma_1 \\ \sigma_2 \\ \sigma_3 \\ \tau_{23} \\ \tau_{31} \\ \tau_{12} \end{bmatrix} = \begin{bmatrix} C_{11} & C_{12} & C_{13} & C_{14} & C_{15} & C_{16} \\ C_{12} & C_{22} & C_{23} & C_{24} & C_{25} & C_{26} \\ C_{13} & C_{23} & C_{33} & C_{34} & C_{35} & C_{36} \\ C_{14} & C_{24} & C_{34} & C_{44} & C_{45} & C_{46} \\ C_{15} & C_{25} & C_{35} & C_{45} & C_{55} & C_{56} \\ C_{16} & C_{26} & C_{36} & C_{46} & C_{56} & C_{66} \end{bmatrix} \begin{bmatrix} \varepsilon_1 \\ \varepsilon_2 \\ \varepsilon_3 \\ \gamma_{23} \\ \gamma_{31} \\ \gamma_{12} \end{bmatrix} \quad (4.13)$$

as the most general expression within the framework of linear elasticity. Actually, the relations in Equation (4.13) are referred to as characterizing anisotropic materials because there are no planes of symmetry for the material properties. An alternative

name for such an anisotropic material is a triclinic material (three axes of the material are all oblique to one another).

If there are two orthogonal planes of material property symmetry for a material, symmetry will exist relative to a third mutually orthogonal plane. The stress-strain relations in coordinates aligned with principal material directions are

$$\begin{bmatrix} \sigma_1 \\ \sigma_2 \\ \sigma_3 \\ \tau_{23} \\ \tau_{31} \\ \tau_{12} \end{bmatrix} = \begin{bmatrix} C_{11} & C_{12} & C_{13} & 0 & 0 & 0 \\ C_{12} & C_{22} & C_{23} & 0 & 0 & 0 \\ C_{13} & C_{23} & C_{33} & 0 & 0 & 0 \\ 0 & 0 & 0 & C_{44} & 0 & 0 \\ 0 & 0 & 0 & 0 & C_{55} & 0 \\ 0 & 0 & 0 & 0 & 0 & C_{66} \end{bmatrix} \begin{bmatrix} \varepsilon_1 \\ \varepsilon_2 \\ \varepsilon_3 \\ \gamma_{23} \\ \gamma_{31} \\ \gamma_{12} \end{bmatrix} \quad (4.14)$$

and are said to define an orthotropic material. Note that there is no interaction between normal stresses $\sigma_1, \sigma_2, \sigma_3$ and shearing strains $\gamma_{23}, \gamma_{31}, \gamma_{12}$ such as occurs in anisotropic materials (by virtue of presence of, for example, C_{14}). Similarly, there is no interaction between shearing stresses and normal strains as well as none between shearing stresses and shearing strains in different planes. Note also that there are now only nine independent constants in the stiffness matrix.

The strain-stress relations for anisotropic and orthotropic material property symmetry cases are shown in Equation (4.15) and (4.16):

Anisotropic (21 independent constants):

$$\begin{bmatrix} \varepsilon_1 \\ \varepsilon_2 \\ \varepsilon_3 \\ \gamma_{23} \\ \gamma_{31} \\ \gamma_{12} \end{bmatrix} = \begin{bmatrix} S_{11} & S_{12} & S_{13} & S_{14} & S_{15} & S_{16} \\ S_{12} & S_{22} & S_{23} & S_{24} & S_{25} & S_{26} \\ S_{13} & S_{23} & S_{33} & S_{34} & S_{35} & S_{36} \\ S_{14} & S_{24} & S_{34} & S_{44} & S_{45} & S_{46} \\ S_{15} & S_{25} & S_{35} & S_{45} & S_{55} & S_{56} \\ S_{16} & S_{26} & S_{36} & S_{46} & S_{56} & S_{66} \end{bmatrix} \begin{bmatrix} \sigma_1 \\ \sigma_2 \\ \sigma_3 \\ \tau_{23} \\ \tau_{31} \\ \tau_{12} \end{bmatrix} \quad (4.15)$$

Orthotropic (9 independent constants):

$$\begin{bmatrix} \varepsilon_1 \\ \varepsilon_2 \\ \varepsilon_3 \\ \gamma_{23} \\ \gamma_{31} \\ \gamma_{12} \end{bmatrix} = \begin{bmatrix} S_{11} & S_{12} & S_{13} & 0 & 0 & 0 \\ S_{12} & S_{22} & S_{23} & 0 & 0 & 0 \\ S_{13} & S_{23} & S_{33} & 0 & 0 & 0 \\ 0 & 0 & 0 & S_{44} & 0 & 0 \\ 0 & 0 & 0 & 0 & S_{55} & 0 \\ 0 & 0 & 0 & 0 & 0 & S_{66} \end{bmatrix} \begin{bmatrix} \sigma_1 \\ \sigma_2 \\ \sigma_3 \\ \tau_{23} \\ \tau_{31} \\ \tau_{12} \end{bmatrix} \quad (4.16)$$

One of the major objectives in studying the strain-stress relation is to be able to conclude what deformation response occurs because of a specific applied stress. The strain-stress relations can be written as,

$$\begin{aligned} \varepsilon_1 &= S_{11}\sigma_1 + S_{12}\sigma_2 + S_{13}\sigma_3 + S_{14}\tau_{23} + S_{15}\tau_{31} + S_{16}\tau_{12} \\ &\cdot \\ &\cdot \\ &\cdot \\ \gamma_{12} &= S_{16}\sigma_1 + S_{26}\sigma_2 + S_{36}\sigma_3 + S_{46}\tau_{23} + S_{56}\tau_{31} + S_{66}\tau_{12} \end{aligned} \quad (4.17)$$

Accordingly, for an applied uniaxial stress $\sigma_1 = \sigma$ (all other stresses are zero):

$$\varepsilon_1 = S_{11}\sigma \quad \varepsilon_2 = S_{12}\sigma \quad \varepsilon_3 = S_{13}\sigma \quad \gamma_{23} = S_{14}\sigma \quad \gamma_{31} = S_{15}\sigma \quad \gamma_{12} = S_{16}\sigma \quad (4.18)$$

For an orthotropic material, the compliance matrix components in terms of the engineering constants are

$$[S_{ij}] = \begin{bmatrix} \frac{1}{E_1} & -\frac{\nu_{21}}{E_2} & -\frac{\nu_{31}}{E_3} & 0 & 0 & 0 \\ -\frac{\nu_{12}}{E_1} & \frac{1}{E_2} & -\frac{\nu_{32}}{E_3} & 0 & 0 & 0 \\ -\frac{\nu_{13}}{E_1} & -\frac{\nu_{23}}{E_2} & \frac{1}{E_3} & 0 & 0 & 0 \\ 0 & 0 & 0 & \frac{1}{G_{23}} & 0 & 0 \\ 0 & 0 & 0 & 0 & \frac{1}{G_{31}} & 0 \\ 0 & 0 & 0 & 0 & 0 & \frac{1}{G_{12}} \end{bmatrix} \quad (4.19)$$

The stiffness matrix, C_{ij} , for an orthotropic material in terms of the engineering constants is obtained by inversion of the compliance matrix, S_{ij} , in Equation (4.19). The nonzero stiffnesses in Equation (4.14) are

$$\begin{aligned} C_{11} &= \frac{1 - \nu_{23}\nu_{32}}{E_2 E_3 \Delta} \\ C_{22} &= \frac{1 - \nu_{13}\nu_{31}}{E_1 E_3 \Delta} \\ C_{12} &= \frac{\nu_{21} + \nu_{31}\nu_{23}}{E_2 E_3 \Delta} = \frac{\nu_{12} + \nu_{32}\nu_{13}}{E_1 E_3 \Delta} \\ C_{23} &= \frac{\nu_{32} + \nu_{12}\nu_{31}}{E_1 E_3 \Delta} = \frac{\nu_{23} + \nu_{21}\nu_{13}}{E_1 E_2 \Delta} \\ C_{13} &= \frac{\nu_{31} + \nu_{21}\nu_{32}}{E_2 E_3 \Delta} = \frac{\nu_{13} + \nu_{12}\nu_{23}}{E_1 E_2 \Delta} \\ C_{33} &= \frac{1 - \nu_{12}\nu_{21}}{E_1 E_2 \Delta} \\ C_{44} &= G_{23} \quad C_{55} = G_{31} \quad C_{66} = G_{12} \\ \Delta &= \frac{1 - \nu_{12}\nu_{21} - \nu_{23}\nu_{32} - \nu_{31}\nu_{13} - 2\nu_{21}\nu_{32}\nu_{13}}{E_1 E_2 E_3} \end{aligned} \quad (4.20)$$

4.3 Stress – Strain Relations For Plane Stress in an Orthotropic Material

Figure 4.2 shows a unidirectional ply under plane stress condition. The 1 and 2 axes are the longitudinal and transverse directions respectively. By assuming two-dimensional orthotropic material properties for each unidirectional ply, number of material properties reduced four.

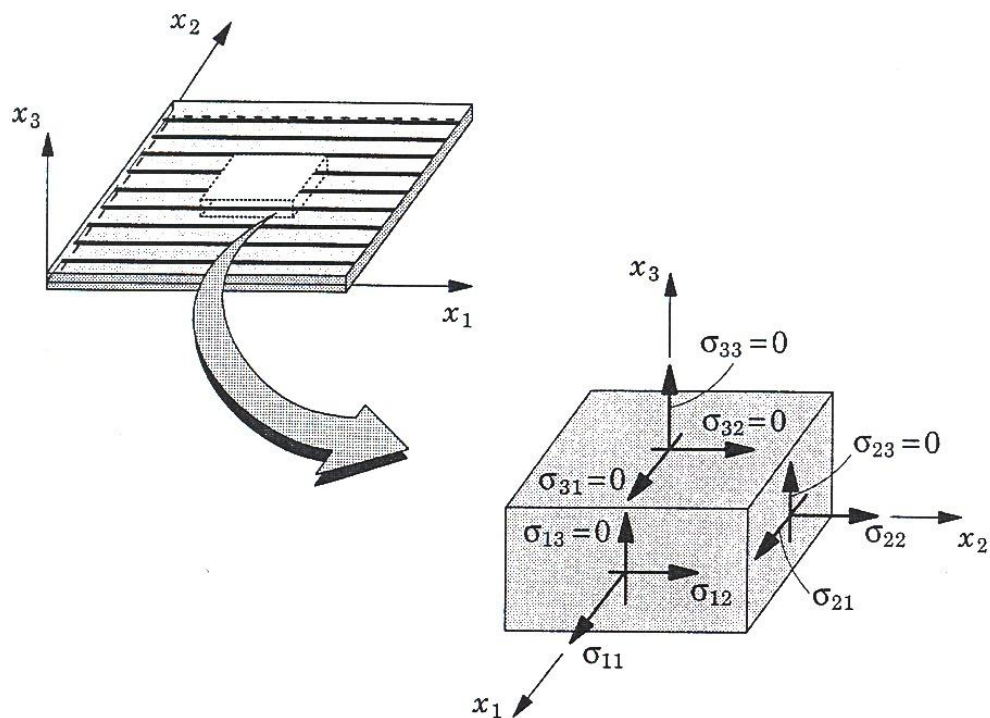


Figure 4.2 A unidirectional fiber reinforced lamina with the material coordinate systems (Reddy,1997)

$$\sigma_3 = \tau_{23} = \tau_{31} = 0 \quad (4.21)$$

In this case, Equation (4.19) reduces to

$$[S_{ij}] = \begin{bmatrix} \frac{1}{E_1} & -\frac{\nu_{21}}{E_2} & 0 \\ -\frac{\nu_{12}}{E_1} & \frac{1}{E_2} & 0 \\ 0 & 0 & \frac{1}{G_{12}} \end{bmatrix} \quad (4.22)$$

where

$$\begin{bmatrix} \varepsilon_1 \\ \varepsilon_2 \\ \gamma_{12} \end{bmatrix} = \begin{bmatrix} S_{11} & S_{12} & 0 \\ S_{12} & S_{22} & 0 \\ 0 & 0 & S_{66} \end{bmatrix} \begin{bmatrix} \sigma_1 \\ \sigma_2 \\ \tau_{12} \end{bmatrix} \quad (4.23)$$

which may be written;

$$\{\varepsilon_\ell\} = [S]\{\sigma_\ell\} \quad (4.24)$$

where ℓ identifies lamina coordinates, and $[S]$, the compliance matrix, relates the stress and strain components in the principal material directions. The Equation (4.23) can be inverted to

$$\{\sigma_\ell\} = [S]^{-1}\{\varepsilon_\ell\} \quad (4.25)$$

or

$$\{\sigma_\ell\} = [Q]\{\varepsilon_\ell\} \quad (4.26)$$

where the matrix Q is defined as the inverse of the compliance matrix and is known as the reduced lamina stiffness matrix.

$$\begin{bmatrix} \sigma_1 \\ \sigma_2 \\ \tau_{12} \end{bmatrix} = \begin{bmatrix} \frac{S_{22}}{S_{11}S_{22}-S_{12}^2} & \frac{S_{12}}{S_{11}S_{22}-S_{12}^2} & 0 \\ \frac{S_{12}}{S_{11}S_{22}-S_{12}^2} & \frac{S_{11}}{S_{11}S_{22}-S_{12}^2} & 0 \\ 0 & 0 & \frac{1}{S_{66}} \end{bmatrix} \begin{bmatrix} \varepsilon_1 \\ \varepsilon_2 \\ \gamma_{12} \end{bmatrix} \quad (4.27)$$

$$\begin{bmatrix} \sigma_1 \\ \sigma_2 \\ \tau_{12} \end{bmatrix} = \begin{bmatrix} \frac{E_1}{1-\nu_{12}\nu_{21}} & \frac{\nu_{12}E_2}{1-\nu_{12}\nu_{21}} & 0 \\ \frac{\nu_{12}E_2}{1-\nu_{12}\nu_{21}} & \frac{E_2}{1-\nu_{12}\nu_{21}} & 0 \\ 0 & 0 & G_{12} \end{bmatrix} \begin{bmatrix} \varepsilon_1 \\ \varepsilon_2 \\ \gamma_{12} \end{bmatrix} \quad (4.28)$$

4.4 Material Orientation

The reduced stiffness and compliance matrices relate stresses and strains in the principal material directions of the composite material. To describe the material response in directions other than these material coordinates, transformation matrices must be developed for the material stiffness. Two sets of coordinate systems are illustrated in Figure 4.3 (Reddy, 1997).

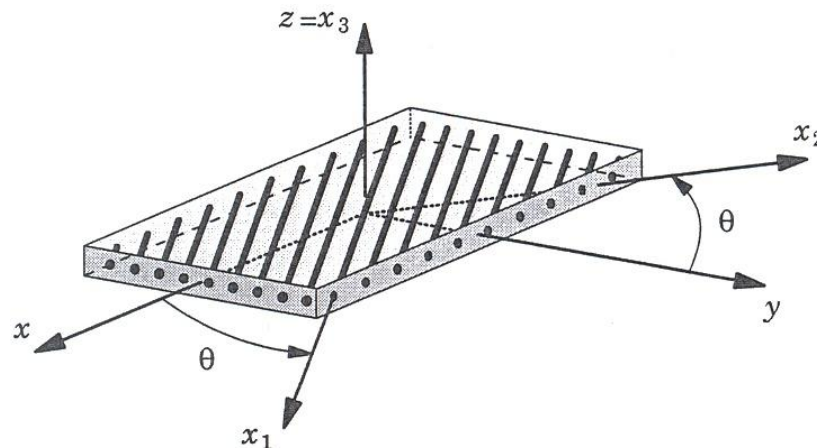


Figure 4.3 A fiber reinforced lamina with global and material coordinate system (Reddy, 1997)

The 1-2 coordinate system corresponds to the principal material directions for a lamina, whereas the x-y coordinates are arbitrary and are related to the 1-2 coordinates through a rotation about the axis out of the plane of the Figure 4.3. The angle, θ , is defined as the rotation from the arbitrary x-y system to the material 1-2 system.

The transformation of stresses from the 1-2 system to the x-y system follows the rules for transformation of tensor components. Hence,

$$\begin{bmatrix} \sigma_x \\ \sigma_y \\ \tau_{xy} \end{bmatrix} = \begin{bmatrix} m^2 & n^2 & -2mn \\ n^2 & m^2 & 2mn \\ mn & -mn & m^2-n^2 \end{bmatrix} \begin{bmatrix} \sigma_1 \\ \sigma_2 \\ \tau_{12} \end{bmatrix} \quad (4.29)$$

or

$$[\sigma_x] = [\theta][\sigma_\ell] \quad (4.30)$$

where $m = \cos(\theta)$ and $n = \sin(\theta)$. The subscript x is used to refer to the laminate coordinate system. The same transformation matrix $[\theta_1]$ can also be used for the tensor strain components. Thus:

$$\begin{bmatrix} \varepsilon_x \\ \varepsilon_y \\ \varepsilon_{xy} \end{bmatrix} = [\theta] \begin{bmatrix} \varepsilon_1 \\ \varepsilon_2 \\ \varepsilon_{12} \end{bmatrix} \quad \text{or} \quad \begin{bmatrix} \varepsilon_x \\ \varepsilon_y \\ 2\varepsilon_{xy} \end{bmatrix} = \begin{bmatrix} m^2 & n^2 & -mn \\ n^2 & m^2 & mn \\ 2mn & -2mn & m^2-n^2 \end{bmatrix} \begin{bmatrix} \varepsilon_1 \\ \varepsilon_2 \\ 2\varepsilon_{12} \end{bmatrix} \quad (4.31)$$

or

$$[\varepsilon_x] = [\theta_2][\varepsilon_\ell] \quad (4.32)$$

Given the transformations for stress and strain to arbitrary coordinate systems, the relations between stress and strain in the composite laminate system can be determined. Substituting Equations (4.29) and (4.31) into Equation (4.25), we calculate as,

$$[\sigma_x] = [\theta_1][Q][\theta_2]^{-1}[\varepsilon_x] \quad (4.33)$$

Hence,

$$[\sigma_x] = [\bar{Q}][\varepsilon_x] \quad (4.34)$$

or

$$\begin{bmatrix} \sigma_x \\ \sigma_y \\ \tau_{xy} \end{bmatrix} = \begin{bmatrix} \bar{Q}_{11} & \bar{Q}_{12} & \bar{Q}_{16} \\ \bar{Q}_{12} & \bar{Q}_{22} & \bar{Q}_{26} \\ \bar{Q}_{16} & \bar{Q}_{26} & \bar{Q}_{66} \end{bmatrix} \begin{bmatrix} \varepsilon_x \\ \varepsilon_y \\ \gamma_{xy} \end{bmatrix} \quad (4.35)$$

where $\gamma_{xy} = 2\varepsilon_{xy}$

The reduced-stiffness matrix $[\bar{Q}]$, relates the stress and strain components in the laminate coordinate system. Here:

$$[\bar{Q}] = [\theta_1][Q][\theta_2]^{-1} \quad (4.36)$$

The terms within $[\bar{Q}]$ are defined by approximate matrix multiplication to be:

$$\begin{aligned} \bar{Q}_{11} &= Q_{11}m^4 + Q_{22}n^4 + 2(Q_{12} + 2Q_{66})m^2n^2 \\ \bar{Q}_{12} &= (Q_{11} + Q_{22} - 4Q_{66})m^2n^2 + Q_{12}(m^4 + n^4) \\ \bar{Q}_{16} &= (Q_{11} - Q_{12} - 2Q_{66})nm^3 + (Q_{12} - Q_{22} + 2Q_{66})n^3m \\ \bar{Q}_{22} &= Q_{11}n^4 + Q_{22}m^4 + 2(Q_{12} + 2Q_{66})m^2n^2 \\ \bar{Q}_{26} &= (Q_{11} - Q_{12} - 2Q_{66})mn^3 + (Q_{12} - Q_{22} + 2Q_{66})m^3n \\ \bar{Q}_{66} &= (Q_{11} + Q_{22} - 2Q_{12} - 2Q_{66})n^2m^2 + Q_{66}(m^4 + n^4) \end{aligned} \quad (4.37)$$

4.5 Tsai-Wu Tensor Failure Criterion

The preceding biaxial failure criteria suffer from various inadequacies in their representation of experimental data. One obvious way to improve the correlation between a criterion and experiment is to increase the number of terms in the prediction equation. Tsai and Wu postulated that a failure surface in six-dimensional stress space exists in the form (Jones, 1999),

$$F_i\sigma_i + F_{ij}\sigma_i\sigma_j = 1 \quad i, j = 1, \dots, 6 \quad (4.38)$$

Wherein F_i and F_{ij} are strength tensors of the second and fourth rank, respectively. Equation (4.38) is obviously very complicated; we will restrict our attention to the reduction of Equation (4.38) to the case of an orthotropic lamina under plane stress conditions,

$$F_1\sigma_1 + F_2\sigma_2 + F_6\sigma_6 + F_{11}\sigma_1^2 + F_{22}\sigma_2^2 + F_{66}\sigma_6^2 + 2F_{12}\sigma_1\sigma_2 = 1 \quad (4.39)$$

Under tensile load,

$$F_1X_t + F_{11}X_t^2 = 1 \quad (4.40)$$

and under compressive load,

$$F_1X_c + F_{11}X_c^2 = 1 \quad (4.41)$$

Upon simultaneous solution of Equations (4.40) and (4.41),

$$F_1 = \frac{1}{X_t} + \frac{1}{X_c} \quad F_{11} = -\frac{1}{X_t X_c} \quad (4.42)$$

Similarly,

$$F_2 = \frac{1}{Y_t} + \frac{1}{Y_c} \quad F_{22} = -\frac{1}{Y_t Y_c} \quad (4.43)$$

Similar reasoning, the shear strength in principal material coordinates is independent of shear stress sign, leads to,

$$F_6 = 0 \quad F_{66} = \frac{1}{S^2} \quad (4.44)$$

Note that for equal strengths in tension and compression ($X_t = -X_c$ and $Y_t = -Y_c$)

$$F_1 = 0 \quad F_{11} = \frac{1}{X^2} \quad F_2 = 0 \quad F_{22} = \frac{1}{Y^2} \quad (4.45)$$

Failure criterion,

$$\frac{\sigma_1^2}{X^2} + 2F_{12}\sigma_1\sigma_2 + \frac{\sigma_2^2}{Y^2} + \frac{\tau_{12}^2}{S^2} = 1 \quad (4.46)$$

Determination of the fourth-rank tensor term F_{12} remains. Basically, F_{12} cannot be found from any uniaxial test in the principal material directions. Instead, a biaxial test must be used. This fact should not be surprising because F_{12} is the coefficient of the product of σ_1 and σ_2 in the failure criterion, Equation (4.39). Thus, for example, we can impose a state of biaxial tension described by $\sigma_1 = \sigma_2 = \sigma$ and all other stresses are zero. Accordingly, from Equation (4.39) (Jones, 1999),

$$(F_1 + F_2)\sigma + (F_{11} + F_{22} + 2F_{12})\sigma^2 = 1 \quad (4.47)$$

Now solve for F_{12} after substituting the definitions just derived for F_1, F_2, F_{11} and F_{22} :

$$F_{12} = \frac{1}{2\sigma^2} \left[1 - \left[\frac{1}{X_t} + \frac{1}{X_c} + \frac{1}{Y_t} + \frac{1}{Y_c} \right] \sigma + \left[\frac{1}{X_t X_c} + \frac{1}{Y_t Y_c} \right] \sigma^2 \right] \quad (4.48)$$

The Tsai-Wu tensor failure criterion is obviously of more general character than the Tsai-Hill or Hoffman failure criteria. Specific advantages of the Tsai-Wu failure criterion include, a) invariance under rotation or definition of coordinates, b) transformation via known tensor-transformation laws, and c) symmetry properties similar to those of the stiffnesses and compliances. The Tsai-Wu failure criterion has several important characteristics (Jones, 1999);

1. Increased curve-fitting capability over the Tsai-Hill and Hoffman criteria because of an additional term in the equation.
2. The additional term, F_{12} , can be determined only with an expensive and difficult-to-perform biaxial test.

3. Graphical interpretations of the results are facilitated by the tensor formulation.

CHAPTER FIVE

EXPERIMENTAL STUDY

5.1 Introduction

Tests have been carried out on single pinned joints in carbon-fiber reinforced epoxy for a range of specimen geometry. For single-hole joints the strengths have been obtained experimentally; the effects of variables such as applied preload moments, moisture, interference-fit, laminate edge and side distances were discussed in the light of the results.

5.2 Fabrication Of Laminated Composites

Carbon/epoxy laminated composites are manufactured from unidirectional Carbon fabric having a weight of 330 g/m² and epoxy resin CY225 with HY225 hardener. [0°]₈ oriented carbon/epoxy composite plate was produced to determine mechanical properties, which are required to carry out failure stress analyses of pinned composite joints. For experimental study on pinned and bolted composite joints, carbon/epoxy laminated composite plate with a lay-up [90/0]_s was produced. For fabrication of laminates, the hand lay-up technique was utilized. After applying this method, these composite plates were cured by using a hot lamination press at 120 °C for 2 hours under a pressure of 0.15 MPa. Then, they were cooled to room temperature at the same pressure. After manufacturing, the test specimens were prepared by cutting from the composite plates.

5.3 Mechanical Test Procedure

Mechanical properties of the composite plates were determined experimentally at room temperatures. Test samples were prepared according to the ASTM standards. All the mechanical tests were performed by using INSTRON tensile test machine. The load was applied to the samples at a constant cross-head speed of 1 mm/min. Each test was repeated three times and the mean values were taken as test results.

Longitudinal Young's modulus E_1 , Poisson's ratio ν_{12} , longitudinal tensile strengths X_t , transverse Young's modulus E_2 and transverse tensile strengths Y_t were measured by using longitudinal and transverse $[0^\circ]_8$ unidirectional composite specimens according to the ASTM D3039-76 standard. The specimens were loaded up to the failure loads in the axial direction. Young moduli, E_1 and E_2 were calculated from the initial slope of the stress-strain curves. The tensile strengths of the unidirectional composite plates, X_t and Y_t , were determined by dividing the failure load to the cross-sectional area of the longitudinal and transverse specimens, respectively. The Illinois Institute of Technology Research Institute (IITRI) compression fixture was used to measure the compressive strength of the unidirectional carbon/epoxy laminated composites. The compression test specimens with 140 mm length were prepared according to ASTM D3410 standard. The width was taken as 6.4 and 12.7 mm for the longitudinal and transverse specimens, respectively. The longitudinal and transverse compressive strengths, X_c and Y_c , are obtained by dividing the failure load to the cross-sectional area of the specimens. The in-plane shear modulus and strength were measured by using Arcan test fixture as shown in Figure 5.1. The specimens with 90° notches were prepared from $[0_8]$ unidirectional carbon/epoxy laminated composites. Tensile force was applied to Arcan test fixture up to the failure load. The in-plane shear strength S_{12} was calculated by

$$S_{12} = \frac{P_{\max}}{wt} \quad (5.1)$$

where P_{\max} is the failure load, w is the width of the specimen at notch location and t is specimen thickness.

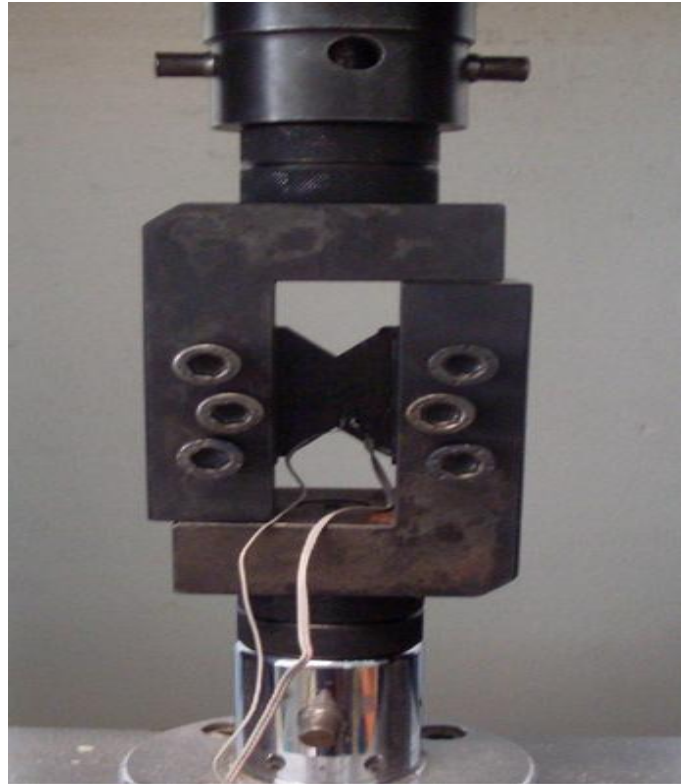


Figure 5.1 Arcan test fixture

Shear modulus G_{12} was measured by using two strain-gage located at the center of the notched section at 45° and -45° to the loading direction. Shear stress s_{12} was obtained by using Equation (5.2). The shear modulus was calculated by using the following equation

$$G_{12} = \frac{\tau_{12}}{\gamma_{12}} \quad (5.2)$$

To determine the interlaminar shear strength, S_i , the double-notch shear test was performed as described in ASTM D3846-79. The specimens having dimensions of a 79,5 mm length, 12,7 mm width and 2,6 mm thickness were prepared from unidirectional reinforced composites. Two parallel notches were machined, one on each face of the specimen, 6,4 mm apart and with a depth equal to half the specimen thickness. The interlaminar shear strength was determined using the following equation

$$S_i = \frac{P_{\max}}{wl} \quad (5.3)$$

where P_{\max} is the failure load, l is the distance between notches, and w the width of the specimen.

To determine the out-plane shear moduli G_{13} and G_{23} , specimens with 15 mm width, 50 mm length and 10 mm thickness were manufactured by using the standard Test Method for Short-Beam Strength as described in ASTM D2344/D2344 M. The strain-gage was glued along the natural axis of longitudinal lateral surface of the specimen at angle of 45° with transverse direction as shown in Figure 5.2 (a) and (b). (In-plane 1–3 for G_{13} , in-plane 2–3 for G_{23}) Maximum shear stresses in natural axis were calculated as given in Equation (5.4). G_{13} and G_{23} can be calculated by using Equation (5.5).

$$\tau_{13} = \frac{3P}{4A} \quad (5.4)$$

where A is the cross-sectional area (width \times thickness) (mm^2) and P static force (N).

$$\gamma_{13} = 2\varepsilon \quad G_{13} = \frac{\tau_{13}}{\gamma_{13}} \text{ [MPa]} \quad (5.5)$$

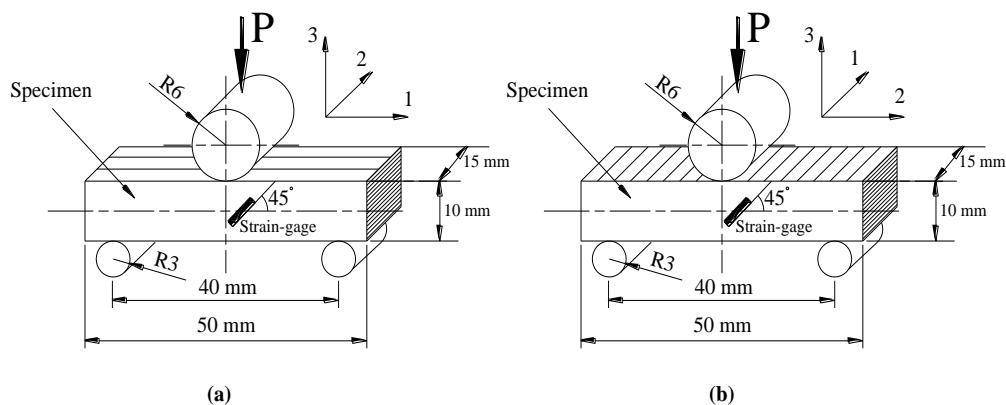


Figure 5.2 Schematic view of three-point bending test for G_{13} and G_{23}

Apart from the mechanical tests, by performing weight and volume measurements, fiber volume fraction and the density of unidirectional carbon/epoxy composite plates were determined as 64.3 % and 1710 kg/m³, respectively. The obtained results from the mechanical tests are given in Table 5.1.

Table 5.1 Mechanical properties of carbon/epoxy composite plate

Mechanical Properties of Carbon/Epoxy Composite Plate	Magnitude
Fiber volume fraction, (V_f)	64.3%
Density, ρ (kg/m ³)	1710
Longitudinal modulus, E_1 (GPa)	150.9
Transverse modulus, E_2 (GPa)	11.2
In-plane shear modulus, G_{12} (GPa)	5.3
Out-plane shear modulus, G_{13} (GPa)	5.3
Out-plane shear modulus, G_{23} (GPa)	1.4
Interlaminar shear strength, S_{13} (MPa)	22.9
In-plane shear strength, S_{12} (MPa)	79.5
Poisson's ratio, ν_{12}	0.29
Longitudinal tensile strength, X_t (MPa)	1858.3
Transverse tensile strength, Y_t (MPa)	25.4
Longitudinal compressive strength, X_c (MPa)	576.8
Transverse compressive strength, Y_c (MPa)	107.3

5.4 Problem Statement

The test specimens for the pinned joints are shown in Fig 5.3. The length and width of the specimens are represented with L and W respectively. L was chosen as 100 mm for all types of specimens. D is the diameter of the hole on the specimen and it has a constant value of 8 mm. t is the thickness of specimens. d is the diameter of the pin. Two different pins with diameter of 8 mm and 8.10 mm were manufactured. The pin with diameter of 8.10 mm was manufactured to investigate the effects of interference-fit on failure loads and failure modes. Geometrical parameters, E/D and W/D, were determined ranging from 1 to 4 and from 2 to 4, respectively.

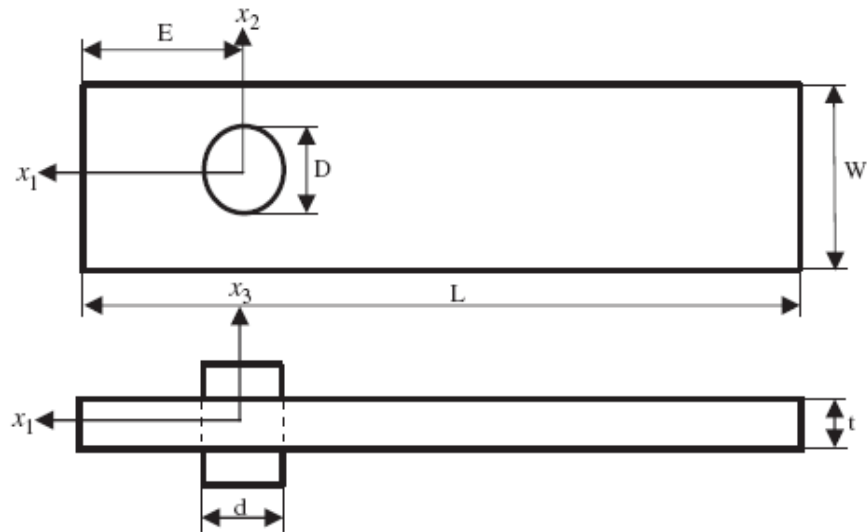


Figure 5.3 Pinned-joint test configuration

A bolted joint is shown in Figure 5.4. A metric 8 bolt was used in the experimental study. The preload moments were applied to the specimens as $M = 3$ Nm and $M = 6$ Nm to observe the failure modes under preload moment.

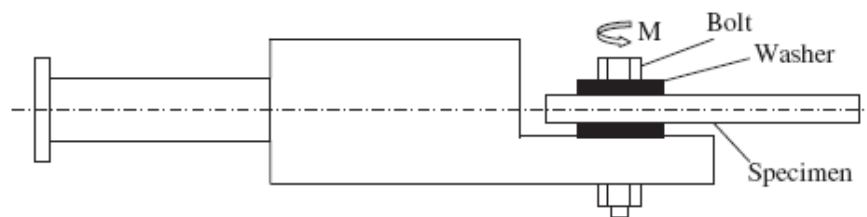


Figure 5.4 Bolted-joint test configuration

Besides, some of specimens were kept for 2 months in sea water to investigate the effect of sea water on bearing strength. These specimens were studied under the preload moments of $M = 0, 3, 6$ Nm and they were compared with the dry specimens.

The experiments were performed in tension mode on the Instron-1114 Tensile Machine of a cross-head speed of 1 mm/min. Then the average bearing strength values were found. The load versus pin displacement curves were plotted in the experiments. To calculate the strength of single pin loaded specimens, the static bearing strength can be written as:

$$\sigma_b = \frac{P}{Dt} \quad (5.6)$$

where P, D and t are the load, pin diameter and the thickness that is equal to 1.6 mm of laminated composite specimen, respectively.

5.5 Results Of Experimental Studies

5.5.1 Failure Modes

Each composite specimen was loaded until the occurrence of the last failure. The general behavior of the composite was found from the load–displacement curves.

In this study, three types of main failure modes and combination of them were observed. They are the shear-out, net-tension and bearing modes. The loads versus displacement curves are almost linear before the failure. The linear zone ends after reaching the first failure load.

The shear-out mode is shown in Figure 5.5. It attains small values in this mode. This failure mode generally occurs for small E/D ratios. The diagram decreases gradually after failure of composite specimens. The maximum force is taken as the failure load.

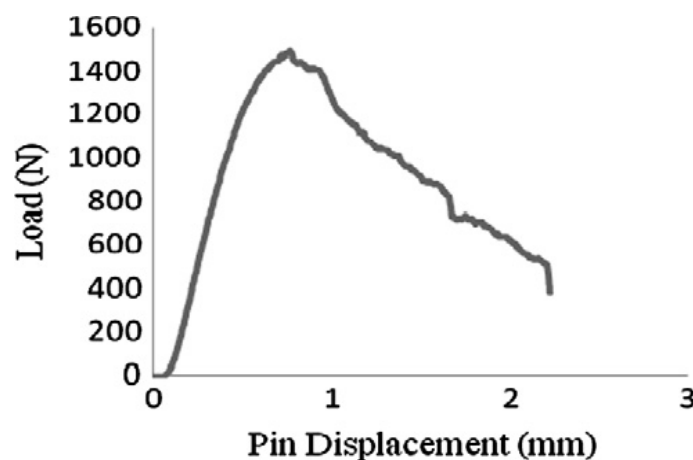


Figure 5.5 Shear-out mode

The net-tension mode is shown in Figure 5.6. This failure mode occurs for small W/D and high E/D ratios. The load decreases suddenly after reaching the ultimate force. Also the tear occurs suddenly in this mode. This mode usually appears under preloads, since the preloads produce high failure loads. Consequently, the high failure loads suddenly produce the failures without occurring to the bearing mode.

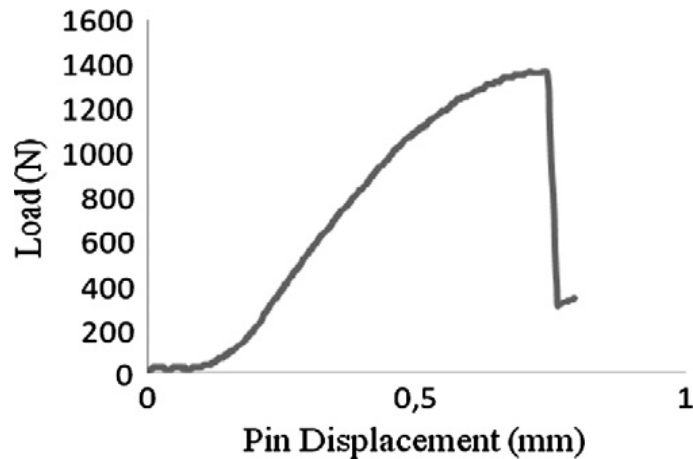


Figure 5.6 Net-tension mode

The bearing mode is shown in Figure 5.7. The failure load increases after first peak and it continues to carry the load. The last failure occurs in large deformations of the pin. It still carries the load in this case; however, the maximum load can be taken as the ultimate load of the specimen. This mode occurs for both high E/D and W/D ratios.

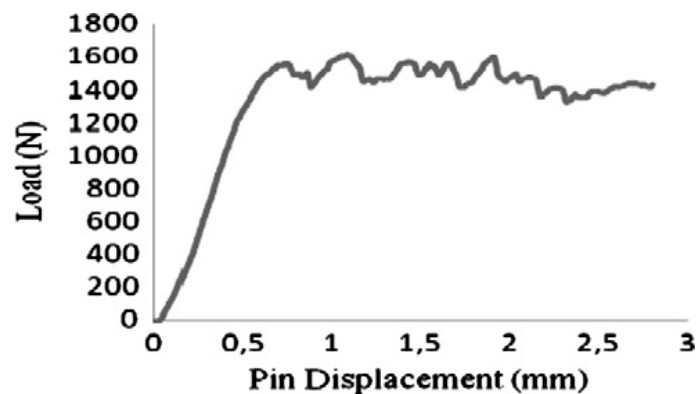


Figure 5.7 Bearing mode

The combined failure modes can be observed in some specimens at different E/D and W/D ratios. They especially occur under preload moments. The failure modes and maximum failure loads of all specimens are given at Table 5.2 and 5.3, respectively.

Table 5.2 Failure modes of specimens (S=Shear-out mode, B= Bearing mode, N=Net-tension mode)

E/D		M = 0 Nm							
		1		2		3		4	
W/D		Dry	Wet	Dry	Wet	Dry	Wet	Dry	Wet
2		S	S	S	B	B	B	B	B
3		S	S	B	B	B	B	B	B
4		S	S	B	B	B	B	B	B
E/D		M = 3 Nm							
		1		2		3		4	
W/D		Dry	Wet	Dry	Wet	Dry	Wet	Dry	Wet
2		S	S	S	B+S	N	B+N	N	N
3		S	S	S	N	B+N	N	N	N
4		B+S	S	S	N+S	B+N	B+N	N	B+N
E/D		M = 6 Nm							
		1		2		3		4	
W/D		Dry	Wet	Dry	Wet	Dry	Wet	Dry	Wet
2		S	S	N	B+N	B+N	N	N	N
3		S	S	N	B+N	B+N	B+N	B+N	N+B
4		S	S	S	B+N	B+N	B+N	N	N+B

Table 5.3 Maximum failure loads of specimens

Maximum Failure Loads (N)							
E/D	W/D	Dry Specimens			Wet Specimens		
		0 Nm	3Nm	6Nm	0 Nm	3Nm	6Nm
1	2	1226	2040	3247	1196	2021	2550
		1098	1795	4139	1226	2943	2138
		1079	1608	3914	1167	2815	2344
	3	1088	1922	4365	1118	2501	2776
		1147	2952	4463	1196	2678	2874
		1216	2383	3355	1069	2844	2992
	4	1118	2226	4914	1089	3276	2266
		912	2501	4326	1138	2442	3345
		1108	2766	4022	1020	2717	3649
2	2	2168	5209	4797	2011	4081	3943
		2197	4100	5562	1736	3992	3404
		2118	4080	4375	2119	3541	4110
	3	1746	4620	5130	1883	4610	5130
		1883	3855	5061	2040	5375	4944
		1873	4071	6268	1765	4130	4502
	4	1912	4277	6768	2158	4365	5111
		2020	3835	6660	2226	3933	5660
		2226	4581	6356	1893	5385	4463
3	2	1854	4326	5228	1697	5091	5199
		1795	4247	6307	1912	4463	5356
		1795	3825	5817	1707	4689	4767
	3	1785	4826	7543	2256	4914	5699
		1481	4394	7691	2119	5709	5738
		1844	4914	7043	1834	5935	5591
	4	1824	5209	5670	2030	5130	6298
		1912	5199	6847	2158	5415	6464
		1922	6278	6916	1344	5287	5915
4	2	2030	5503	7328	2060	4669	5817
		1785	5091	6484	2011	5581	6533
		2109	5709	7269	1824	5071	5699
	3	2040	6425	6690	2217	5836	6945
		1932	6916	7416	1697	6592	6268
		1746	6405	8161	2021	5572	6347
	4	2050	6405	7769	2001	6249	6749
		2079	6582	7455	2050	6150	5925
		2109	6464	7004	2050	5111	6533

As seen in this table, for the case without preload moment, the shear-out mode occurs in $E/D = 1$ at both dry and wet specimens. The bearing failure mode is observed for $E/D = 2-4$ at dry and wet specimens. When the effects of geometric parameters and sea water on failure modes are investigated, the similar results have been obtained by Aktaş and Uzun (2008).

Under $M = 3$ N m preload moment, the shear-out mode appears for $E/D = 1$ at both dry and wet specimens. For $E/D = 2-4$, the net-tension or combined modes generally occur at both dry and wet specimens. Since failure load reaches high values, the net-tension generally appears at the specimens under $M = 3$ Nm preload moments.

Under $M = 6$ Nm preload moment, the shear-out mode occurs for $E/D = 1$ at both dry and wet specimens. For $E/D = 2-4$, the net-tension or bearing modes occur at both dry and wet specimens.

5.5.2 The Effect Of End Distance – Pin Diameter Ratio (E/D)

First and ultimate failure bearing strength values depends on the E/D ratio while W/D ratio is considered constant. Ultimate bearing strengths for $W/D = 2$ and $E/D = 1-4$ are shown in Figure 5.8(a). As seen in this figure, the dry and the wet specimens represent the close results. The similar results are shown in Figure 5.8(b) and (c) for $W/D = 3, 4$ and $E/D = 1-4$. It is seen that the bearing strengths do not vary significantly for the specimens which were kept in sea water for 2 months. An investigation conducted by Aktas and Uzun (2008) has indicated that the bearing values obtained from the specimens kept into sea for 1, 2 and 4 months are about 10% lower than that of the unimmersed specimens. The difference between the results is probably due to the fact that carbon/epoxy and glass/epoxy composites have the different mechanical and absorption properties. In addition, the specimens were tied to a ship making voyage in sea, differently from the present study. Making voyage in sea may increase the corrosion and then the strength of the composite specimens decrease.

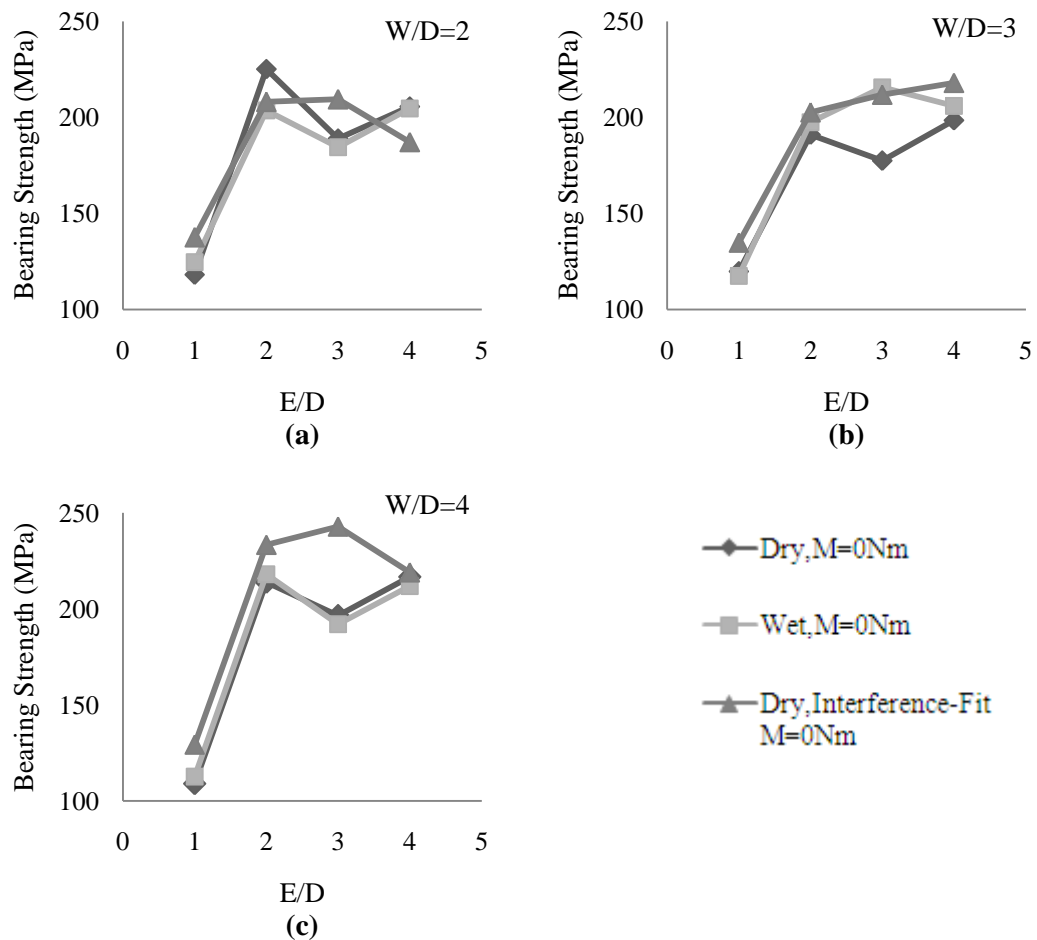


Figure 5.8 The effect of E/D on ultimate bearing strengths

5.5.3 The Effect Of The Preload Moment $M=3$ And $M=6$ Nm

The bearing strength under $M = 3$ and 6 Nm preload moments for $W/D = 2$ and $E/D = 1-4$ is shown in Figure 5.9(a). It generally increases with increasing E/D ratio. It depends on the E/D ratio and preload moment. When the preload moment increases the bearing strength reaches high values. In the study conducted by Sayman et al. (2007), preload moments of 2.5 and 5 Nm were applied onto composite joints. The similar results with the present study were obtained in terms of the effect of preload moment on bearing strength. The mean value of the bearing strength is almost the same for the dry and the wet specimens under $M = 3$ Nm preload moment. However, it reaches high values under $M = 6$ Nm preload moment for the dry specimens.

The bearing strength under $M = 3$ and 6 Nm preload moments for $W/D = 3, 4$ and $E/D = 1-4$ is shown in Figure 5.9(b) and (c) respectively. The bearing strength is almost similar for dry and wet specimens under $M = 3$ Nm preload moment. It is observed that the bearing strength of the dry specimens are higher than the wet specimens under $M = 6$ Nm preload moment.

The mean values of the bearing strength of the dry specimens under $M = 3$ and 6 Nm preload moments are 153% and 241% higher than that of the dry specimen without a preload moment. It is seen that the bearing strength increases with increasing of the preload moment.

The mean values of the bearing strengths of the wet specimens under $M = 3$ and 6 Nm preload moments are 155% and 176% higher than that of the wet specimens without a preload moment. The mean value of the dry specimens are almost the same in comparison with the wet specimens under $M = 3$ Nm. However, the mean values of the dry specimens are higher than that of the wet specimens under $M = 6$ Nm preload moment.

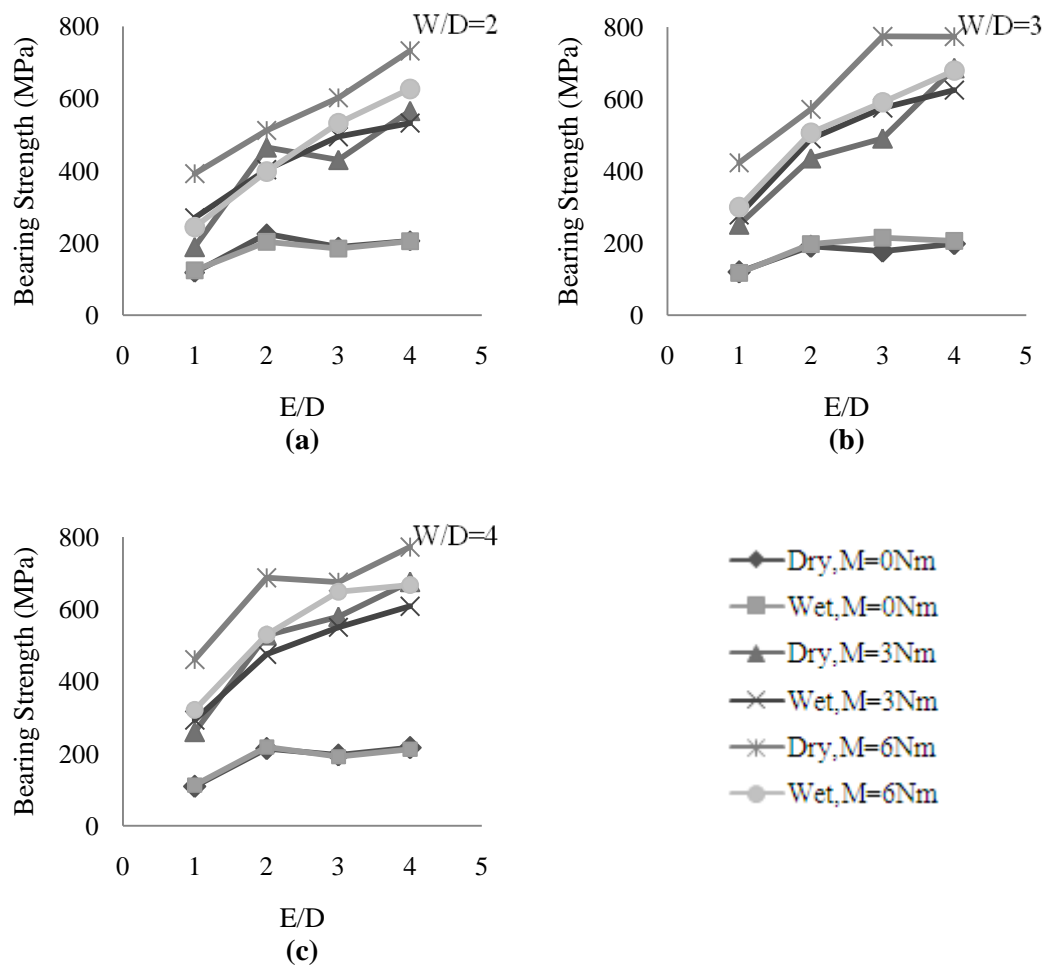


Figure 5.9 The effect of E/D on ultimate bearing strengths

5.5.4 The Effect Of Side Distance – Pin Diameter Ratio (W/D)

Bearing strength generally changes by increasing the W/D ratio, while E/D ratio is held constant under $M = 0$ Nm preload moment, as shown in Figure 5.10(a–d).

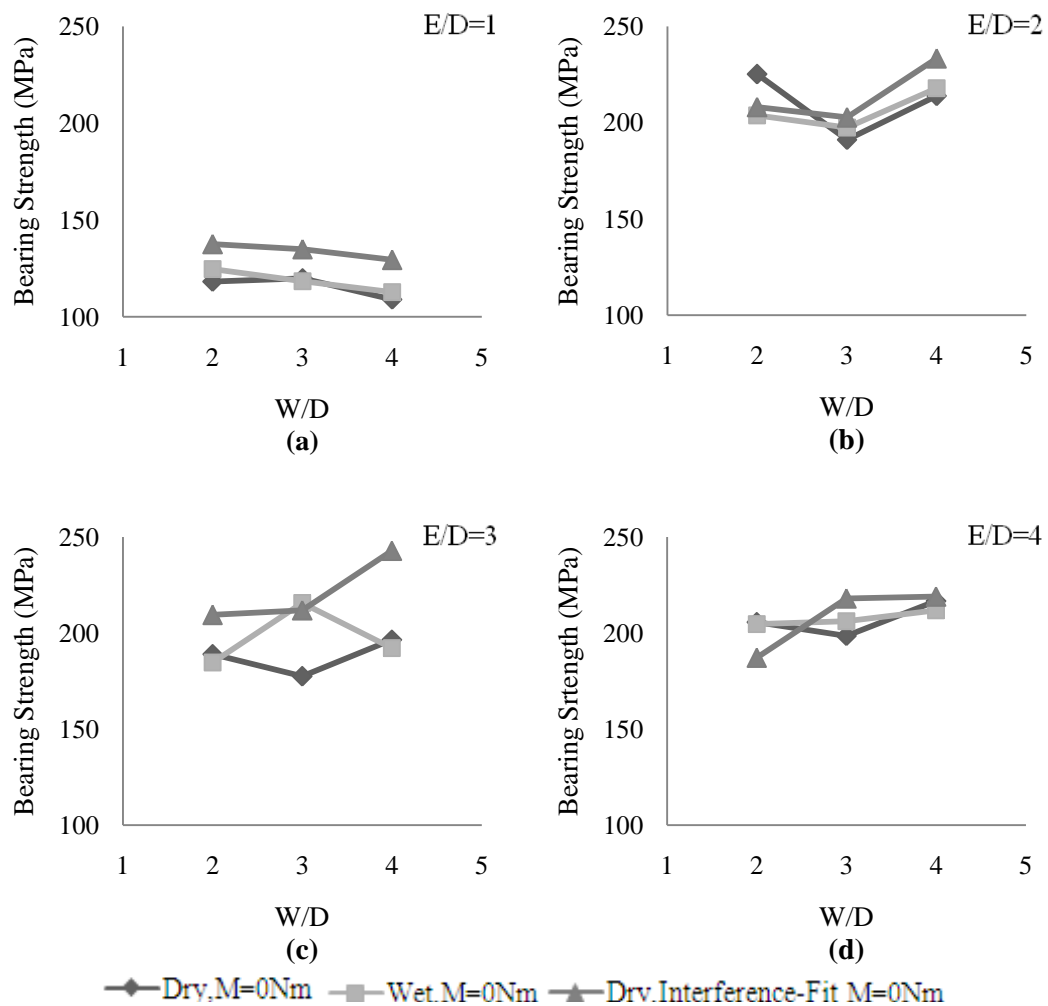


Figure 5.10 The effect of W/D on ultimate bearing strengths

The bearing strength increases by increasing W/D ratio, while E/D is held constant under $M = 3$ and 6 Nm preload moment, for the dry and wet specimens as shown in Figure 5.11(a). Dry and wet specimens give a close results under $M = 3$ Nm preload moment. Nevertheless, the bearing strength of the dry specimens reaches highest values under $M = 6$ Nm preload moment.

For $E/D = 2$ and $W/D = 2-4$, the bearing strength increases both dry and wet specimens under $M = 3$ and 6 Nm preload moments as shown in Figure 5.11(b). It is observed that the bearing strength under 3 Nm preload moment gives close results for the dry and wet specimens. The dry specimens under 6 N m preload moment have the highest values of the bearing strength.

The bearing strength is shown in Figure 5.11(c), by changing W/D ratio while E/D is held constant as 3 under M = 3 and 6 Nm preload moment. It increases under preload moments for the dry and wet specimens with respect to the specimens without a preload moment. The highest values are obtained at the dry specimens under M = 6 Nm preload moment.

For E/D = 4 and W/D = 2–4, the bearing strength is shown in Figure 5.11(d), under M = 3 and 6 Nm preload moments. It is evident that the preload moments increase the bearing strength. Especially, M = 6 Nm preload moment in the dry specimens causes the increasing of the bearing strength to 774 MPa.

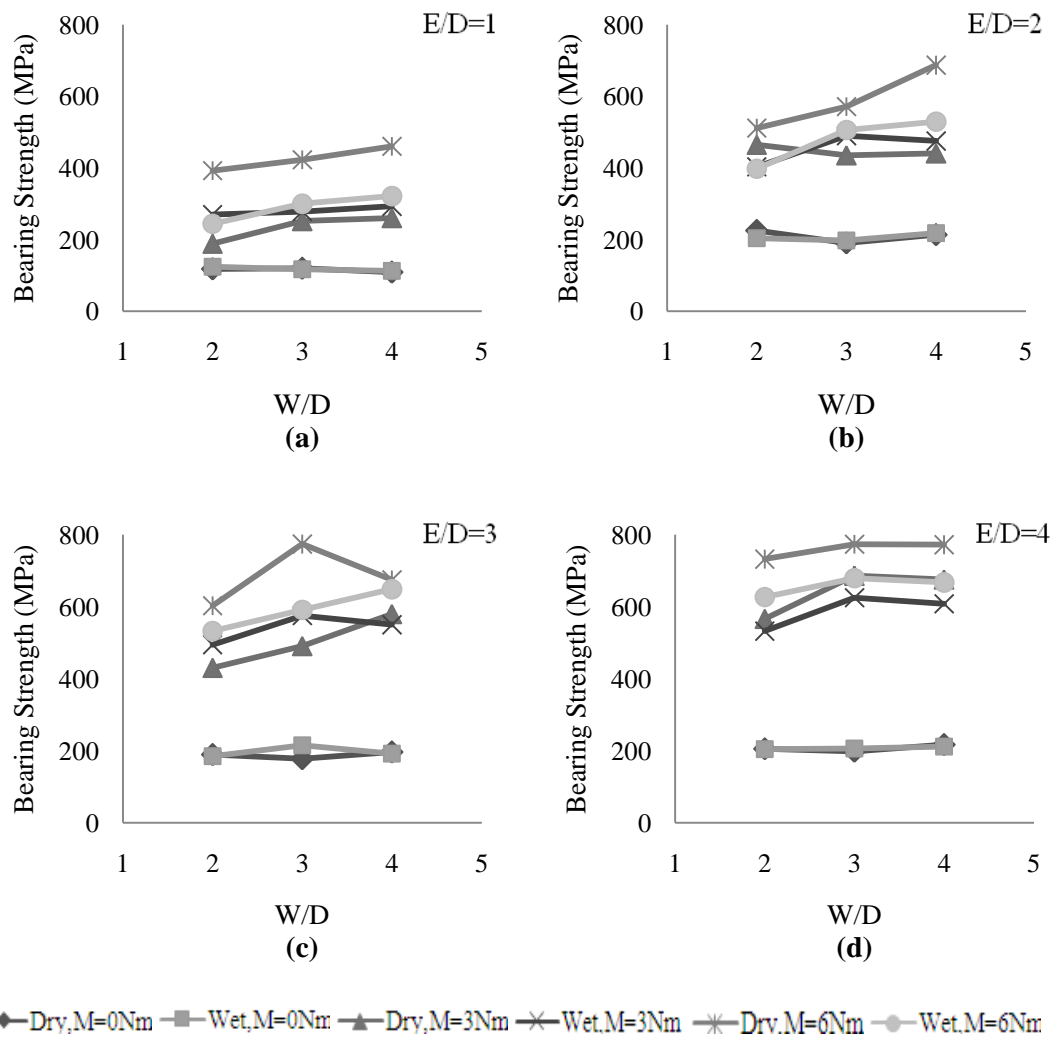


Figure 5.11 The effect of W/D on ultimate bearing strengths

5.5.5 The Effect Of The Interference-Fit On The Failure Mode

Besides the mentioned investigations, the effect of the interference-fit on the failure mode was studied. To this end, the pin was manufactured in the diameter of 8.10 mm, while the diameter of the circular hole was 8 mm. Only the dry specimens were tested and preload moment was not applied on these specimens. The effect of interference-fit on the failure modes and failure loads was investigated. It is found that mean value of the ultimate bearing strength of the interference-fitted specimens is 8% higher than the mean value of free-fitted specimens. The similar results have been obtained by Kiral (2010) in terms of interface-fit effects. In the mentioned study, mean value of the ultimate bearing strength of the interference-fitted specimens is 8% higher than the mean value of free-fitted specimens. Therefore, in addition to the selection of the optimal values of W/D and E/D ratios, interference-fit in pinned composite joints may also be used. The failure modes and maximum failure loads in this case are given at Table 5.4 and 5.5 respectively. The shear-out mode was generally observed for small E/D values.

Table 5.4 Failure modes of interference-fit specimens (S=Shear-out mode, B= Bearing mode, N=Net-tension mode)

W/D	E/D=1		E/D=2		E/D=3		E/D=4	
	Free Fit	Interference Fit	Free Fit	Interference Fit	Free Fit	Interference Fit	Free Fit	Interference Fit
2	S	N	S	S	B	B	B	B
3	S	N+S	B	B	B	B	B	B
4	S	N+S	B	B	B	B	B	B

Table 5.5 Maximum failure loads of interference-fit specimens

Maximum Failure Loads (N)			
W/D	E/D	Free-fit	Interference-fit
1	2	1226	1364
		1098	1383
		1079	1216
	3	1088	1344
		1147	1344
		1216	1197
	4	1118	1305
		912	1128
		1108	1294
2	2	2168	1834
		2197	2128
		2118	2031
	3	1746	2070
		1883	1835
		1873	1933
	4	1912	2178
		2020	2374
		2226	2168
3	2	1854	2090
		1795	1991
		1795	1950
	3	1785	1991
		1481	2109
		1844	2000
	4	1824	2511
		1912	2246
		1922	2236
4	2	2030	1982
		1785	1609
		2109	1800
	3	2040	2031
		1932	2168
		1746	2080
	4	2050	2119
		2079	2109
		2109	2080

CHAPTER SIX NUMERICAL STUDY

6.1 Modeling of The Composite Plates and Applying The Boundary Conditions

Composite plates were modeled and solved using commercial finite element analysis program ANSYS. A static failure analysis was carried out for the first failure loads. For composite plates, solid layered 46 element (Figure 6.1) which has 8 nodes was used. For steel pin, solid 92 element (Figure 6.2) which has 10 nodes was used. Composite plate and steel pin are modeled for each different configuration of actual experiment specimens. One of them is illustrated in Figure 6.3.

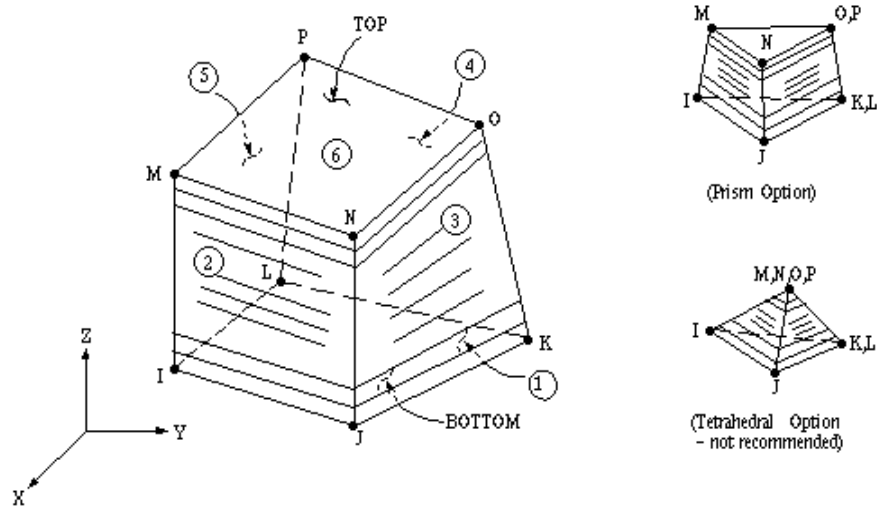


Figure 6.1 Solid 46 element (ANSYS Release 10.0 Documentation, 2005)

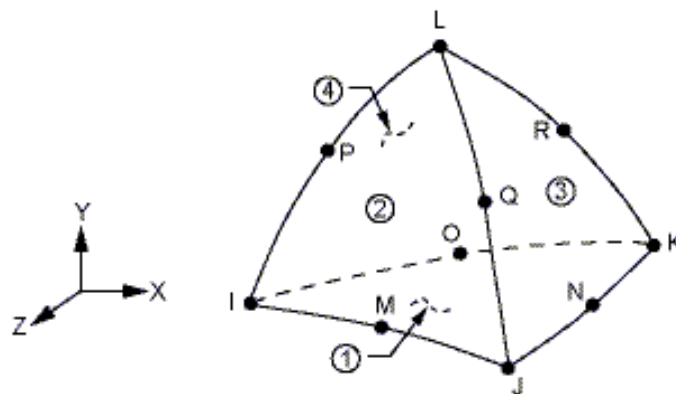


Figure 6.2 Solid 92 element (ANSYS Release 10.0 Documentation, 2005)

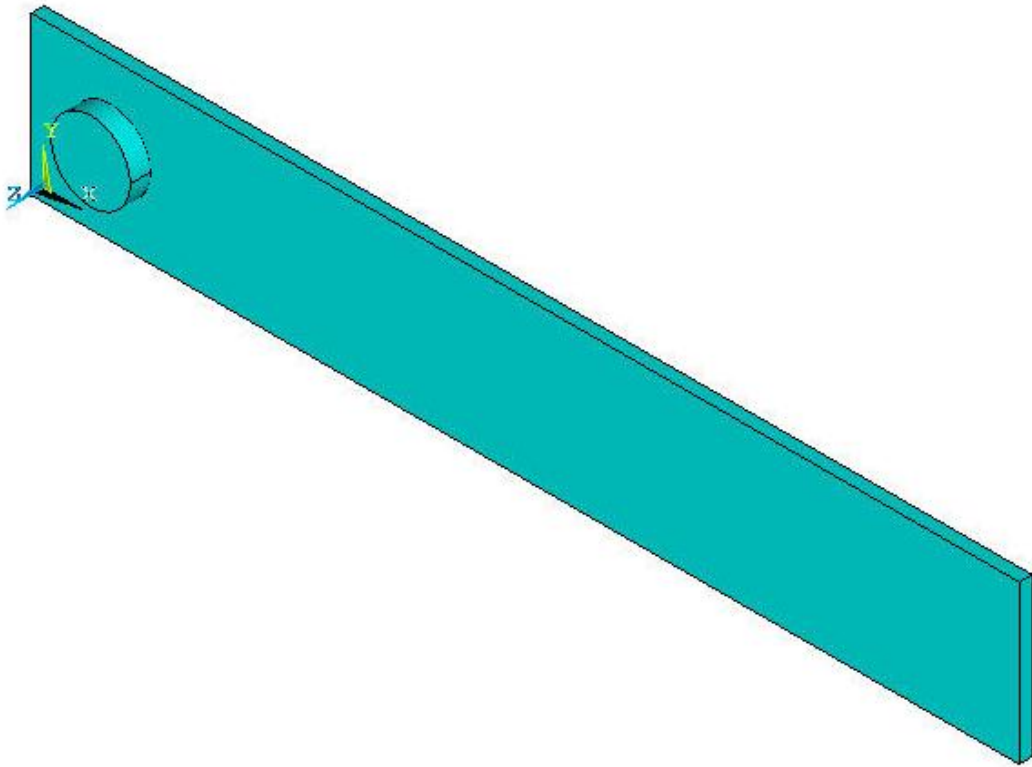


Figure 6.3 Composite plate and steel pin

To generate a tight mesh around the pin hole, each quarter line of circumference of the hole was divided into 15 pieces using Mesh Tool feature of ANSYS. Each width line on the corners of the composite plate was also divided into 4 pieces.

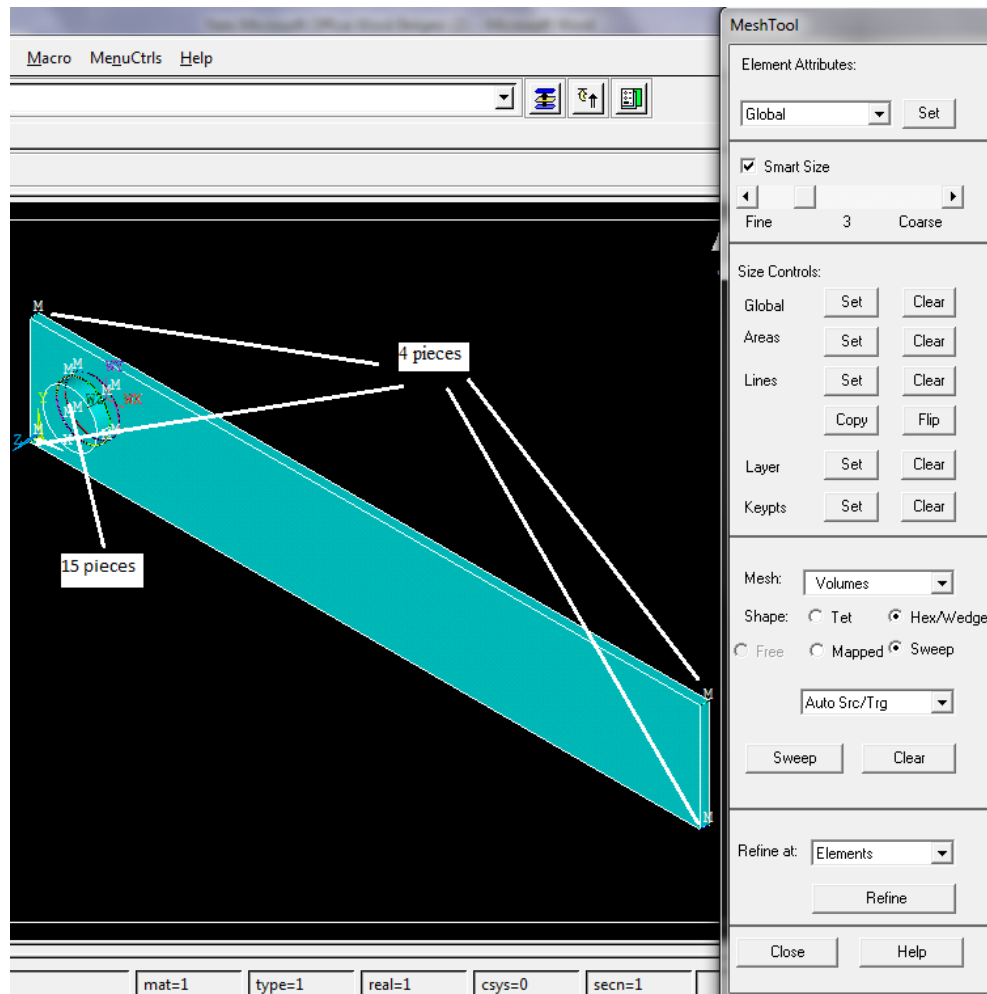


Figure 6.4 Composite plate meshing

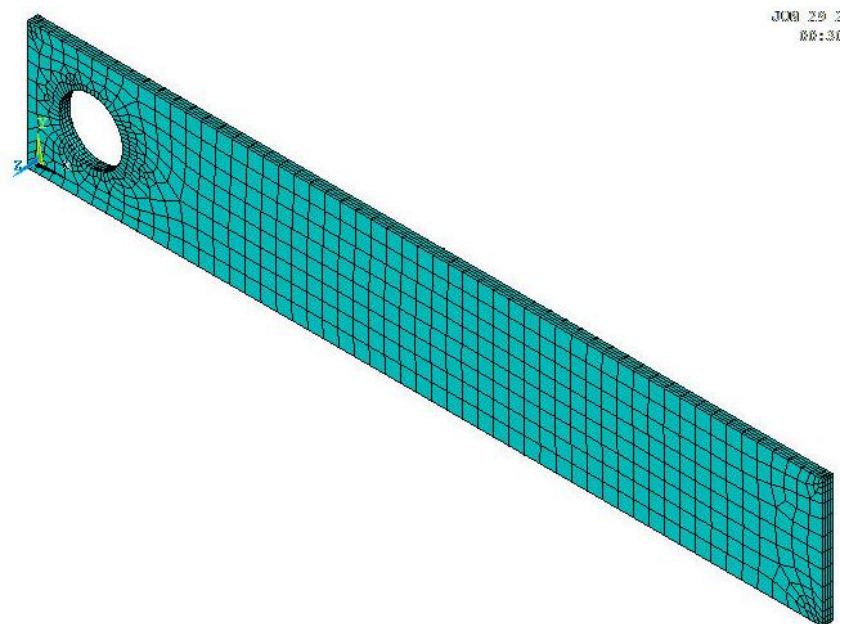


Figure 6.5 Meshed composite plate

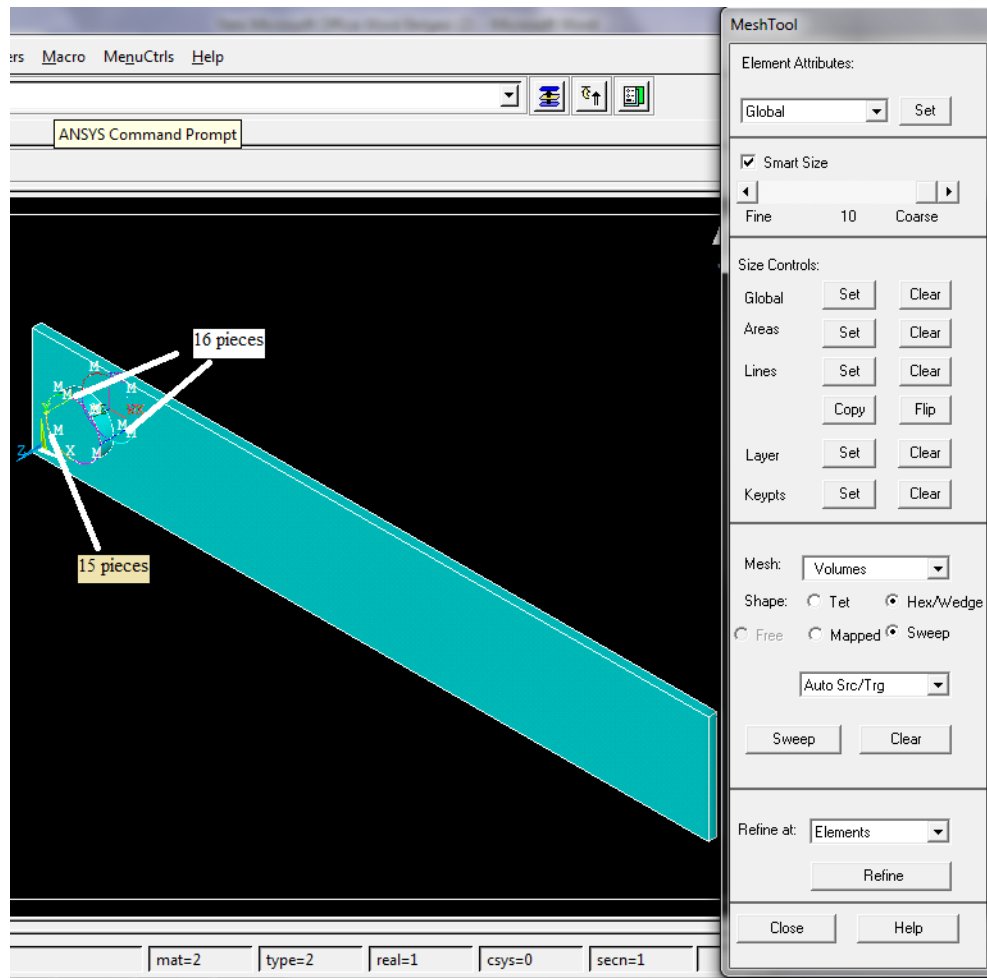


Figure 6.6 Steel pin meshing

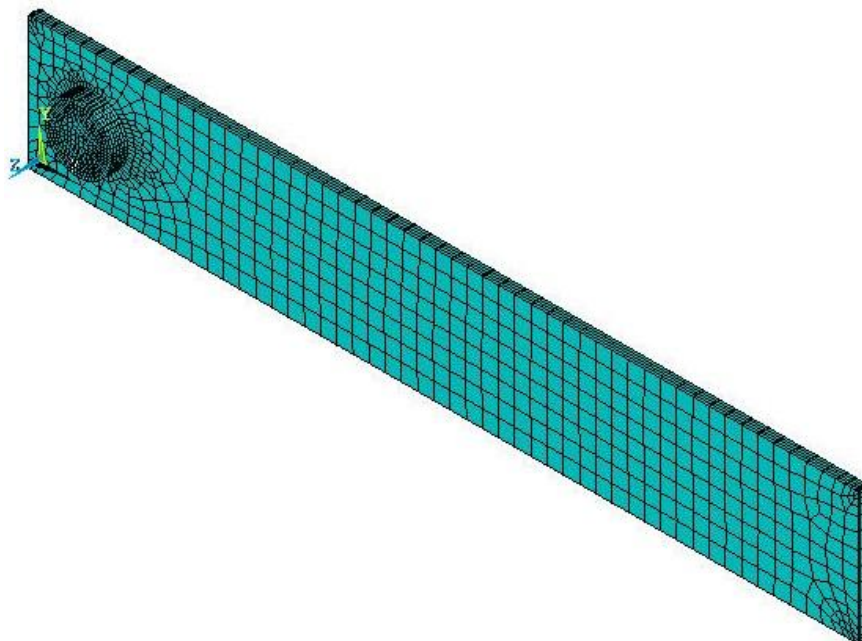


Figure 6.7 Meshed composite plate and steel pin

A contact region was defined between composite plate and steel pin. To define the contact region, ANSYS Contact Pair tool was used. In the Contact Pair tool, the composite plate was defined as Target and the steel pin was defined as the Contact. The coefficient of friction between the parts was defined as 0,15.

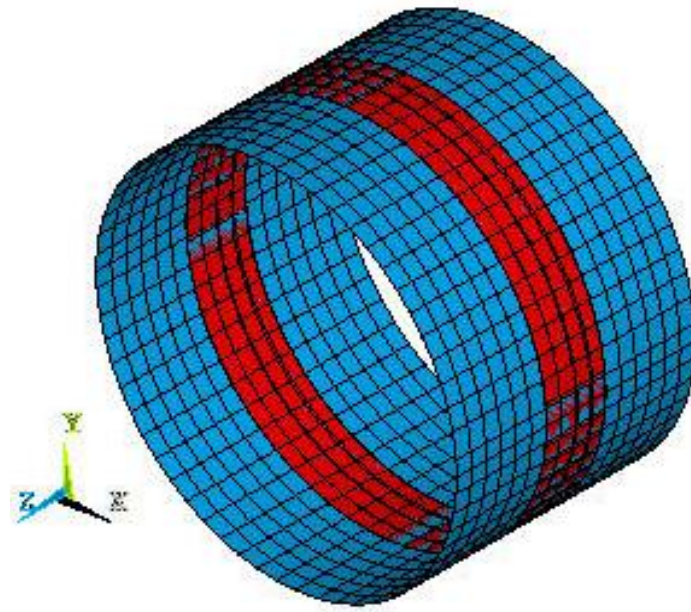


Figure 6.8 Contact region

First failure loads were determined from the force-displacement curves and applied to the free edges of the composite plates as pressure, by dividing the force by cross-sectional area. To fix the assembly, nodes on the both sides of the pin were constrained with All Dof option. Program solutions were checked for Tsai-Wu failure criterion. Same procedures were conducted for interference-fit specimens.

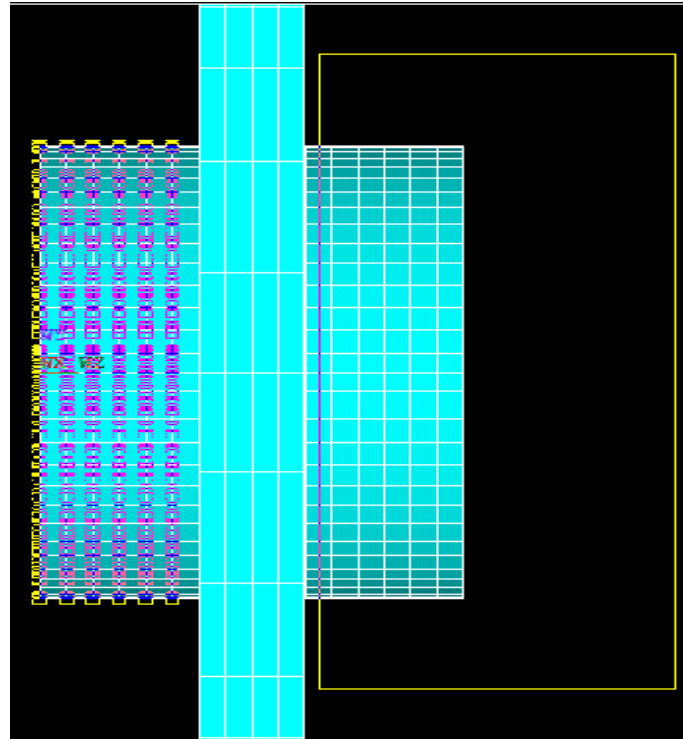


Figure 6.9 Choosing the nodes on the both sides of the pin

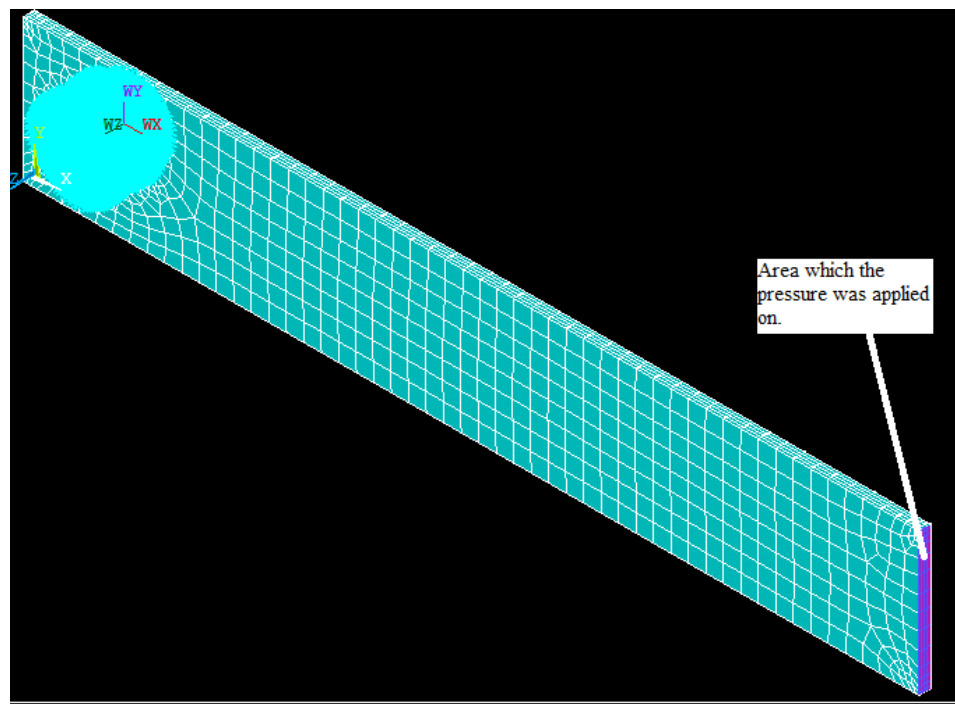


Figure 6.10 Applying the pressure on edge area of the composite plate

After preceding explanations, result figures of solutions for free and interference-fit specimens can be seen in further pages, respectively.

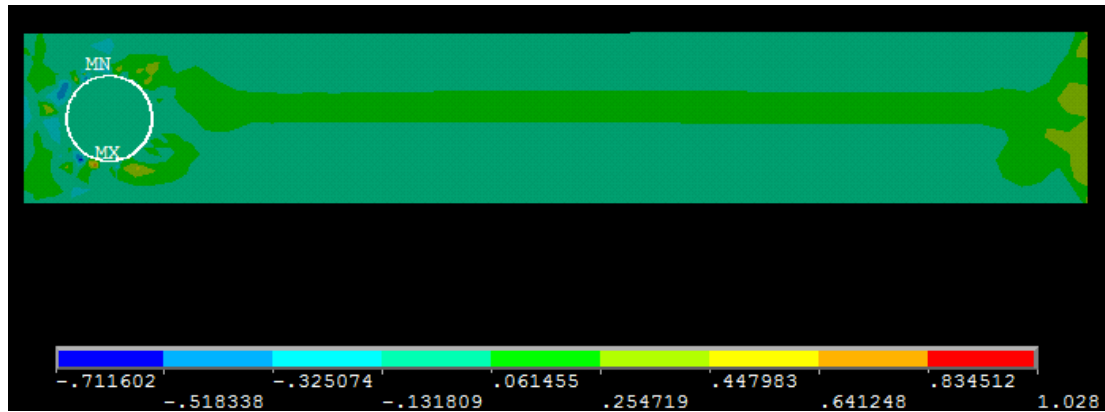


Figure 6.11 Tsai-Wu failure criterion index in $W/D = 2$, $E/D = 1$ for $d = 8.00$ mm

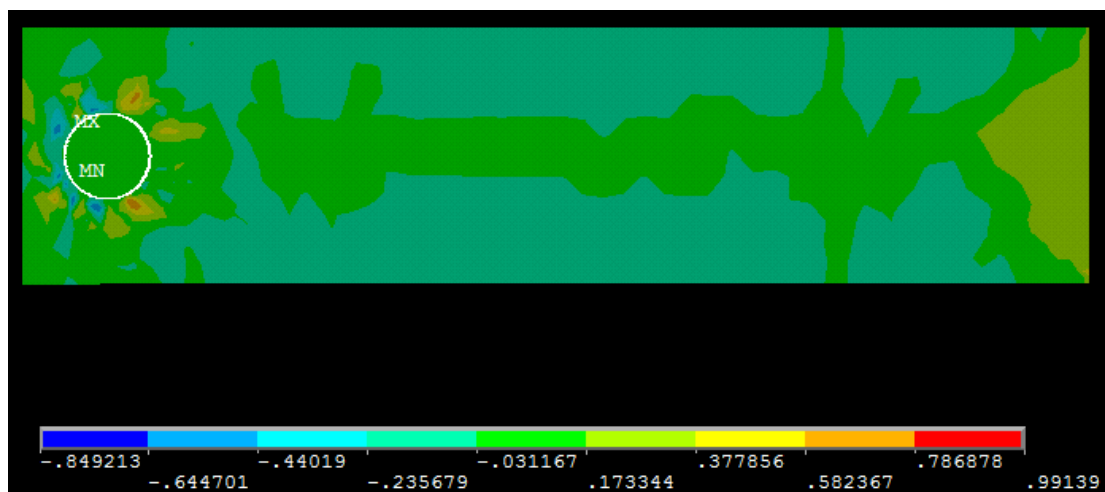


Figure 6.12 Tsai-Wu failure criterion index in $W/D = 3$, $E/D = 1$ for $d = 8.00$ mm

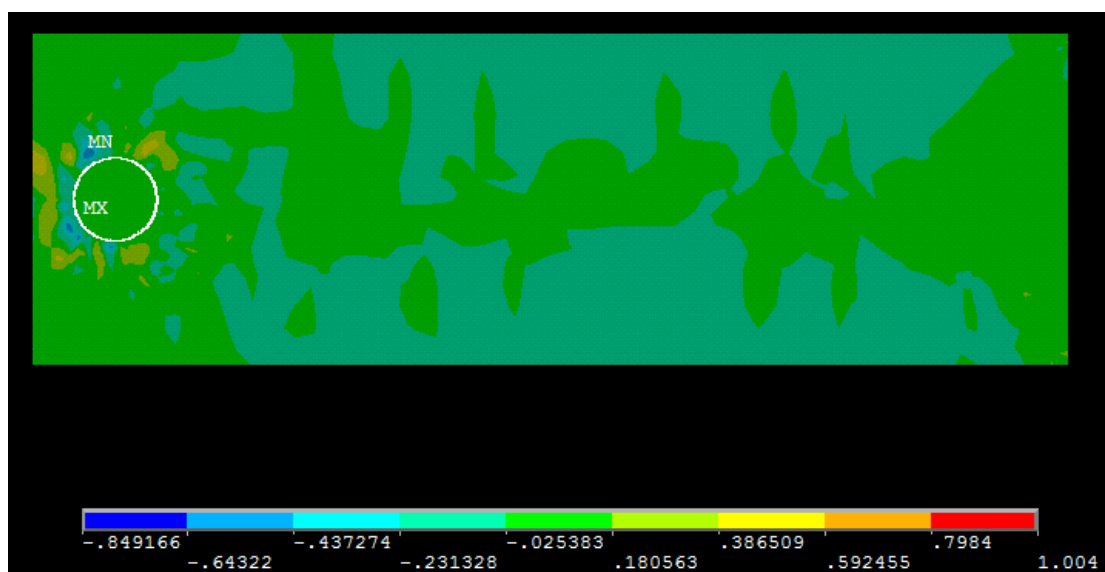


Figure 6.13 Tsai-Wu failure criterion index in $W/D = 4$, $E/D = 1$ for $d = 8.00$ mm

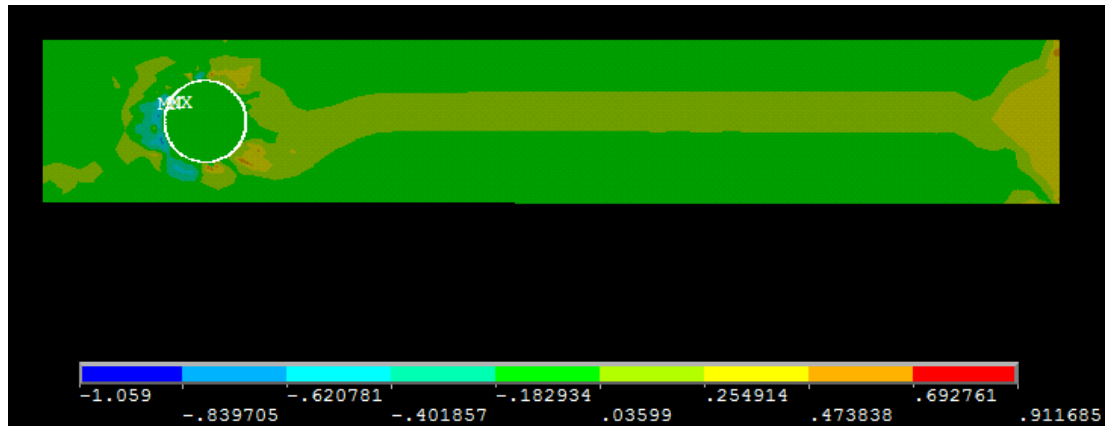


Figure 6.14 Tsai-Wu failure criterion index in $W/D = 2$, $E/D = 2$ for $d = 8.00$ mm

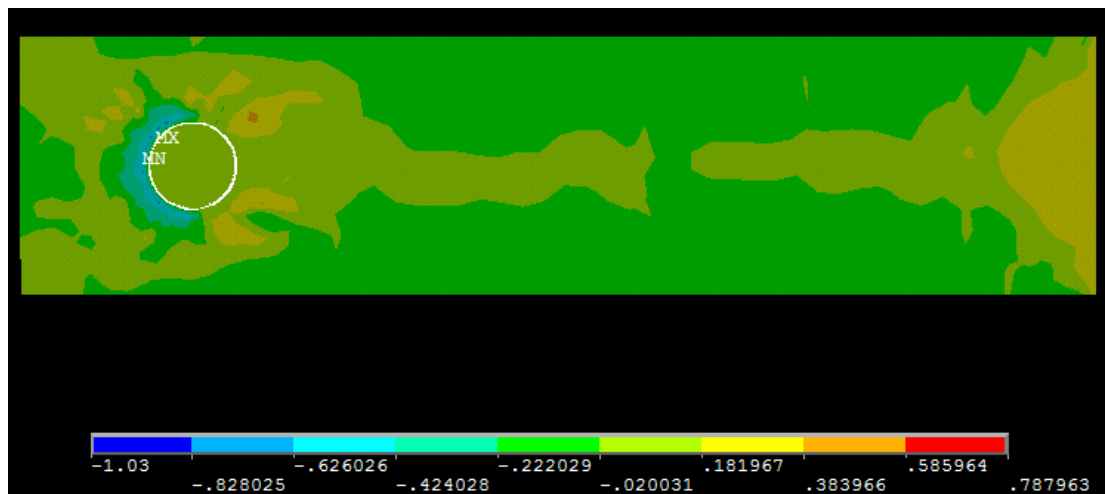


Figure 6.15 Tsai-Wu failure criterion index in $W/D = 3$, $E/D = 2$ for $d = 8.00$ mm

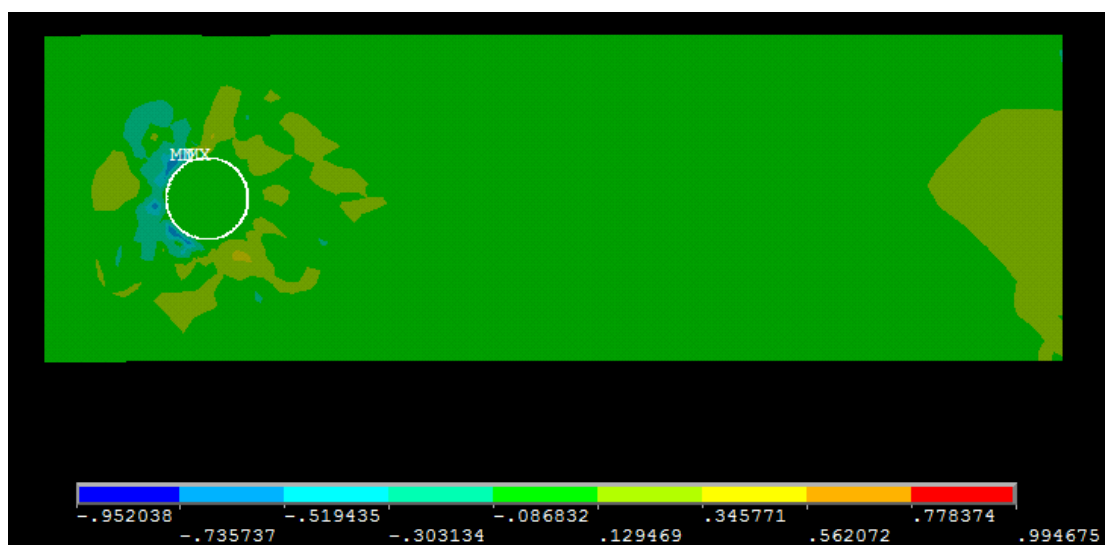


Figure 6.16 Tsai-Wu failure criterion index in $W/D = 4$, $E/D = 2$ for $d = 8.00$ mm

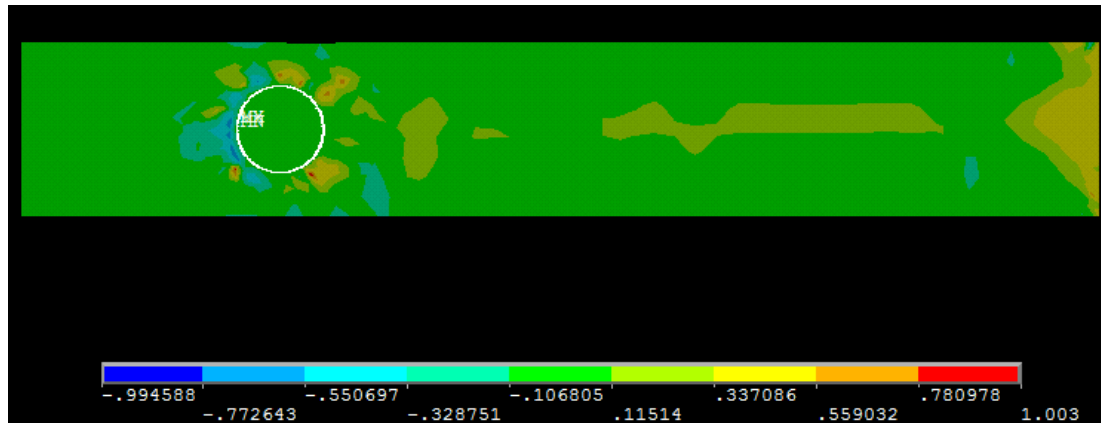


Figure 6.17 Tsai-Wu failure criterion index in $W/D = 2$, $E/D = 3$ for $d = 8.00$ mm

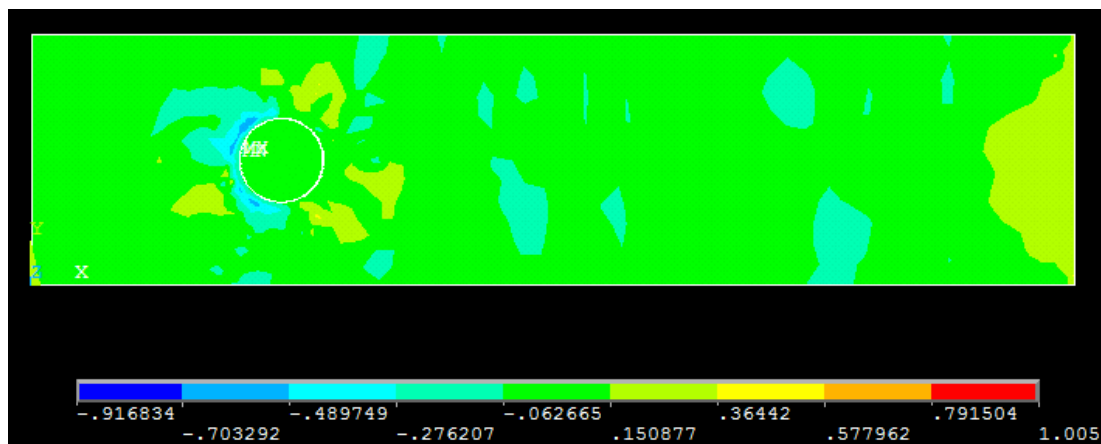


Figure 6.18 Tsai-Wu failure criterion index in $W/D = 3$, $E/D = 3$ for $d = 8.00$ mm

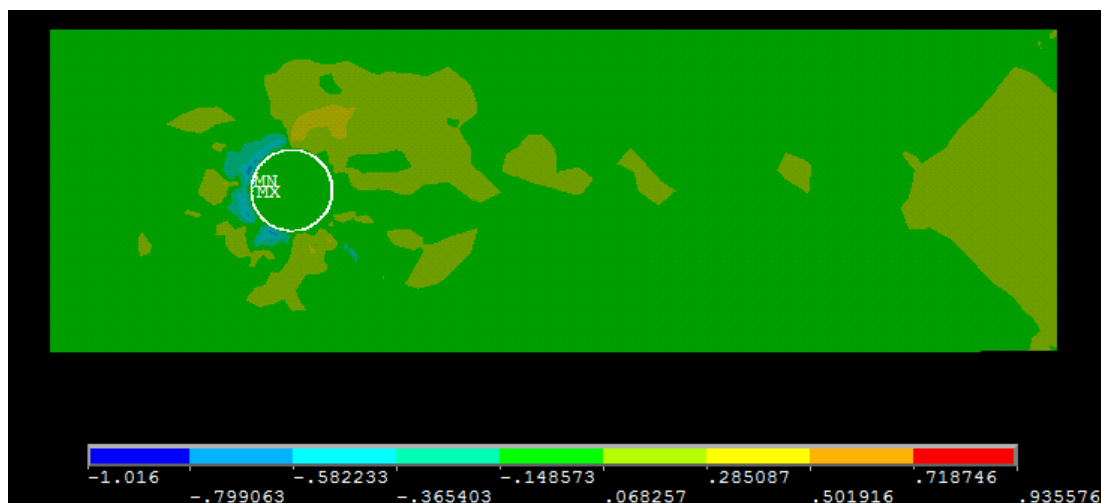


Figure 6.19 Tsai-Wu failure criterion index in $W/D = 4$, $E/D = 3$ for $d = 8.00$ mm

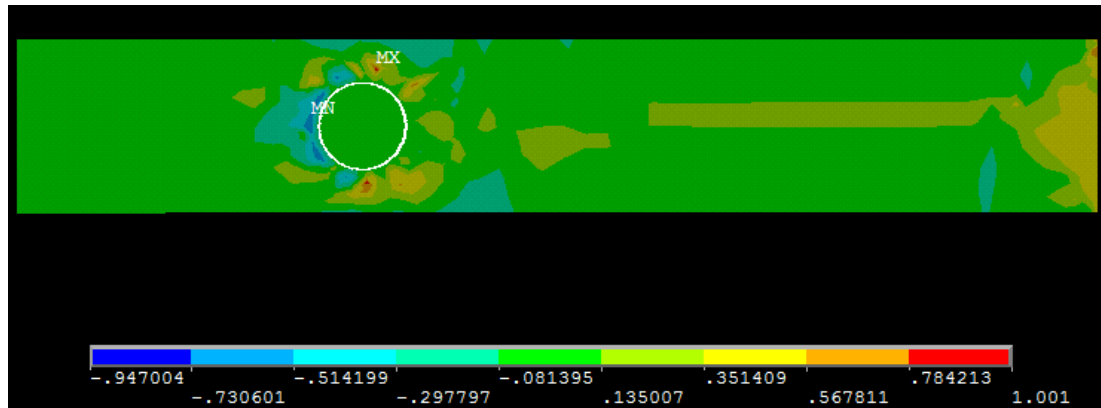


Figure 6.20 Tsai-Wu failure criterion index in $W/D = 2$, $E/D = 4$ for $d = 8.00$ mm

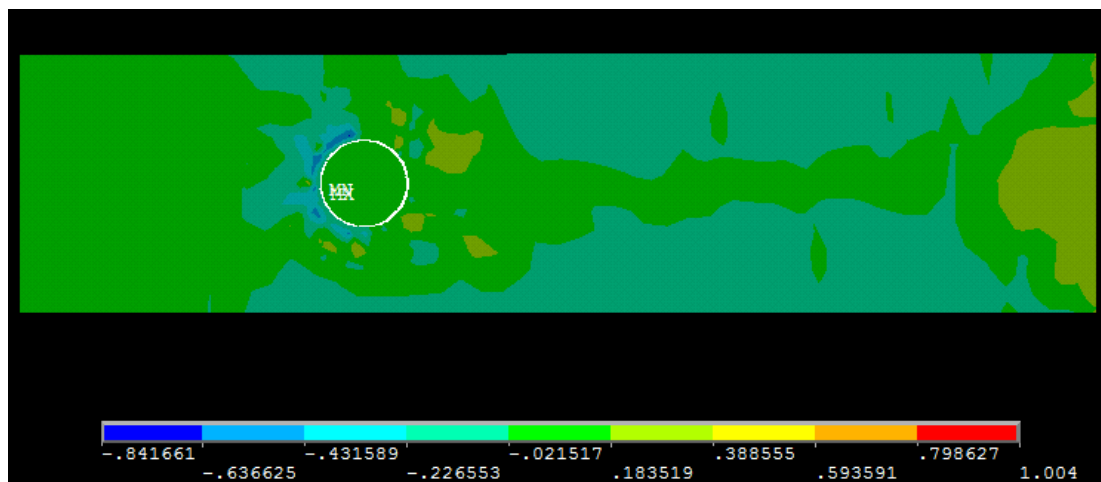


Figure 6.21 Tsai-Wu failure criterion index in $W/D = 3$, $E/D = 4$ for $d = 8.00$ mm

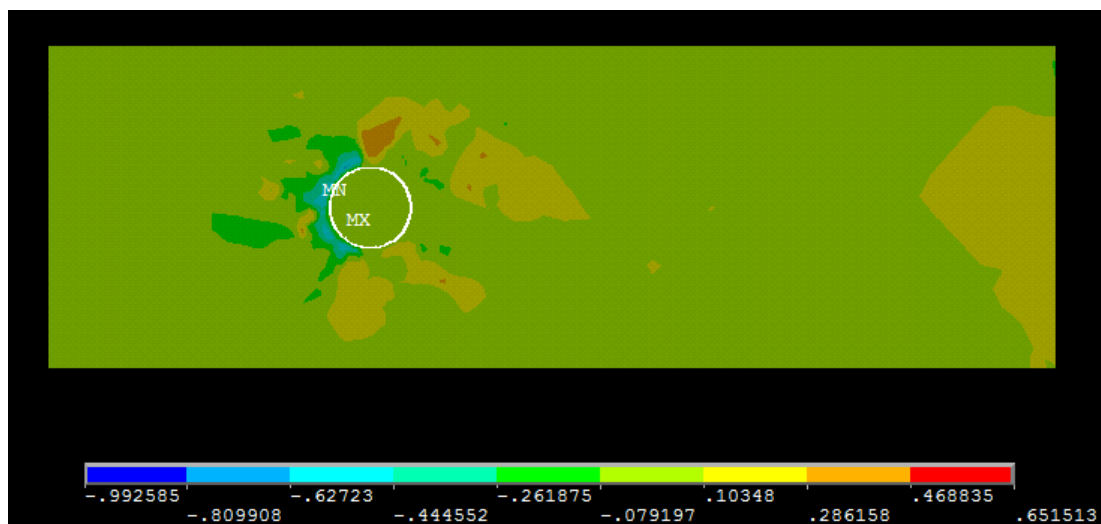


Figure 6.22 Tsai-Wu failure criterion index in $W/D = 4$, $E/D = 4$ for $d = 8.00$ mm

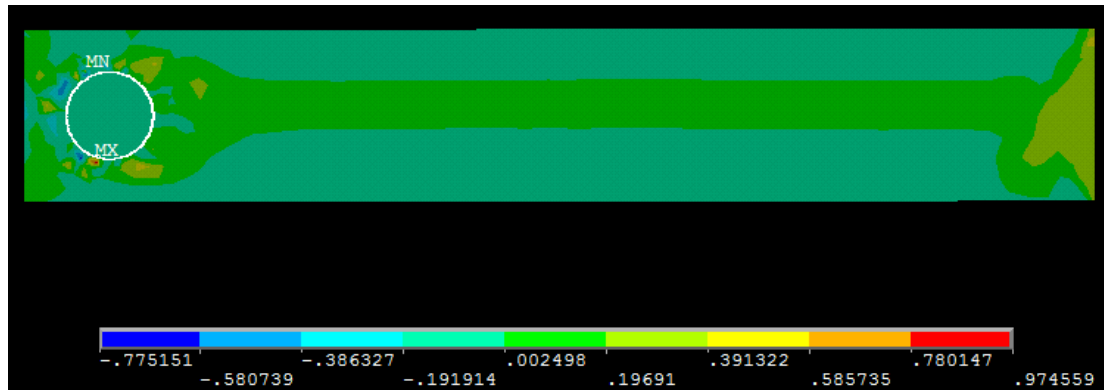


Figure 6.23 Tsai–Wu failure criterion index in $W/D = 2$, $E/D = 1$ for $d = 8.1$ mm

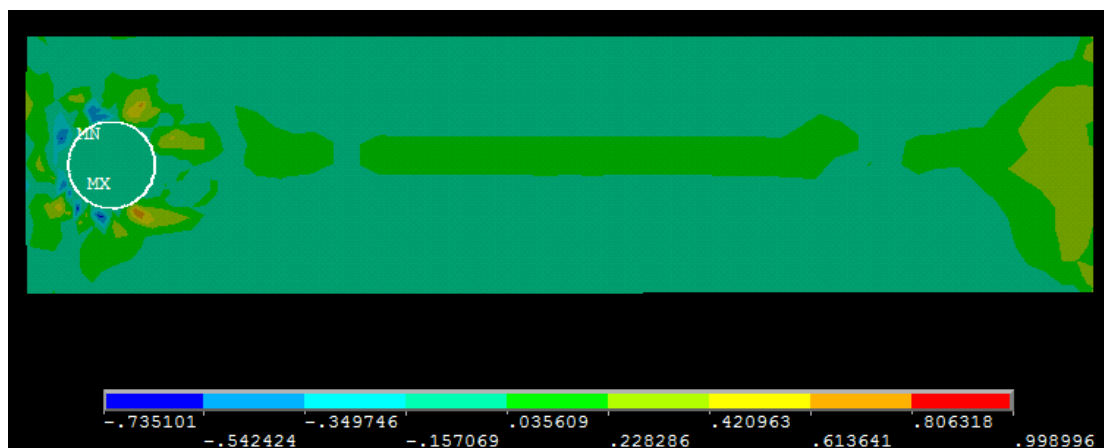


Figure 6.24 Tsai–Wu failure criterion index in $W/D = 3$, $E/D = 1$ for $d = 8.1$ mm

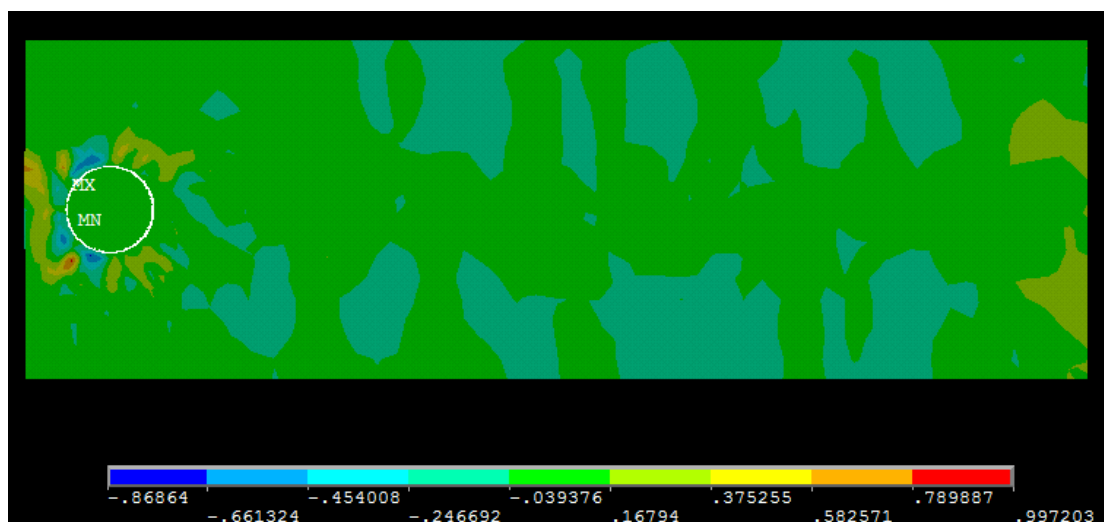


Figure 6.25 Tsai–Wu failure criterion index in $W/D = 4$, $E/D = 1$ for $d = 8.1$ mm

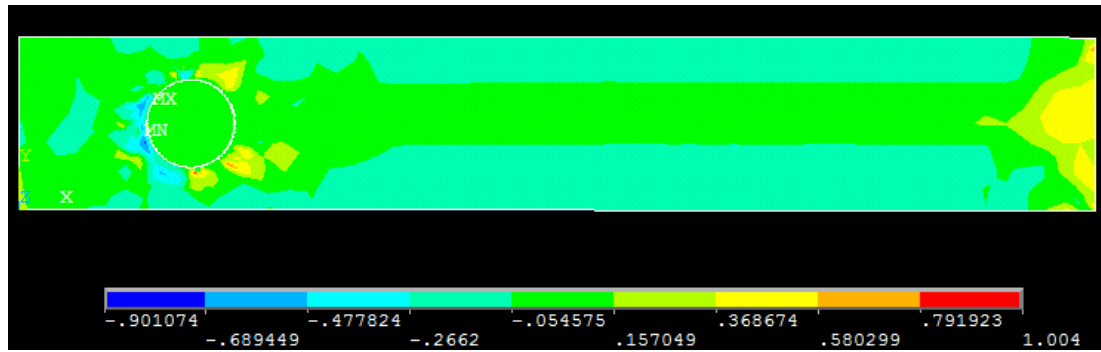


Figure 6.26 Tsai-Wu failure criterion index in $W/D = 2$, $E/D = 2$ for $d = 8.1$ mm

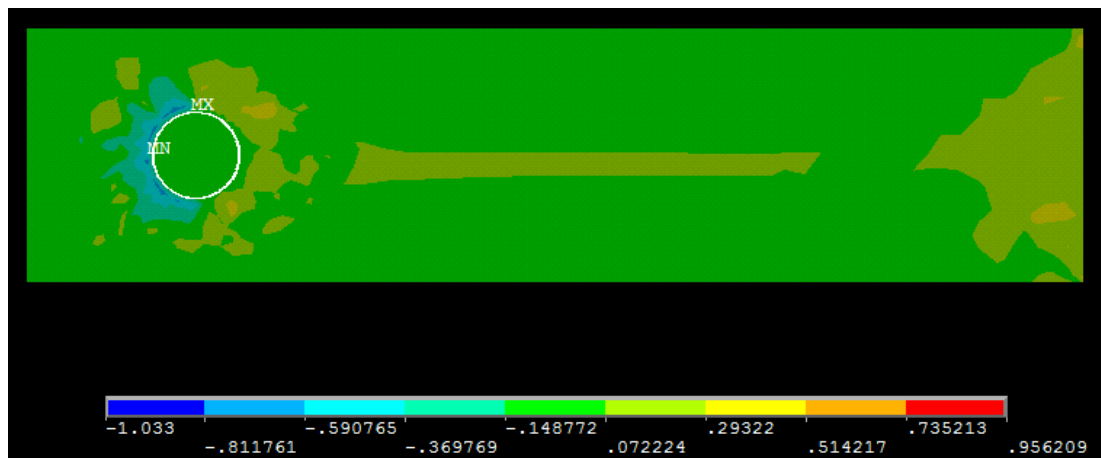


Figure 6.27 Tsai-Wu failure criterion index in $W/D = 3$, $E/D = 2$ for $d = 8.1$ mm



Figure 6.28 Tsai-Wu failure criterion index in $W/D = 4$, $E/D = 2$ for $d = 8.1$ mm

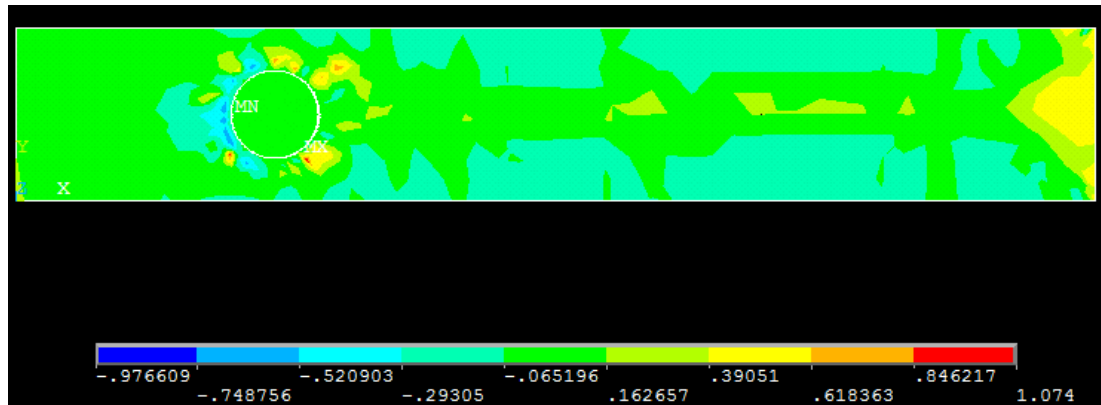


Figure 6.29 Tsai-Wu failure criterion index in $W/D = 2$, $E/D = 3$ for $d = 8.1$ mm

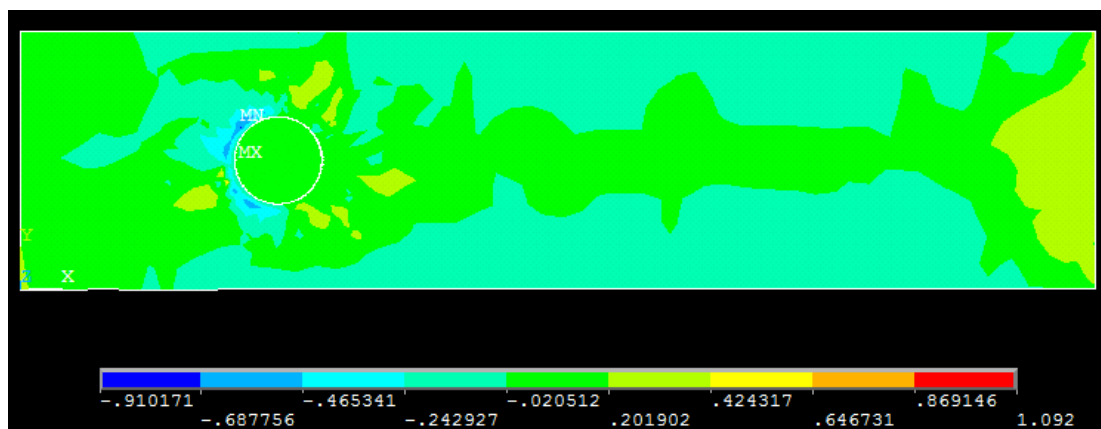


Figure 6.30 Tsai-Wu failure criterion index in $W/D = 3$, $E/D = 3$ for $d = 8.1$ mm



Figure 6.31 Tsai-Wu failure criterion index in $W/D = 4$, $E/D = 3$ for $d = 8.1$ mm

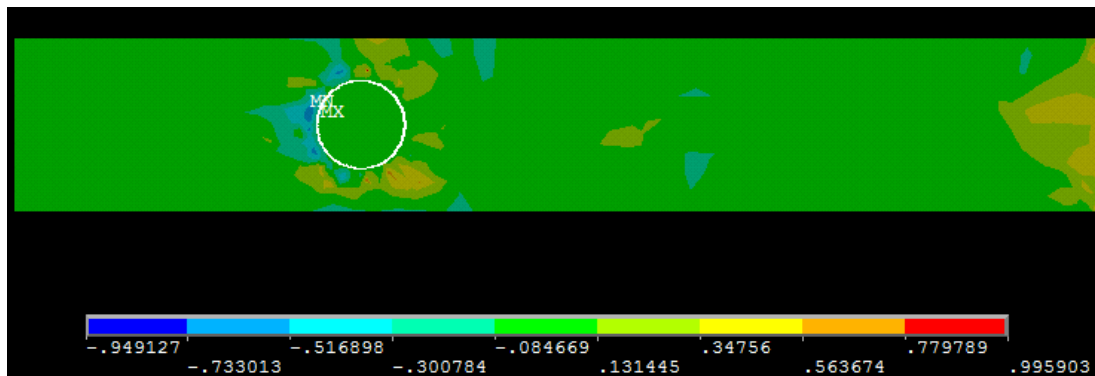


Figure 6.32 Tsai-Wu failure criterion index in $W/D = 2$, $E/D = 4$ for $d = 8.1$ mm

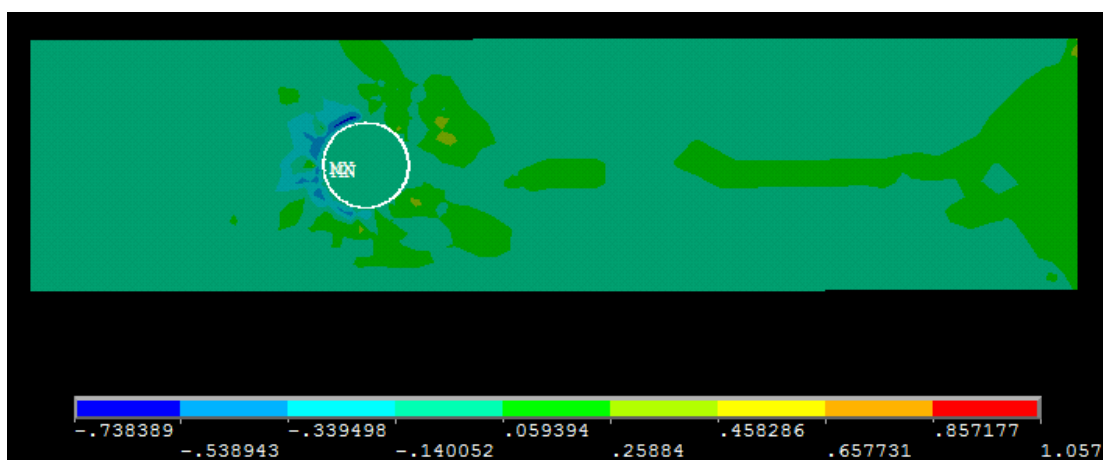


Figure 6.33 Tsai-Wu failure criterion index in $W/D = 3$, $E/D = 4$ for $d = 8.1$ mm

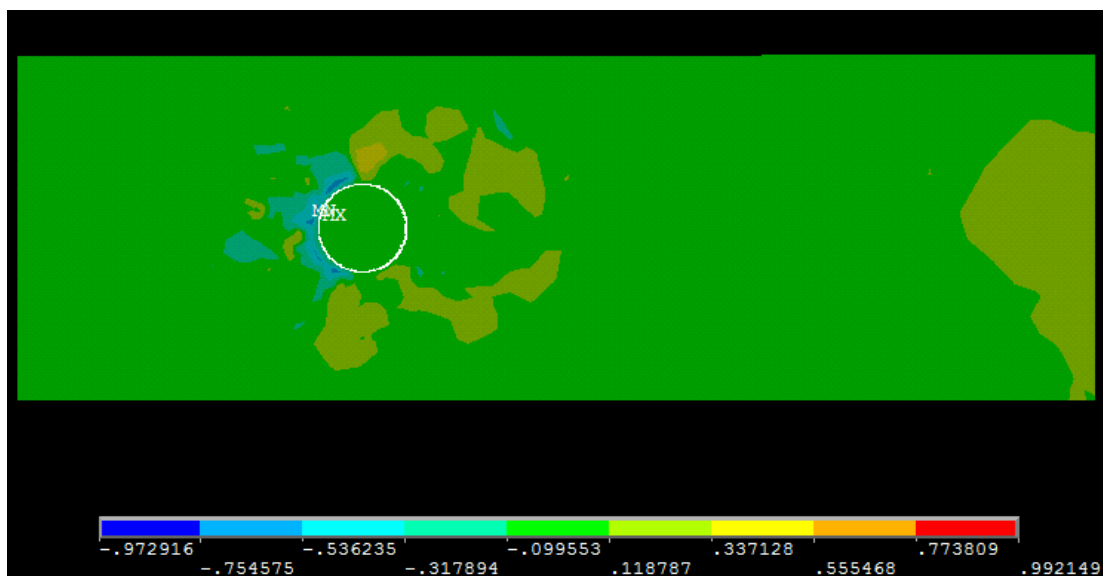


Figure 6.34 Tsai-Wu failure criterion index in $W/D = 4$, $E/D = 4$ for $d = 8.1$ mm

In the following two tables, comparison of the experimental and the numerical solutions for free and interference-fit specimens can be seen, respectively.

Table 6.1 Comparison of first failure loads obtained experimentally and numerically for free fit

	W/D=2		W/D=3		W/D=4	
	Experimental	Numerical	Experimental	Numerical	Experimental	Numerical
E/D=1	1000	1341.6	1020	1872	1100	1680.64
E/D=2	1854	1726.4	1750	1872	1610	1776.32
E/D=3	1680	1934.4	1410	1747.2	1600	1851.2
E/D=4	1850	1913.6	1560	1638	1700	1768

Table 6.2 Comparison of first failure loads of interference-fit specimens

	W/D=2		W/D=3		W/D=4	
	Experimental	Numerical	Experimental	Numerical	Experimental	Numerical
E/D=1	1320	1453.92	1300	1769.04	1245	1826.24
E/D=2	1890	1872	1950	1950	2060	1747.2
E/D=3	2040	2038.4	2000	1872	1950	1913.6
E/D=4	1610	1705.6	1670	1622.4	1796.67	1830.4

CHAPTER SEVEN

CONCLUSIONS

In this study, the failure modes and the bearing strengths of carbon–epoxy pinned composite plates were investigated both experimentally and numerically. Also, the effects of preload moment, seawater and interference-fit on failure modes and loads were studied. According to the experimental and numerical results, the following conclusions can be drawn:

1. When E/D ratio is 1, failure modes are shear-out for all W/D ratios under all conditions. When E/D ratio equals to 2–4, the net-tension and bearing mode are generally observed for all types of specimens. The bearing strength values are always the lowest for E/D = 1.
2. The bearing strengths reach higher values in preloaded specimens than non-preloaded ones. Furthermore, the mean value of the bearing strength of the wet specimens under M = 3 and 6 N m preload moments are 155% and 176% higher than that of the non-preloaded wet specimens. The mean bearing strength value of the dry specimens are almost the same in comparison with the wet specimens under M = 3 N m. However, the mean value of dry specimens under M = 6 N m preload moment is 22% higher than that of wet specimens.
3. The mean bearing strength values of the dry interference-fit specimens are 8% higher than that of the dry neat-fit nonpreloaded specimens. In comparison, the dry free-fit nonpreloaded specimens with dry interference-fit specimens, failure modes for E/D = 1 change from shear-out to net-tension while failure modes for E/D = 2–4 stay almost same.
4. When numerical and experimental bearing strengths are compared, it is seen that numerical results are in good agreement with experimental results.

REFERENCES

- Aktaş, A., & Karakuzu, R. (1999). Failure analysis of two-dimensional carbon-epoxy composite plate pinned joint. *Mechanics of Composite Materials and Structures*, 6, 347-361.
- Aktaş, A., & Dirikolu, M. H. (2003). The effect of stacking sequence of carbon epoxy composite laminates on pinned-joint strength. *Composite Structures*, 62(1), 107–111.
- Aktaş, A. & Uzun, İ. (2008). Sea water effect on pinned-joint glass fibre composite materials. *Composite Structures*, 85, 59-63.
- ANSYS Inc. (2005). *ANSYS Release 10.0 Documentation*. Canonsburg, PA.
- Baker, A. A., Dutton, S., & Kelly, D. (2004). *Composite Materials for Aircraft Structures* (2nd ed.). Virginia: American Institute of Aeronautics and Astronautics, Inc.
- Choi, J. H., Ban, C. S., & Kwean, J. H. (2008). Failure load prediction of a mechanically fastened composite joint subjected to a clamping force. *Journal of Composite Materials*, 42 (14), 1415-1429.
- İçten, B. M., & Karakuzu, R. (2002). Progressive failure analysis of pin-loaded carbon-epoxy woven composite plates. *Composite Science and Technology*, 62, 1259-1271.
- İçten, B. M., & Sayman, O. (2003). Failure analysis of pin-loaded aluminum-glass-epoxy sandwich composite plates. *Composites Science and Technology*, 63(5), 727-737.

- Kiral, B. G. (2010). Effect of clearance and interference-fit on failure the pin-loaded composites. *Materials and Design*, 31, 85-93.
- Kootsookos, A. & Mouritz, A. P. (2004). Seawater durability of glass-and carbon-polymer composites. *Composite Science and Technology*, 64, 1503-1511.
- Mallick, P. K. (1993). *Fiber-Reinforced Composites Materials, Manufacturing, and Design* (2nd ed.). New York: Marcel Dekker.
- Mallick, P. K. (1997). *Composite Engineering Handbook* (1th ed.). USA: Marcell Dekker, Inc.
- Mallick, P. K. (2007). *Fiber-Reinforced Composites Materials, Manufacturing, and Design* (3rd ed.). USA: CRC Press LLC.
- Mazumdar, S. K. (2001). *Composites Manufacturing - Materials, Product, and Process Engineering* (1th ed.). USA: CRC Press LLC.
- Okutan, B. (2001). *Stress and failure analysis of laminated composite pinned joints.*, İzmir: PhD Thesis, Dokuz Eylül University.
- Okutan, B. (2002). The effects of geometric parameters on the failure strength for pin-loaded multi-directional fiber-glass reinforced epoxy laminate. *Composites Part B: Engineering*, 33(8), 567-578.
- Peters, S. T. (1998). *Handbook of Composites* (2nd ed.). London: Chapman &Hall.
- Pierron, F., Cerisier, F., & Grediac, M. (2000). A numerical and Experimental Study of Composite Pin-Joints. *Journal of Composite Material*, 34, 1028-1054.

- Pradhan, B., & Babu, P. R. (2007). Assessment of beneficial effect of interference-fit in pin-loaded FRP composites. *Journal of Reinforced Plastics and Composites*, 26, 771-788.
- Reddy, J. N. (1997). *Mechanics of Laminated Composite Plates Theory and Analysis* (1th ed.). US: CRC Press.
- Shokrieh, M. M., & Lessard, L. B. (1996). Effects of material non-linearity on the three-dimensional stress state of pin-loaded composite laminates. *Journal of Composite Materials*, 30(7), 839-861.
- Staab, G. H. (1999). *Laminar Composites* (1th ed.). USA:Butterworth-Heinemann.
- Sayman, O., Siyahkoç, R., Sen, F., & Ozcan, R. (2007). Experimental Determination of Bearing Strengths in Fiber Reinforced Laminated Composite Bolted Joints under Preload. *Journal of Reinforced Plastics and Composites*, 26, 1051-1063.
- Whitworth, H. A., Othieno, M., & Barton, O. (2003). Failure Analysis of Composite Pin Loaded Joints. *Composite Structures*, 59(2), 261–266.
- Zhang, C., Ganesan, R., & Hoa, S. V. (2000). Effects of Friction on Three-Dimensional Contact Stresses in Pin-Loaded Laminated Composites. *Journal of Composite Materials*, 34, 1382-1415.